

**DEVELOPING A METHODOLOGY FOR INTEGRATED FLOOD
RISK ASSESSMENT IN A TRANSBOUNDARY RIVER BASIN
USING MULTI-PLATFORM DATA UNDER GLOBAL CHANGE–
THE CASE OF THE MEGHNA RIVER BASIN**

A Dissertation

Submitted to the National Graduate Institute for Policy Studies (GRIPS)
and International Centre for Water Hazard and Risk Management (ICHARM),

Public Works Research Institute (PWRI)

in Partial Fulfillment of the Requirements for the Degree of

Ph.D. in Disaster Management

by

Md Khairul Islam

September 2019

Declaration

Except where specific reference has been made to the work of others, the work embodied in this thesis is the result of investigation carried out by the author. No part of this thesis has been submitted or is being concurrently submitted in candidature for any degree at any other institution.

Md. Khairul Islam

Abstract

Flood risk has been tremendously increasing due to changes in climate, population, and land use. To reduce such risk through mitigations measures, flood risk assessment (FRA) is required for strengthening preparedness and building back better. However, lack of various observed data makes FRA difficult to perform in local river basins. Performing FRA is even more difficult in transboundary basins due to unavailability of upstream data. Because of these limitations, FRA hasn't been implemented in transboundary basins, though useful, if implemented, to acquire policy level information for sustainable development. Accordingly, this study proposed a research framework to develop an Integrated FRA (IFRA) model in the Meghna river basin that shares the wettest areas of India upstream and economically important north-eastern rural Bangladesh downstream. An IFRA model consists of three main components: assessment of flood hazard, vulnerability, and exposure. Flood hazard assessment requires reliable basin-wide rainfall data, which is unavailable in the Meghna basin beyond Bangladesh border. Therefore, a reference rainfall dataset was developed using locally available ground and globally available satellite estimates. The potential of the dataset was successfully investigated by calibrating and validating a hydrological model to simulated streamflows. Such dataset overcome the data limitation issues and produced hazard maps in terms of depths, duration, and extent for a past flood across the basin.

Flood vulnerability was assessed through a field survey data due to the lack of recorded flood damage data. Vulnerability curves for Boro rice (main crop of the area), house building, and in-house property damage were established using the survey data. Findings revealed that Boro plants can tolerate the inundation without any damage up to an average height of 25 cm (at which rice tiller evolves), though rice damage becomes ~100% at 70–75 cm water height (at which grains start to flourish). Findings also showed that the

household damage is mainly dependent on inundation height above floor level and construction method and building material of different house types.

Flood exposure, third component of the IFRA model, was assessed for Boro rice and households using a rice extent map (provided by the International Rice Research Institute) and a household distribution map (prepared using population distribution and average household size), respectively. By combining the hazard, vulnerability, and exposure maps, potential flood damage to Boro rice and households were estimated for 2017 flood and satisfactorily validated with the damage reported for the flood.

Using the validated IFRA model, flood risk to Boro rice was assessed under the global changes in climate and land use. Future hazard parameters were produced using global climate models' outputs. Established damage functions (at present value) and rice extent maps predicted for future climate were respectively used for vulnerability and exposure assessment. The results revealed that the effect of climate change will increase the vulnerability of the study area by increasing both depth and extent of inundation. Boro rice damage is expected to increase by about 124%, in future.

Based on findings, new policy implications are recommended to reduce flood disaster risk through structural and non-structural measures. However, the non-structural measures, such as near-real-time flood forecasting and warning, dissemination and implementation of hazard maps, allowing excess water into the Boro fields up to a 25 cm or more water height, and introduction of flood insurance program, were found more effective and environmentally friendly than the structural measures. These recommended non-structural measures have to be promoted by the government as well as non-governmental organizations to reduce increasing flood risk in the study area in order to achieve sustainable development goals and building back better.

Acknowledgement

First, I express my profound and sincere gratitude to the almighty Allah (SWT) for blessing me with physical and mental strength to successfully complete this study.

This study is a product of endless supports, suggestions and efforts from many remarkable individuals. I first would like to express sincere gratitude to my supervisor, respected sensei Associate Prof. Abdul Wahid Mohamed RASMY for his overall supervision, invaluable suggestions and passionate encouragement in every aspect of my study. It is indeed a superb experience to work with him.

I would also like to thank my sub-supervisors Prof. Toshio KOIKE and Prof. Kuniyoshi TAKEUCHI for their enormous support and continuous encouragement to successfully accomplish my study. Without their generous and kind guidance, this study couldn't have seen the light.

I would also like to thank Associate Prof. Miho OHARA for co-authoring and reviewing a journal paper with her insightful comments. Also, I would like to thank Nikolaos Mastrantonas, a former ICHARM intern, for providing computational scripts, literature review and descriptions related to some bias correction and merging techniques of satellite rainfall products. I am also thankful to Yukie OKAWA and Keiko ASAMI for their continuous administrative assistance and making necessary arrangements in different stages of my personal and family life.

I would like to express deepest respect to the authority of National Graduate Institute for Policy Studies (GRIPS) for selecting and supporting me as a Doctoral Program student. I am indebted to International Centre for Water Hazard and Risk Management (ICARM) and Public Works Research Institute (PWRI) for allowing me to work as a research assistant and supporting me to smoothly carry out my study in Japan.

Hereby, I would like to thank the Director General and many other officials of my organization, Bangladesh Water Development Board (BWDB) for approving my leave as deputation and providing necessary data to accomplish my study.

Here, I express heartfelt gratitude to my father, wife and daughter for their continuous encouragement and mental support which helped me to complete the study.

Finally, I beg forgiveness from those whose names I have failed to mention but without whose support this study wouldn't have materialized. The fault for such omission lies entirely with me.

I dedicate this study to my departed mother Mst Khadiza Begum who breathed her last on July 20, 2014.

Table of Contents

Declaration	ii
Abstract	iii
Acknowledgement.....	v
Table of Contents.....	vii
List of Figures	x
List of Tables.....	xv
List of Abbreviations	xvi
Chapter 1: Introduction.....	1
1.1 Background of the Study.....	1
1.2 Problem statement.....	3
1.3 Literature review and way forward.....	5
1.4 Objectives of the Study.....	9
1.5 Scope of the Study	9
1.6 Structure of the Dissertation.....	11
Chapter 2: Material and methods.....	12
2.1 Introduction.....	12
2.2 Study area.....	12
2.3 Methodology	15
2.3.1 Development of a reference rainfall data to generate hazard maps.....	16
2.3.2 Establishment of damage functions to assess vulnerability	17
2.3.3 Flood damage assessment for a past flood	17
2.3.4 Flood risk assessment under global changes.....	17
Chapter 3: Development of Reference Rainfall	19
3.1 Introduction.....	19
3.2 Study area.....	19
3.3 Literature review	20
3.4 Data	24
3.4.1 Topographic Data.....	24
3.4.2 Hydro-meteorological Data.....	25
3.4.2.1 Rainfall.....	25
3.4.2.2 Water Level and Streamflow.....	30
3.5 Methods.....	31
3.5.1 Performance Evaluation of GSRPs	32
3.5.2 Bias Correction of GSRPs.....	34
3.5.2.1 Linear Correction Method	34
3.5.2.2 Modified Linear Correction (MLC) Method	36
3.5.2.3 Quantile Mapping (QM) Method	37
3.5.3 Merging of GSRPs	38
3.5.3.1 Simple Average (SA) Merging.....	39
3.5.3.2 Error Variance (EV) Merging	39

3.5.3.3 Inverse Error Variance Weighting (IEVW) Merging	40
3.5.4 Combination of Merging and Bias Correction	40
3.5.5 Performance Evaluation of the Bias-Corrected and Merged Products	41
3.5.6 Streamflow Simulations	41
3.6 Results and Discussion.....	43
3.6.1 Performance Evaluation of GSRPs on the Daily Scale	43
3.6.2 Performance Evaluation of GSRPs on the Monthly Scale	46
3.6.3 Evaluation of Bias-Corrected GSRPs	48
3.6.4 Evaluation of Merged Products.....	51
3.6.5 Combined Use of Merging and Bias Correction	52
3.6.6 Validation of the IMLC product outside Bangladesh	57
3.6.7 Streamflow simulations with the improved dataset (IMLC product)	59
3.7 Conclusions.....	61
Chapter 4: Establishment of flood damage functions	64
4.1 Introduction.....	64
4.2 Flood vulnerability and literature review	64
4.3 Study area.....	66
4.4 Methods.....	66
4.4.1 Outline of questionnaire survey	67
4.4.1.1 Boro rice damage survey	73
4.4.1.2 Household damage survey	73
4.4.2 Development of flood damage functions	74
4.5 Results and discussion	76
4.5.1 Development of agricultural damage curves.....	77
4.5.2 Development of household damage curves.....	82
4.5.2.1 House building damage curves.....	82
4.5.2.2 Household property damage curves	87
4.6 Conclusions.....	90
Chapter 5: Flood damage assessment.....	93
5.1 Introduction.....	93
5.2 Literature review	93
5.3 Study area.....	95
5.4 Methods.....	95
5.4.1 Generation of hazard maps	97
5.4.2 Estimation of vulnerability.....	97
5.4.3 Exposure assessment.....	98
5.4.4 Flood damage assessment	100
5.5 Results and discussions	102
5.5.1 Calibration and validation of RRI model	102
5.5.2 Generation of hazard parameters	104
5.5.3 Flood damage curves to estimate vulnerability	104
5.5.4 Flood damage to Boro rice.....	105
5.5.5 Household damage assessment	107
5.5.5.1 Damage to house buildings	108
5.5.5.2 Damage to in-house properties.....	109

5.6 Conclusions.....	110
Chapter 6: Flood risk assessment under global change.....	112
6.1 Introduction.....	112
6.2 Literature review	112
6.3 Study area.....	113
6.4 Methods.....	113
6.4.1 Flood hazard.....	114
6.4.2 Flood vulnerability.....	117
6.4.3 Flood exposure.....	117
6.5 Results and discussion	118
6.5.1 Flood hazard estimation for future climate	118
6.5.2 Agriculture land cover change	122
6.5.3 Flood damage functions	123
6.5.4 Future damage assessment	123
6.5.5 Agricultural risk reduction	126
6.6 Conclusion	130
Chapter 7: Summary and conclusions.....	131
7.1 Overall summary.....	131
7.1.1 Summary and findings on hazard assessment	132
7.1.2 Summary and findings on vulnerability assessment	133
7.1.3 Summary and findings on exposure assessment	134
7.1.4 Summary and findings on flood damage assessment	134
7.1.5 Summary and findings on risk assessment due to global change.....	135
7.2 Contribution and applicability of the study.....	136
7.3 Limitations of the study	140
Chapter 8: Policy implications	142
8.1 Existing policy approaches	142
8.2 Policy recommendations	142
Appendix A.1.....	147
Appendix A.2.....	149
Appendix B.....	151
References.....	152

List of Figures

- Figure 1.1: The Ganges-Brahmaputra-Meghna River basins in the Asian continent. The red circles indicate the locations of the entry points of those rivers inside Bangladesh. 2
- Figure 2.1: Topographic features of the study area. (a) Meghna basin in the Asian continent (inset), showing major rivers and administrative details (green shaded area is northeastern Bangladesh); (b) Topography of northeastern Bangladesh; two pink bounded area are sub-districts used for conducting questionnaire survey to collect damage data; (c) Topography of the Meghna basin; and (d) land cover of the Meghna basin. 13
- Figure 2.2: Flowchart of the research methodology used in this study for integrated flood risk assessment for sustainable development in a transboundary river basin. 16
- Figure 3.1: Meghna basin with detailed river network, including 20 meteorological stations (red bubbles) and two hydrological stations (green bubbles) inside Bangladesh; 25
- Figure 3.2: Meghna basin showing GHCN-D global gauges and CPC unified 0.5°-grid centres that—along with other observed datasets—were used to produce the GSRP rainfall estimates on (a) 25 July 2010, and (b) 17 May 2016. The local rainfall stations are also shown (red dots). 30
- Figure 3.3: Flow chart of the method used for comparing four GSRPs, creating a reference rainfall dataset, and investigating that dataset’s applicability when simulating streamflows in the Meghna basin. 32
- Figure 3.4: Cumulative rainfall of daily estimates calculated for the ground gauges and GSRPs throughout the wet season (March–October) of the study period (2009–2016), at the 20 rain-gauge stations (a–t) located within the Bangladesh portion of the Meghna basin. 45
- Figure 3.5: Scatterplots of daily GSRP estimates against daily ground rainfall for the wet seasons during the entire study period (2009–2016) at the 20 rain-gauge stations (a–t). Comparison indices are included inside the plot for each station. 46
- Figure 3.6: Scatterplots of mean monthly accumulated GSRP estimates against the ground rainfall for the wet seasons during the entire study period (2009–2016) at the 20 rain-gauge stations (a–t). Statistical indices are included inside the plot for each station. 47
- Figure 3.7: Mean monthly accumulated rainfall of the ground gauges and CHIRPS, GSMaP-G, TMPA-G, and MSWEP for the months of the rainy season (March–October) during the study period (2009–2016) at 20 gauge stations (a–t). 48
- Figure 3.8: Taylor diagram illustrating statistical comparison between original, bias-corrected GSRP estimates and gauge rainfall (obs mark), as calculated for the wet seasons of 2009–2016 at five validation stations (a–e). The CCs are related to the azimuthal angle (grey lines), which denote a similarity in pattern between the satellite and gauge fields. NSDs (green contours) indicate the amount of variance between the satellites and the gauge time series, and is proportional to the radial distance from the origin. The NRMSD (blue contours) between the satellite products and the rain-gauge fields is

proportional to the distance from the point on the x -axis identified as obs. For details, refer to Taylor (2001).	50
Figure 3.9: Taylor diagram illustrating a statistical comparison between satellite products (original and merged) and ground rainfall (obs mark) for the wet seasons of 2009–2016 at the 20 rain-gauge stations (a–t). Instructions for reading a Taylor diagram are given in Figure 3.8.	52
Figure 3.10: Taylor diagram with the statistical comparison of the original GSRPs, the MLC-corrected GSRPs, and the IEVW-based merged product of the original GSRPs (both without and with the MLC bias correction) against ground rainfall for the wet seasons of 2009–2016 at the five validation stations (a–e). Instructions for reading a Taylor diagram are given in Figure 3.8.	54
Figure 3.11: Taylor diagrams plotted for the (a) daily, (b) monthly, and (c) annual time series of the original GSRPs and the IMLC product vs. the ground rainfall collectively calculated for the five validation stations for the period of 2009–2016. Instructions for reading a Taylor diagram are given in Figure 3.8.	56
Figure 3.12: Annual average rainfall distribution at 0.25° grid resolution for (a) CHIRPS, (b) GSMaP-G, (c) TMPA-G, (d) MSWEP, and (e) IMLC product during the study period (2009–2016).	56
Figure 3.13: Taylor diagram with a comparison of the monthly accumulated district-average rainfall estimates (calculated from the original GSRPs) and IMLC product (the improved dataset created in this study) relative to the observed rainfall of nine districts (a–i) located inside the Indian portion of the Meghna basin for the period of 2012–2016. Instructions for reading a Taylor diagram are given in Figure 3.8.	58
Figure 3.14: Daily observed streamflows (black) and simulated streamflows (red) produced by the improved rainfall dataset (the IMLC product) for the periods of (a) calibration (2009–2012) and (b) validation (2013–2016) using the RRI model at the Bhairab Bazar stream gauge. See Table 3.4 for the statistical metrics used to evaluate the simulated streamflows.	60
Figure 3.15: Daily observed streamflows (black) and simulated streamflows (red) produced by the improved rainfall dataset for additional validation of the RRI model at the Amalshid stream gauge during the entire study period (2009–2016). See Table 3.4 for the statistical metrics used to evaluate the simulated streamflows.	60
Figure 4.1: Flow chart of the methodology used for establishing reliable damage curves for agriculture and household damage in the northeastern part of Bangladesh.	67
Figure 4.2: Different types of houses according to building materials. (a) Mud: made of mud/soil, straws, bamboo sticks, jute sticks, and corrugated iron sheet; (b) Brick: made of mud/cement, bricks, and corrugated iron sheet; (c) Concrete: made of bricks, cement, brick/stone chips, and steel rods.	74
Figure 4.3: Comparison between the collected dataset of two sub-districts using four statistical indices, and performed for the flood duration of (a) 1–3 days, (b) 4–7 days, and (c) above 7 days.	78

Figure 4.4: Distribution of rice yield loss against selected flood heights, plotted in box and whisker plots with the collected 196 target samples for the flood duration of (a) 1–3 days, (b) 4–7 days, and (c) above 7 days.	79
Figure 4.5: Damage curves predicted by five regression models for each set of flood duration of (a) 1–3 days, (b) 4–7 days, and (c) above 7 days.	80
Figure 4.6: Flood damage curves of Boro rice developed via the data of a questionnaire survey conducted in the study area for the duration range of (a) 1–3 days, (b) 4–7 days, and (c) above 7 days. Standard deviation ($\pm 1\sigma$) is added to show the uncertainty bands.	82
Figure 4.7: Comparison between the collected datasets of two sub-districts using four statistical indices for (a) Mud, (b) Brick, and (c) Concrete houses.	83
Figure 4.8: Distribution of house building damage against selected flood heights, plotted in box and whisker plots with the collected 165 target samples for the house types of (a) Mud, (b) Brick, and (c) Concrete.	84
Figure 4.9: Depth-damage relationships predicted by five regression models for the house types of (a) Mud, (b) Brick, and (c) Concrete.	86
Figure 4.10: Flood damage curves developed through the data of the questionnaire survey conducted in the study area for (a) Mud, (b) Brick, and (c) Concrete type of houses. Standard deviation ($\pm 1\sigma$) is added to show the uncertainty bands.	87
Figure 4.11: Comparison between the in-house property damage data of the two sub-districts performed with four statistical indices and for the house type of (a) Mud, (b) Brick, and (c) Concrete.	88
Figure 4.12: Distribution of the damage to household properties against selected flood heights, plotted in box and whisker plots with the collected 165 target samples for the house types of (a) Mud, (b) Brick, and (c) Concrete.	88
Figure 4.13: Household property damage and depth relationships predicted by five regression models for the house types of (a) Mud, (b) Brick, and (c) Concrete.	89
Figure 4.14: Flood damage curves developed for in-house properties through the data of the questionnaire survey for (a) Mud, (b) Brick, and (c) Concrete type of houses. Standard deviation ($\pm 1\sigma$) is added to show the uncertainty bands.	90
Figure 5.1: Flowchart of the research structure used in this research for flood damage assessment in the northeastern part of Bangladesh.	96
Figure 5.2: Boro extent map for the study area provided by IRRI.	98
Figure 5.3: 500-m grid distribution maps of the study area for (a) population extracted from 1-km grid LandScan 2016 and (b) houses prepared using LandScan population and the average family size by district.	100
Figure 5.4: Comparison of streamflows simulated by RRI model with the observed streamflows at Bhairab Bazar station for the period of model's (a) calibration and (b) validation.	103

Figure 5.5: Validation of water levels simulated by RRI model along the river channel with the observed water levels measured at 15 stations (a) on 5 th April 2017 and (b) for 30 days of the 2017 flood (30 th March to 28 th April).	103
Figure 5.6: Potential inundation maps at 500-m grid generated by RRI model in terms of (a) flood depths and (b) flood duration across the study area during the 2017 flood event (30 th March to 28 th April).	104
Figure 5.7: Synthetic type of damage curves developed through the data of a questionnaire survey conducted in the study area for (a) Boro rice, (b) house buildings, and (c) in-house properties. Standard deviation ($\pm 1\sigma$) is included as uncertainty bands to avoid the differences between actual and collected damage.	105
Figure 5.8: Distributed damage map produced for the Boro rice considering its average yield for the 2017 flash flood in the study area.	106
Figure 5.9: Estimated and reported area with Boro rice damage caused by the 2017 flood for each administrative district of the study area.	106
Figure 5.10: Comparison of the estimated and reported number of affected households caused by the 2017 flood for each administrative district of the study area.	108
Figure 5.11: Estimated house building damage for each grid cell of the study area considering the flood event of 2017.	109
Figure 5.12: In-house property damage for each grid cell of the study area considering the flood event of 2017.	110
Figure 6.1: Flowchart of the methodology used in this chapter for future flood risk assessment in the northeastern part of Bangladesh due to global changes.	114
Figure 6.2: Past and predicted land cover maps of Boro rice in the study area.	118
Figure 6.3: Basin averaged extreme rainfall of each selected GCM for the past (1981-2000) and future climate (2040-2059) drawn for the months of March and April considering (a) 1-day and (b) 5-day accumulated maximum rainfall.	119
Figure 6.4: Flood inundation maps in terms of maximum depths for the past and future climates.	120
Figure 6.5: Comparison of flood inundation areas for past and future climates considering different sets of flood inundation depths.	121
Figure 6.6: Land cover change from past to future for the Boro rice of two classes.	123
Figure 6.7: Flood damage maps estimated for Boro rice damage for different future flood events considering the changes in global climate and land use.	124
Figure 6.8: Total amount of flood damage to Boro rice in future calculated for the study area considering the flood events of each selected GCM.	125
Figure 6.9: Hazard maps generated for the MIROC5 model (a) without and (b) with the structural measure (river channel dredging and widening).	127

Figure 6.10: Comparison of flood inundation areas for different sets of flood inundation depths without and with the structural measure (river channel dredging and widening)...	127
Figure 6.11: Flood damage to Boro rice without and with the structural measure (river channel dredging and widening).	128
Figure 6.12: Hazard maps generated without and with the non-structural measure.	129
Figure 6.13: Flood damage to Boro rice without and with the non-structural measure.	129

List of Tables

Table 3.1: Salient features of the 20 rain-gauge stations located in the Bangladesh portion of the Meghna basin for the study period of 2009–2016.	26
Table 3.2: Salient features of the GSRPs used in the study for the period of 2009–2016.	29
Table 3.3: Categorical statistics calculated for daily GSRP rainfall estimates relative to daily ground rainfall in the wet season throughout the study period (2009–2016).	44
Table 3.4: Statistical indices used to measure the performance of the RRI model simulations in the calibration, validation, and additional-validation phases.	61
Table 4.1: Total population size, standard minimum sample size, and collected number of actual sample size by sub-district.	69
Table 4.2: Name and equations of the regression models used in this study.	76
Table 4.3: Characteristics of Boro rice in the sample area.	77
Table 4.4: Results of five regression models performed with 196 target samples collected for Boro rice damage due to flood.	80
Table 4.5: Characteristics of different house types observed in the study area.	83
Table 4.6: Results of five regression models performed with 165 target samples collected for flood damage to three types of houses.	85
Table 4.7: Results of different regression models performed with the household property damage data collected for 165 samples.	89
Table 5.1: Cultivable extent of Boro rice by district extracted from IRRI map; the extent is compared with the area provided by DAE.	99
Table 5.2: Comparison of LandScan (2016) population and the calculated number of houses by district with those of the figure obtained from Bangladesh census data (BBS-2011)	100
Table 5.3: Comparison of estimated and reported damage of Boro rice for the 2017 flood.	107
Table 6.1: Selected GCMs with their performance scores obtained for the nine climatic variables considered in this study.	116

List of Abbreviations

AIC	Akaike's Information Criterion
APHRODITE	Asian Precipitation - Highly-Resolved Observational Data Integration Towards Evaluation of Water Resources
BBS	Bangladesh Bureau of Statistics
BWDB	Bangladesh Water Development Board
CHIRPS	Climate Hazards Group InfraRed Precipitation with Station data
CMIP5	fifth Coupled Model Inter-comparison Project
CMORPH	Climate Prediction Centre (CPC) MORPHing method
CPC	Climate Prediction Centre
DAE	Department of Agricultural Extension
DDM	Department of Disaster Management
DIAS	Data Integration and Analysis System
GBM	Ganges, Brahmaputra, and Meghna basins
GCMs	Global Climate Models
GHCN-D	Global Historical Climatology Network's Daily
GPCC	Global Precipitation Climatological Centre
GPM	Global Precipitation Measurement mission
GSMaP	Global Satellite Mapping of Precipitation
GSRPs	Gauge-adjusted Satellite Rainfall Products
HydroSHEDS	Hydrological data and maps based on Shuttle Elevation Derivatives at multiple Scales
IDW	Inverse Distance Weighting
IEVW	Inverse Error Variance Weighting
IFRA	Integrated Flood Risk Assessment

IMERG	Integrated Multi-satellite Retrievals for GPM
IPCC	Intergovernmental Panel on Climate Change
IRRI	International Rice Research Institute
JICA	Japan International Cooperation Agency
JAXA	Japan Aerospace Exploration Agency
LULC	Land Use Land Cover
MLC	Modified Linear Correction
MSWEP	Multi-Source Weighted-Ensemble Precipitation
NASA	National Aeronautics and Space Administration
NMSE	Normalised-Mean-Squared Error
NOAA	National Oceanic and Atmospheric Administration
NRT	Near-Real Time
ORNL	Oak Ridge National Library
PERSIANN	Precipitation Estimation from Remotely Sensed Information using Artificial Neural Networks
RCP	Representative Concentration Pathways
REs	River Embankments
RMSE	Root-Mean-Squared Error
RRI	Rainfall-Runoff-Inundation
SDGs	Sustainable Development Goals
SEs	Submergible Embankments
SRTM	Shuttle Radar Topography Mission
TMPA	TRMM Multi-satellite Precipitation Analysis
TRMM	Tropical Rainfall Measuring Mission

Chapter 1: Introduction

1.1 Background of the Study

Floods are natural hazards necessary for healthier existence of the eco-system on the one hand. However, on the other hand, they can lead to a disaster with widespread damage. Flood damage and associated disaster risk have been tremendously increasing due to the effect of climate change, rapid urbanization, global population change and land use changes, which are posing threat to the sustainable development of many countries throughout the world, particularly of developing countries (IPCC, 2014; Felbermayr and Gröschl, 2014). To reduce such increasing flood damage and risk through structural and non-structural measures for strengthening preparedness (resource allocation, rescue operation, etc.) and building back better, flood risk assessment (FRA) is required according to the Sendai framework and globally supported sustainable development goals (SDGs). However, due to the lack of various observed data, FRA becomes difficult to perform in the local river basins, for developing countries, in particular. Performing FRA is even more difficult in transboundary river basins due to unavailability of upstream data. Because of all these limitations, FRA has not yet been implemented in transboundary river basins though it is essential to acquire evidence-based policy-level information for sustainable development. Accordingly, this study was conducted to propose a research framework to develop an Integrated FRA (IFRA) methodology by utilizing present state-of-art observations and numerical modelling in a transboundary river basin called the Meghna, which shares areas of eastern-most India and northeastern rural Bangladesh.

Bangladesh is a deltaic country formed at the confluence of three transboundary rivers, the Ganges, Brahmaputra, and Meghna (GBM). The total GBM catchment area is about 1.75 million sq. km., almost 92 percent of which is located outside Bangladesh, i.e.,

in India, Nepal, Bhutan and China (Nishat and Rahman, 2009; FAO, 2012). Figure 1.1 shows the location of Bangladesh in the GBM basins.

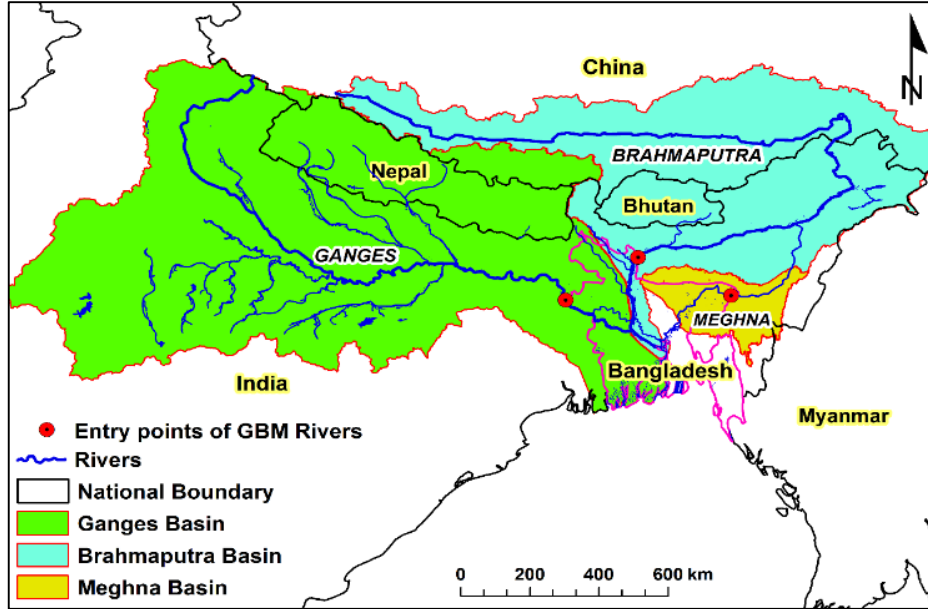


Figure 1.1: The Ganges-Brahmaputra-Meghna River basins in the Asian continent. The red circles indicate the locations of the entry points of those rivers inside Bangladesh.

Although Bangladesh occupies only 8 percent of the GBM basins area, 97 percent of the GBM discharges flow through the country into the Bay of Bengal (Brammer, 1990; Hofer and Messerli, 1997; Wolf et al., 1999; Nishat and Rahman, 2009). As a result, flooding, among the major natural hazards, is a frequent phenomenon in Bangladesh. Almost every year, one fifth to one third of the country gets flooded as its rivers overflow during both pre-monsoon (March through May) and monsoon (June through September) periods, causing widespread damage to the nation (Chowdhury, 2000; Mirza, 2003; Paul and Routray, 2010). The flood damage mainly include loss of life, income loss, and economic damage to agriculture, households, transport, and livestock, though it may vary depending on different types of floods (e.g., monsoon riverine floods, pre-monsoon flash floods, local rainwater floods, and storm-surge floods).

1.2 Problem statement

Although whole Bangladesh recurrently suffers from monsoon riverine floods, agriculture-dominated northeastern Bangladesh, located downstream of the Meghna river basin, predominantly encounters both pre-monsoon flash floods and monsoon riverine floods mainly due to the complex geographical structure of the Meghna basin, abundant precipitation originating from the world's rainiest places (which are within the Meghna catchment located at the foothills of Meghalaya mountain range) with an annual average rainfall of about 12 000 mm, and the prolonged duration of flooding due to flow obstructions (either from the combined flow of the Ganges and the Brahmaputra or from the back-water effect caused by tidal influence) (Shah, 2001; Mirza, 2003; Mirza et al., 2003; Chowdhury and Ward, 2004). Moreover, due to the effect of climate change, floods are expected to increase in the Meghna river basin, making northeastern Bangladesh more vulnerable in the future (Mirza et al., 2003; Kamal et al., 2013; Masood et al., 2015 & 2016).

In addition to the points discussed in the previous paragraph, many distinctive attributes make the Meghna river basin very important than the Ganges and Brahmaputra basins. The Ganges and Brahmaputra basins together consist of 59% of Bangladesh, whereas only 5% of their catchment area belongs to Bangladesh. The Meghna basin, on the other hand, occupies 24% of the Bangladesh territory, but 40% of its catchment area belongs to the country, indicating that the basin can effectively be managed by Bangladesh alone (FAO, 2014). The basin also plays a vital role in the national economy as its Bangladesh part is a home to agriculture and aquaculture activities. The area contributes more than 18% of rice production to the nation total, provides livelihood for

about twenty million people, and thus support the country and its economy (Quddus, 2009; Alam et al., 2010; Rabby et al., 2011; Kamruzzaman and Shaw, 2018).

Currently, Bangladesh has been adopting three structural and non-structural measures for reducing flood risk in the Meghna basin area. Structural measures include submergible embankments (SE) and river embankments (RE). SE are earthen embankments constructed circling around Haors (internal draining depressions in which the main crop of the area, Boro rice, is cultivated once a year). They protect Boro fields from floods up to certain level and then allows water to enter to submerge the Haors for fish culture. RE, on the other hand, are discontinuously constructed along river banks to reduce damage to structures, such as houses, properties, mosques, historical places, etc. An inundation map with a 3-day probabilistic forecasting, as a non-structural measure, is produced by assuming fixed river discharge and water level at the country's border, in order to warn the residents of the area to save their lives and assets. However, these existing measures didn't work in reducing agricultural or structural damage during the past floods in 2004, 2010, 2016, and 2017. Therefore, to acquire evidence-based policy-level information for reducing flood risk in the Meghna basin area, IFRA should be conducted under current as well as future climates.

However, as is the case for many other transboundary river basins (e.g., Niger, Mekong, Nile, La Plata, Volta, Euphrates, etc.), IFRA remains a challenge for Bangladesh to perform in the Meghna river basin due to the unavailability of transboundary data (such as rainfall and river flow data needed for hydrological modelling) together with the lack of various local observed data (such as distributed local rainfall data, integrated damage data).

1.3 Literature review and way forward

To the best of the author's knowledge, no established methodology was found in literature to overcome the limitations and data scarcity issues (local as well as basin-wide) in a transboundary river basin, and no developed methodology for IFRA considering the global changes (such as climate and land use) was reported in literature for practicing better flood risk management in a transboundary river basin. Some previous studies mainly focused on flood risk management in either a single flood event, river or country (Enserink, B. et al., 2003; Mudelsee et al., 2003; Dixit, 2003; Tol et al., 2003; Steen and Pellenberg, 2004). Other studies focused on water institutions and their management related to water resources, in particular (Biswas, 2004; Gopalakrishnan et al., 2005; Blomquist and Schlager, 2005). Very few studies were found in literature which focused on the issues of transboundary river basins and floods (Marsalek et al., 2006; Drieschova et al., 2008; Bakker, 2009a, b; Kibler et al., 2014). However, all these studies mainly pointed out the affairs and issues of institutional capacity between the riparian countries of transboundary basins, rather than focusing on how to overcome data scarcity issues in the absence of international treaty for effective flood risk management in transboundary river basins. This study, thus, as a first step, attempted to overcome the transboundary and local data limitation issues and developed a methodology to conduct IFRA in the Meghna river basin by utilizing multi-platform data, such as ground data, satellite data, field survey data, climate and land use change data, etc.

Conducting IFRA in a river basin mainly involves three components: assessment of flood hazard, flood vulnerability, and flood exposure (Messner et al., 2007; Crichton, 2008; Kwak et al., 2012; Foudi et al., 2015, Kefi et al., 2018). Therefore, in support of the framework, this research first focused on the flood hazard assessment for present and

future climate based on the locally available ground data, globally available satellite data, and Global Climate Models (GCMs) outputs. Secondly, flood vulnerability was assessed based on the results of a structured field survey conducted in the pilot sub-districts of northeastern Bangladesh. Thirdly, flood exposure maps were produced, prepared, and predicted using globally available observed and satellite information. By integrating the hazard, vulnerability, and exposure maps, multiple present and future risk maps were produced. Finally, policy implications were proposed for the decision makers to reduce and manage flood disaster risk for sustainable development of the study area.

Basin-wide reliable rainfall information is required to simulate the flood hazard parameters (depths and duration) by hydrological modelling (Zappa et al., 2008; Viviroli et al., 2009). However, hydrological modelling is difficult to perform in the Meghna basin because 60% of the basin area is located in India, which doesn't share any hydro-meteorological data with Bangladesh (Ahmad and Ahmed, 2003; Mirza, 2003; Bakker 2009b; Balthrop and Hossain, 2010). In addition, ground-based rainfall measurements inside Bangladesh are sparse in both time and space. To overcome such limitations, freely available global satellite rainfall products that include rainfall estimates with high spatial and temporal resolutions anywhere in the globe, are recognized as alternative. However, prior to their use, these data must be verified with ground observations, because such data are affected by systematic and random biases mainly produced by their indirect estimation from radiances and from rainfall-retrieval algorithms (Hay and Clark, 2003; Ines and Hansen, 2006; Christensen et al., 2008; Piani et al., 2010; Teutschbein and Seibert, 2012; Ehret et al., 2012; Chen et al., 2016). Using satellite rainfall products, a number of studies were conducted in Bangladesh, and they are mainly of two kinds. The first kind was to study the spatial and temporal variability of satellite rainfall estimates by comparing them

with the ground rainfall measurements (Islam and Uyeda, 2007; Islam et al., 2010; Prasanna et al., 2014). The second line of studies were conducted beyond data comparisons, investigating the potential use of satellite rainfall in rainfall-runoff modelling (Nishat and Rahman, 2009; Valeriano et al., 2010; Hopson and Webster, 2010; Siddique-E-Akbor et al., 2014). While half of these studies were limited to check the validity of satellite rainfall products, the remaining studies were focused on the hydrological modelling forced with these products without performing any appropriate bias correction. Even though they suggested the promising prospect of using satellite rainfall products in hydrological studies of data-scarce river basins, such as the Meghna, none of the previous researchers evaluated more than two products together with suitable bias correction to investigate their potential for use as a reference dataset in simulating the hydrological responses of that basin. To support this study's research framework, a reference data was developed for the Meghna basin using four satellite products, rainfall estimates of which were improved by using the local gauge rainfall and employing several bias correction and merging techniques. The potential of this dataset was successfully investigated by calibrating and validating a hydrological model to the simulated streamflows. Finally, a hazard map for a past flood (2017) was produced through the calibrated hydrological model forced with a basin wide rainfall data created using the above methodology. The very same model forced with GCMs outputs, was used to generate future hazard maps for this study.

One of the three important components of IFRA model is the estimation of flood vulnerability that is usually represented by flood damage curves (Okazumi et al., 2014a, b; Shrestha et al., 2016). Flood damage curves can be of two types as empirical and synthetic. Empirical damage curves are developed using actual damage data collected

after flood events, whereas the synthetic damage functions are developed based on damage data collected by questionnaire survey (Merz et al., 2010; Win et al., 2018). However, due to the lack of integrated and consistent flood damage data, the empirical type of flood damage functions are yet to be developed in Bangladesh. Therefore, synthetic approach of developing flood damage curves is the best alternative in Bangladesh. However, such synthetic damage curves to assess flood vulnerability in Bangladesh have yet not been established. Few researchers attempted to calculate potential flood risk in the urban areas of Bangladesh (mainly in Dhaka city) by assuming vulnerability as proportional to the population density or by calculating vulnerability as indices assuming several weight factors according to land use classes (Tingsanchali and Karim, 2005; Khan et al., 2012; Masood and Takeuchi, 2012). Two recent studies (Gain and Hoque, 2013; Gain et al., 2015), conducted for flood risk assessment in the eastern part of Dhaka, also estimated vulnerability either by assuming land use-based weight factors or by using stage-damage relationships or equations that were obtained from several other studies. However, many other researchers and government agencies worldwide attempted to establish synthetic flood damage curves for the areas with different content characteristics and established stage-damage relationships through survey results of various damage categories (e.g., agricultural or residential damage) (MOC, 1996b; MLIT, 2005; Zhai et al., 2005; Shrestha et al., 2016; Velasco et al., 2016; Hasanzadeh Nafari et al., 2017; Kefi et al., 2018; Win et al., 2018). Other researchers also used depth-damage functions obtained from other countries due to the fact of bearing similar regional content characteristics (Shrestha et al., 2016a & 2016b). For the northeastern part of Bangladesh, the fact is that there are no regional scale damage functions with identical content characteristics, and thus establishing of such functions

on a local scale is necessary. As a first attempt, this study thus developed reliable flood damage functions to assess vulnerability for agriculture and residential damage by conducting a structured questionnaire survey in the study area.

The third component of the IFRA model is the flood exposure assessment which usually requires land-use land-cover (LULC) maps to detect flood-exposed areas of agriculture and built ups. Gridded population data are also required to identify the number of affected people exposed to inundation. However, due to the lack of such observed land use and population data, globally available observed and satellite information were utilized to produce, prepare, and predict the flood exposure maps for this study.

1.4 Objectives of the Study

The overall objective of this study is to develop an IFRA framework in the Meghna river basin to provide evidence-based information to the residents as well as decision makers for practicing an effective flood risk management in the basin for sustainable development. To do so, the main objective is divided into five sub-categories: (1) Development of a reliable reference rainfall dataset to simulate hydrological responses of the basin; (2) Establishment of reliable flood damage functions for agriculture and household damage; (3) Assessment and verification of potential flood damage to agriculture and households for past climate, considering 2017 flash flood; (4) Assessment of agricultural flood risk under the changes in global climate and land use; and (5) Investigation of flood risk mitigation measures under climate change through structural and non-structural means.

1.5 Scope of the Study

This study mainly focuses on proposing a research framework to develop an IFRA methodology in the Meghna river basin by using present state-of-art observations and

numerical modelling. The methodology covers the following scopes despite various uncertainty and limitations.

(1) Local and transboundary rainfall data scarcity issues are addressed, and as a first attempt, a reliable distributed reference rainfall dataset is created for simulating hydrological responses of the basin, such as hazard mapping. To do so, globally available satellite rainfall data and locally available ground observations are used.

(2) Limitations of consistent flood damage data bank in Bangladesh is addressed, and as a first attempt, reliable flood damage functions for agriculture and households are established in order to estimate their flood vulnerability. To do so, a structured questionnaire survey is undertaken to collect flood damage data for the aforementioned damage classes.

(3) An Integrated Flood Risk Assessment (IFRA) model is developed, performed, and validated for agriculture and household damages considering a recent past flood of 2017 by combining flood hazard, vulnerability, and exposure maps of the damage classes. Hazard maps in terms of flood inundation depths, duration and extent are produced using a hydrological model forced with the created rainfall data. Estimation of vulnerability are performed using the established damage functions. Exposure for agriculture is assessed by globally available observed land cover maps, and that for households is prepared using population distribution and average household size.

(4) Agricultural flood risk assessment for future climate is performed under global climate and land use change by using the validated IFRA model. In doing so, Global Climate Models (GCMs) outputs are used for hazard estimation, future land-cover maps are predicted for exposure assessment, and established damage functions at present value are used for vulnerability estimation.

(5) Finally, flood risk mitigation and countermeasures under climate change through structural and non-structural means are proposed based on results and findings for improving existing conditions by providing evidence-based information for building back better and achieving sustainable development goals.

1.6 Structure of the Dissertation

The dissertation is organized as follows. Chapter 2 introduces the study area and methodology of the study. Chapter 3 presents the methodology and results of developing reliable reference rainfall. The methodology and results of establishing flood damage functions are described in Chapter 4. Chapter 5 describes flood damage assessment methodology and results of past flood damage assessment with validation. Flood risk assessment under global change of climate and land use is outlined in Chapter 6. Summary and conclusions are drawn in Chapter 7, and finally policy implications are discussed in Chapter 8.

Chapter 2: Material and methods

2.1 Introduction

This chapter of the dissertation describes the study area and methodology used to address the study objectives. First, the area chosen for this study is described in detail with necessary figures and references. Second, a flowchart is drawn to graphically visualize the study methodology, and finally the important components of the methodology are shortly described chronologically.

2.2 Study area

The area selected for this comprehensive study is the northeastern region of Bangladesh, which is located downstream of the Meghna river basin. The Meghna basin, which is also called the Upper Meghna basin, is a transboundary river basin and shares the area between Bangladesh and India (Figure 2.1a). The river originates in the hills of Meghalaya, Assam, and Manipur States of India and flows down to the agriculturally dominated northeastern Bangladesh (Figure 2.1a). About 40% of the basin area falls within Bangladesh, and the remaining 60% lies in Indian Territory. Specifically, the basin encompasses the mountainous Meghalaya, Assam, Manipur, Tripura, and Mizoram regions of India and the predominantly agricultural land of Bangladesh [22.75-26.00°N, 89.50-94.50°E]. The topography of the basin changes rapidly in its northern and eastern areas, and the altitude varies from 1 to 2888 m with a mean of 362 m a.s.l. (Lehner et al., 2008) (Figure 2.1c). However, the basin topography in Bangladesh is relatively flat, and thus highly vulnerable to flooding (Figure 2.1b).

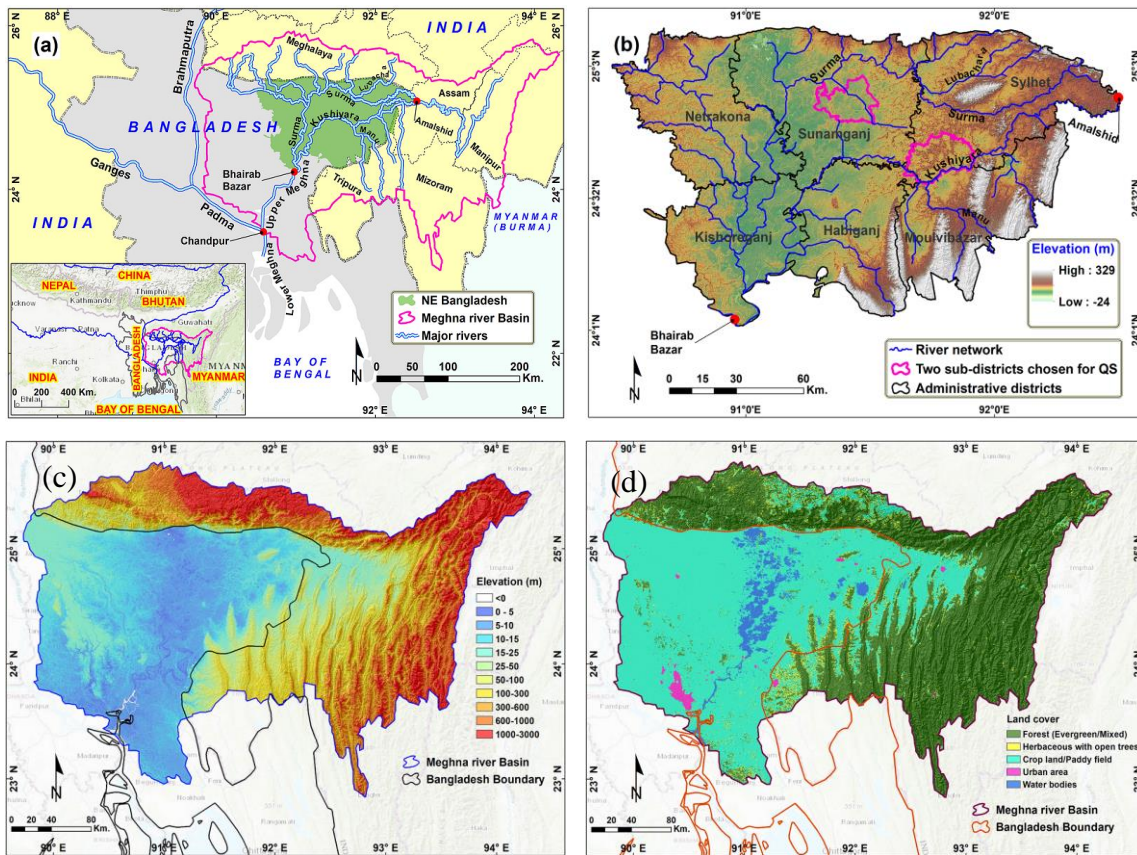


Figure 2.1: Topographic features of the study area. (a) Meghna basin in the Asian continent (inset), showing major rivers and administrative details (green shaded area is northeastern Bangladesh); (b) Topography of northeastern Bangladesh; two pink bounded area are sub-districts used for conducting questionnaire survey to collect damage data; (c) Topography of the Meghna basin; and (d) land cover of the Meghna basin.

The Barak River, one of the prime sources of the Meghna River, bifurcates into the Surma and Kushiya Rivers at Amalshid, which is in Sylhet district near the Bangladesh-India border (Figure 2.1a). Discharges from the steep and highly flashy rivers (e.g., the Lubachara, Jadukata, and Chela River) originating in the Khasi and Jaintia Hills—which are the wettest places in the world with an annual average rainfall of about 12 000 mm (Shah, 2001; Parry, 2013)—contribute to the Surma River through its right bank. On the other hand, the Kushiya River receives water from the rivers that originate in the Tripura Hills (e.g., the Manu and Khowai River). The channels of these two main

rivers, along with those of many other rivers in the Bangladesh part of the basin, run from the northeast to the southwest through the Bhairab Bazar stream gauge station (outlet of the basin) as the Upper Meghna to join the Padma at Chandpur, and finally flows into the Bay of Bengal as the Lower Meghna (Figure 2.1a). The drainage area of the Upper Meghna is about 76 000 km²; about 62% of this area is comprised of forested, mountainous (or hilly) terrain, whereas 29% is comprised of irrigated cropland and pastures (Tateishi et al., 2014) (Figure 2.1d).

The Bangladesh part of the Meghna basin (northeastern Bangladesh), consisting of six major administrative districts, mainly lies in the Surma-Kushiyara river system. Between the Surma and Kushiyara rivers are many low-land regions, internal draining depressions (i.e., locally called *Haors*), meandering flood channels, and abandoned river courses, which get flooded in every pre-monsoon (March-May) and monsoon (June-September) season. The area is famous for agriculture and aquaculture activities. The main agricultural product in this region is the Boro rice. Since a number of *Haors* (about 423 nos. – they are surrounded by submergible embankment – earthen embankment that protect the Boro rice from flood up to a certain level and then allows water to enter and submerge the *Haors* for fish culture) are located in this region and most of them remain inundated for about 4–7 months in a year, people of this area thus can grow rice only once a year. The area contributes more than 20% of rice production to the nation total, provides livelihood for about twenty million people, and thus support the country and its economy (Quddus, 2009; Alam et al., 2010; Rabby et al., 2011; Kamruzzaman and Shaw, 2018). However, it is unfortunate that the pre-monsoon flash floods, which hit this area almost every year, damage the Boro rice paddy just before its harvesting, causing numerous socio-economic damage to the nation.

In 2017, a massive flash flood devastated this region due to heavy rainfall as well as surge of water from upstream of the Meghna basin and affecting about one million people and one third of the households in this area. Both the Surma and Kushiya rivers exceeded their danger levels at various points and inundating vast areas of croplands. The Department of Disaster Management in Bangladesh reported that 219,840 hectares of crops, mainly the Boro rice at the nearly-ready-for-harvesting stage, were damaged. Moreover, approximately 30,000 households lost their houses fully or partially.

To simulate the hydrological responses of the Meghna river basin for addressing the study objectives, the basin is delineated based on the Hydrological data and maps based on Shuttle Elevation Derivatives at multiple Scales (HydroSHEDS) (Lehner et al., 2008), considering the outlet at the Bhairab Bazar stream gauge station (Figure 2.1a). This station is selected for two main reasons; the total flow of the basin contributes most at this station, and the streamflow for the entire basin is also measured there. The climatic year in the basin can be divided into wet and dry seasons. Given rainfall intensity and monthly accumulated rainfall, this study defines March through October as the wet season and November through February as the dry season.

2.3 Methodology

To address the study objectives, a research framework is first designed. Figure 2.2 shows the flowchart of the research method used in this study. As depicted in the figure, the methodology first addresses the assessment of flood hazard, vulnerability and exposure followed by flood damage and risk assessment for agriculture and residential damage. Each component of the methodology was shortly described in the following subsections.

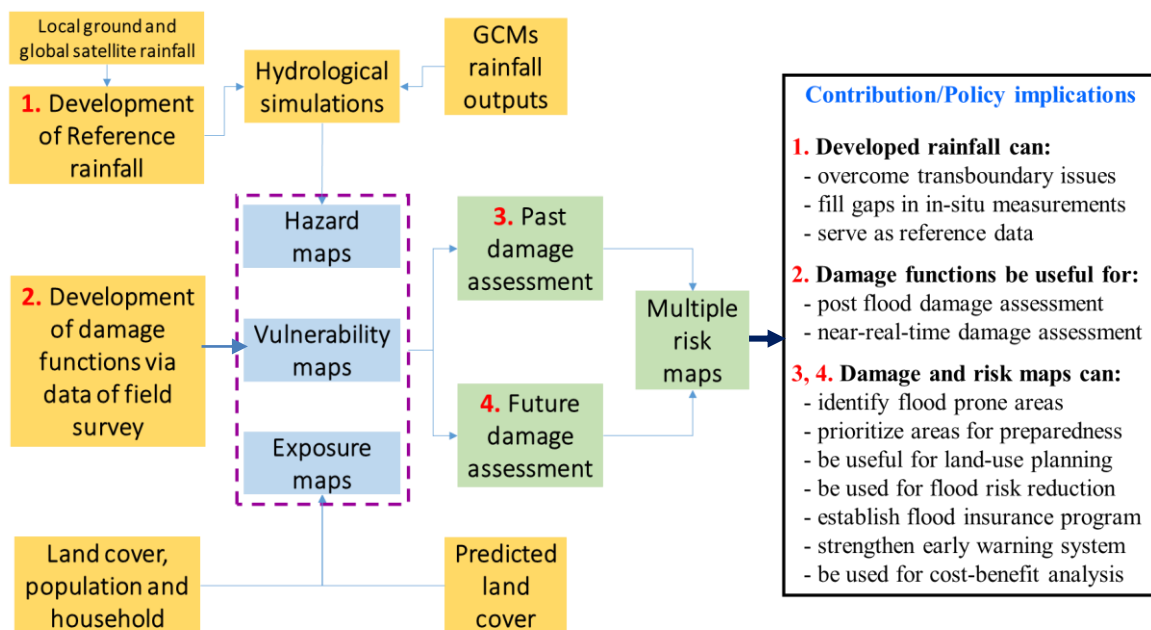


Figure 2.2: Flow chart of the research methodology used in this study for integrated flood risk assessment for sustainable development in a transboundary river basin.

2.3.1 Development of a reference rainfall data to generate hazard maps

Flood inundation depth, duration, and extent for a given flood are usually considered as flood hazards. A 2D distributed hydrological model called Rainfall-Runoff-Inundation (RRI) (Sayama et al., 2012 & 2015a, b) is used in this study to generate the hazard parameters. However, the input rainfall to drive the RRI model for the Meghna basin is not available since 60% of the basin area is located outside Bangladesh in India and any hydro-meteorological data are not being shared between these two countries. Therefore, a reference data was first developed for the basin using freely-available global gauge-adjusted satellite rainfall products which were further corrected and improved by locally available ground rainfall. This developed dataset was then used to calibrate and validate the RRI model, and accordingly the calibrated model was used to generate hazard maps for both present and future climate. The details of developing and validating the reference rainfall dataset is described in the next chapter.

2.3.2 Establishment of damage functions to assess vulnerability

Flood vulnerability is defined by depth-damage relationships, frequently known as damage functions. Flood damage functions can be of empirical (developed from actual damage data) or synthetic (developed from the data of questionnaire surveys) types. However, due to lack of integrated damage data, this study conducted a structured questionnaire survey to collect various damage data, and accordingly established damage functions for the Boro rice (main crop of the study area) and households to estimate flood vulnerability for flood damage and risk assessment in the study area. The details of the conducted questionnaire survey and the methodology of establishing damage functions are described in Chapter 4.

2.3.3 Flood damage assessment for a past flood

Potential flood damage to the Boro rice, house building, and household properties were estimated and validated for the 2017 flood by combining the hazard and vulnerability maps with the exposure maps. Exposure maps for any damage class (e.g., agriculture, built up, etc.) are usually derived using land-use land-cover maps. However, due to the lack of such observed maps, globally available observed and satellite information were utilized to produce and prepare exposure maps in this study. The details of this component of the framework is described in Chapter 5.

2.3.4 Flood risk assessment under global changes

Flood risk due to the changes in climate and land use was also assessed in support of this study's framework. The calibrated and validated RRI model was forced with the average of several GCM rainfall outputs to simulate future hazard parameters. Using a land change modeler, future land cover for the Boro rice was predicted based on the past land cover maps. Finally, flood risk to the Boro rice in changing climate and also

considering land use changes was estimated by integrating future hazard and exposure maps with present vulnerability maps. The details of assessing flood risk due to the changes in climate and land use are shown and described in Chapter 6.

Chapter 3: Development of Reference Rainfall¹

3.1 Introduction

Bangladesh part of the Meghna basin (northeastern Bangladesh) experiences frequent floods that cause severe human and economic losses. Being the downstream nation in the basin, Bangladesh receives no hydro-meteorological and water use data from India for effective flood risk management. To address such issues, satellite rainfall products are recognized as an alternative. However, they are affected by biases and thus must be calibrated and verified using ground observations. This chapter of the dissertation introduces a methodology to create an improved rainfall dataset in the Meghna river basin using freely available global satellite rainfall products. This improved dataset can overcome the limitations of poor data availability in the basin and can serve as a reference rainfall dataset for wide range of applications (e.g., flood modelling and forecasting, flood damage and risk assessment, irrigation planning, and climate change adaptation planning). In addition, the proposed methodology of creating a reference rainfall dataset based on satellite rainfall estimates can also be applicable to other poorly gauged and inaccessible transboundary river basins, thus providing reliable rainfall information and effective flood risk and water resource management for sustainable development.

3.2 Study area

The area studied for the component of this chapter is the Meghna river basin, which is described in detail under Chapter 2.

¹A similar version/parts of the contents of this chapter is published as an Article in Remote Sensing Journal; Remote Sens. 2018, Vol. 10, Issue 6, Article 828, <https://doi.org/10.3390/rs10060828>

3.3 Literature review

In recent times, many satellite-based rainfall estimates with high spatial and temporal resolutions have been generated at the global scale and have become available at no cost and in near-real time (NRT). These globally available NRT satellite-based rainfall products include Global Satellite Mapping of Precipitation (GSMaP) from the Japan Aerospace Exploration Agency (JAXA), Tropical Rainfall Measuring Mission (TRMM) Multi-satellite Precipitation Analysis (TMPA) from the National Aeronautics and Space Administration (NASA), Integrated Multi-satellitE Retrievals for GPM (IMERG) from NASA, the Climate Prediction Centre (CPC) MORPHing method (CMORPH) from the National Oceanic and Atmospheric Administration (NOAA), and Precipitation Estimation from Remotely Sensed Information using Artificial Neural Networks (PERSIANN) from the University of California, Irvine. These sets of satellite-based information are highly valuable and have immense potential in flood risk and water resource management, particularly for inaccessible transboundary and poorly gauged river basins. Given the absence of upstream rainfall data from India's portion of the Meghna basin, satellite data (that includes rainfall estimates for both inside and outside Bangladesh) can overcome the limitations of poor data availability and can also be used as gridded reference data to generate basin-wide hydrological responses or to practice effective and timely management of water resources and water-related disasters.

However, satellite data come with the caveat that they must be verified with ground observations prior to their application since such data are subject to systematic and random errors because they rely on indirect estimation from radiances; because of issues with their sampling frequency and rainfall-retrieval algorithms; and because they depend on elevation, latitude, rainfall type, and climate (Hay and Clark, 2003; Ines and

Hansen, 2006; Christensen et al., 2008; Piani et al., 2010; Teutschbein and Seibert, 2012; Ehret et al., 2012; Chen et al., 2016). Therefore, many NRT satellite products have recently been supplemented with gauge adjustments based on global gauge observations, both for research purposes and for use in a wide range of applications. They are available at no cost, usually 10-20 days after the end of each month. The most important of these products are the Climate Hazards Group InfraRed Precipitation with Station data (CHIRPS), adjusted GSMaP (GSMaP_Gauge); TRMM 3B42 (3 hourly or daily) and 3B43 (monthly) Version 5 (V5), Version 6 (V6), and Version 7 (V7); corrected CMORPH Version 1 (CMORPH_V1.0_CRT) and blended CMORPH Version 1 (CMORPH_V1.0_BLD); adjusted PERSIANN (PERSIANN-CDR); and Multi-Source Weighted-Ensemble Precipitation (MSWEP). Some of these gauge-adjusted products include in situ measurements for the Meghna basin as well, both inside and outside Bangladesh, so they may have greater potential than the NRT products for use as a reference rainfall dataset for long-term hydrological applications in the basin. However, before these products can be used, further bias correction may be necessary, as the global validation stations (provided by NASA, NOAA, JAXA, CPC, and many other global databases) are limited and usually far away and thus may not sufficiently represent the actual rainfall characteristics of the basin. Another reason could be that bias originates from various correction algorithms and methods. For instance, (1) the CHIRPS algorithm uses satellite imagery with the available time series of global station data for a month, producing daily CHIRPS data in the third week of the following month; (2) the adjusted GSMaP product combines standard and re-analysis based satellite estimates with 0.5°-grid CPC global gauge analysis (CPC grid box contains the average rainfall of the available gauges located within that box); and (3) the corrected daily TRMM 3B42 is a disaggregated product from

corrected monthly TRMM 3B43 that is produced by calibrating monthly TRMM 3B42RT estimates (NRT version) with the monthly Global Precipitation Climatological Centre's (GPCC) and CPC's rain-gauge analysis. Missing rainfall records and the limited number of such records in the global database may also affect the accuracy of these gauge-adjusted satellite products demanding further bias correction.

Several studies have been conducted on the Bangladesh portion of the Ganges-Brahmaputra-Meghna (GBM) basins, using both NRT and gauge-adjusted, satellite-based rainfall products. In an effort to understand the climatic characteristics of rainfall in Bangladesh, Islam and Uyeda (2007) depicted that TRMM 3B42 (V6), without further correction, overestimated the rainfall in the pre-monsoon period and underestimated it in the monsoon period; they also found that the biases were mainly seasonal- and location-dependent. Blended with concurrent ground observations wherever available, Nishat and Rahman (2009) used TRMM 3B42 (V6) satellite data to model the GBM basins for streamflow prediction. In their study, the monthly flow volume simulated with a lumped kind (sub-basin scale) of model differed from the actual streamflows in all three basins, which suggested that their GBM model forced with satellite data has limited potential for water resource management. Valeriano et al. (2010) attempted to generate discharge in the Meghna basin using TRMM 3B42 (V6) estimates. They further improved the satellite data using two approaches: by applying a simple ratio-correction method at the available local gauge stations and then transferring the correction factors to other grids (according to Thiessen polygon areas of influence) inside Bangladesh, and by applying the nearest-neighbour method to the area outside Bangladesh. Rather than a daily time-series comparison, their study involved a comparison of the total discharge for the rainy season throughout 2001-2004 with the observed discharge from the same period. To learn the

causes of the 2007 Bangladesh flood, Islam et al. (2010) compared the mean monthly rainfall, as calculated from 3-hourly TRMM-3B42 (V6) estimates (without further corrections), with that of the historical rainfall for the flood period. They found that a larger volume of rainfall was accumulated in July 2007 than in the same month in either of the previous two years, causing flooding in Bangladesh. Over the domain of the GBM basins, Prasanna et al. (2014) developed a merged rainfall dataset (0.5° resolution) for 1998-2007 using TRMM-3B42 (V6) estimates and gauge rainfall data collected from India and Bangladesh; they consequently predicted the possibility of using this dataset for flood forecasting. However, no hydrological models were either calibrated or validated in their study so as to check the streamflow generation; such a step is desirable for flood forecasting. Siddique-E-Akbor et al. (2014) ran a distributed hydrological model forced with datasets from two NRT satellite-precipitation products (TRMM-3B42RT and CMORPH) to investigate the feasibility of water management in the GBM basins. However, they mainly focused on hydrological simulation of the Brahmaputra and Ganges basins and did not provide any bias correction of the NRT satellite products.

None of the researchers in those previous studies—even though they hinted at the promise of using satellite-based rainfall products in hydrological studies of data-scarce river basins such as the Meghna basin—evaluated more than two products together with suitable bias correction to investigate their potential for use as reference dataset in simulating the hydrological responses of that basin for water resource management. Therefore, this chapter is focused on developing a reference rainfall dataset for the Meghna basin using satellite products. It first evaluates the performance of four Gauge-adjusted Satellite Rainfall Products (GSRPs): CHIRPS, GSMaP_Gauge (termed GSMaP-G), TRMM-3B42 Version 7 (termed TMPA-G), and MSWEP during 2009-2016 by

identifying their biases relative to the ground rainfall measurements for the area inside Bangladesh. Then, it applies several bias-correction and merging techniques to further remove biases from the GSRPs. The bias-correction and merging techniques are conducted at the available gauge stations inside Bangladesh to calculate correction factors and merging weights, respectively. These station-based correction factors and merging weights are spatially distributed using the inverse distance weighting (IDW) interpolation method (Shepard, 1968; Dirks et al., 1998; Heistermann and Kneis, 2011) to produce grid-based correction-factor and merging-weight maps that cover the entire Meghna basin. The original GSRPs are then multiplied or added to these factor maps (multiplication or addition is dependent on the bias-correction and merging techniques), resulting in an improved dataset. This chapter further investigates the improved dataset's potential for use as a reference rainfall data for streamflow simulations of the Meghna basin.

The component presented in this chapter therefore has three key objectives: (1) to evaluate the performance of the GSRPs relative to the locally available ground rainfall measurements; (2) to further improve the GSRPs' rainfall estimates by applying several bias-correction and merging techniques, thus creating an improved rainfall dataset; and (3) to investigate the applicability of the improved dataset as a reference rainfall data in simulating streamflows of the basin.

3.4 Data

3.4.1 Topographic Data

Topographic data are required to set up hydrological models. These data include digital elevation models, river networks, drainage basins, flow directions, and flow accumulation, and they are collected from the U.S. Geological Survey's HydroSHEDS.

The HydroSHEDS (Lehner et al., 2008) data are produced using NASA's Shuttle Radar Topography Mission (Farr et al., 2007) and are in a consistent format for regional- and global-scale applications. These data are freely available at 3-, 15-, and 30-second resolutions.

3.4.2 Hydro-meteorological Data

3.4.2.1 Rainfall

As discussed, Bangladesh does not receive any observed rainfall data for beyond its borders, and the available data are only from inside the country. Out of all the in situ stations maintained by the Bangladesh Water Development Board (BWDB), 20 are sparsely located within the Bangladesh portion of the Meghna basin. Figure 3.1 shows the locations of these stations (red bubbles), and Table 3.1 outlines the statistics for these the 20 rain-gauge stations for the study period (2009-2016).

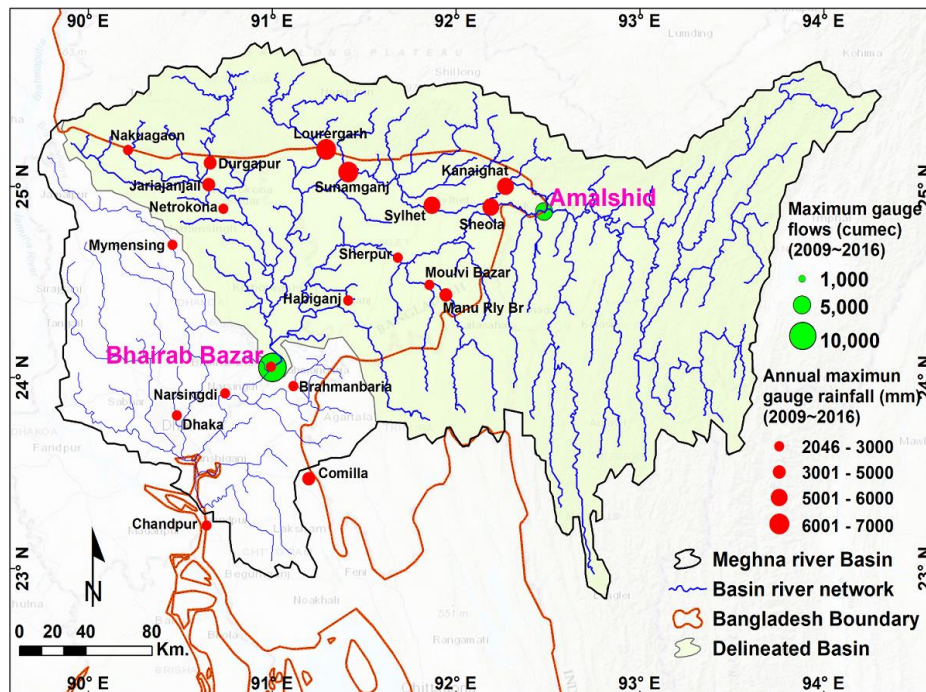


Figure 3.1: Meghna basin with detailed river network, including 20 meteorological stations (red bubbles) and two hydrological stations (green bubbles) inside Bangladesh;

Table 3.1: Salient features of the 20 rain-gauge stations located in the Bangladesh portion of the Meghna basin for the study period of 2009–2016.

Sl.	Rain-Gauge Station Name	North Latitude (°)	East Longitude (°)	Elevation (m a.s.l.) (90 m SRTM)	Available Daily Records	Missing Daily Data (%)	Mean Annual Rainfall (mm)
1	Lourergarh	25.1941	91.2941	16	2892	1.03	5130
2	Sunamganj	25.0760	91.4147	14	2875	1.61	5015
3	Sylhet	24.8764	91.8571	20	2922	0.00	4156
4	Kanaighat	25.0011	92.2708	23	2844	2.67	3926
5	Sheola	24.8922	92.1910	20	2447	16.26	3536
6	Durgapur	25.1227	90.6645	20	2152	26.35	2926
7	Netrokona	24.8832	90.7356	14	2842	2.74	2333
8	Habiganj	24.4036	91.4151	11	2692	7.87	2320
9	Comilla	23.4705	91.2000	17	2922	0.00	2312
10	Nakuagaon	25.1900	90.2180	31	2228	23.75	2211
11	Manu RlyBr	24.4324	91.9462	19	1762	39.70	2137
12	Sherpur-Sylhet	24.6277	91.6848	18	1645	43.70	2134
13	Jariajanjail	25.0092	90.6557	9	2669	8.66	2070
14	Moulvi Bazar	24.4849	91.8570	19	2712	7.19	1882
15	Narsingdi	23.9159	90.7456	9	2890	1.10	1815
16	Mymensingh	24.6940	90.4594	10	2410	17.52	1807
17	Chandpur	23.2254	90.6440	10	2780	4.86	1802
18	Brahmanbaria	23.9555	91.1177	17	2922	0.00	1752
19	Dhaka	23.7840	90.5278	10	2725	6.74	1609
20	Bhairab Bazar	24.0559	90.9950	8	2922	0.00	1390

The percentages of the daily rainfall records that are missing in the study period vary from 1.03% to 43.70% for the rain-gauge stations (Table 3.1). Because some of the daily data are missing, the rain-gauge network is sparse and located only inside Bangladesh, and since the gauge records are merely point measurements, it is desirable to have a dense network of rainfall estimates that covers the entire Meghna basin so as to simulate its hydrological responses, as recommended also by Romilly and Gebremichael (2011). Given this, this study investigates rainfall estimates of four GSRPs (CHIRPS, GSMaP-G, TMPA-G, and MSWEP) that contain global gauge information for the basin, both inside and outside Bangladesh. The study includes the products that are freely available in near-present time (usually 10–20 days after the end of each month) and that have as high a spatial resolution as possible. The details on each GSRP are as follows.

CHIRPS has been created in collaboration with scientists at the U.S. Geological Survey Earth Resources Observation and Science Centre, and it incorporates 0.05°- and 0.25°-resolution satellite-measured rainfall time series blended with in situ station data. The blending algorithm uses satellite imagery and station data to produce a preliminary information product with a latency of about two days and a final product with an average latency of about three weeks. The station processing stream used to produce CHIRPS incorporates data from many public data streams and from several private archives, such as the Global Historical Climatology Network's daily (GHCN-D) (Menne et al., 2012) and monthly archives, the Global Summary of the Day database, and the World Meteorological Organization's Global Telecommunication System. Additional observations come from various national meteorological agencies. The data for 1981 through the near present (after a 1–3 week delay) are freely available with a daily temporal resolution. For more information on CHIRPS, refer to Funk et al. (2014, 2015).

GSMaP, which is produced by JAXA, integrates geostationary infrared data from three satellites (MTSAT, METEOSAT-7/-8, and GOES-11/12) along with passive microwave data from sensors mounted on various low-Earth-orbiting satellites with an infrared-microwave combined algorithm (Kubota et al., 2007; Okamoto et al., 2008; Aonashi et al., 2009), a backward-and-forward morphing technique from infrared images (Joyce et al., 2004), and a Kalman filter (Ushio et al., 2009). The rain types from the TRMM precipitation radar, the melting-layer model, and the scattering algorithm are used in the radiative transfer model calculation to improve the rain/no-rain classification methods (Seto et al., 2005) over land (Takahashi and Awaka, 2005). The gauge-adjusted GSMaP version, i.e., GSMaP_Gauge (termed GSMaP-G) is used for this study. GSMaP-G is adjusted from the GSMaP_MVK (standard) and GSMaP_RNL (reanalysis) estimates

and includes global gauge analysis (CPC Unified Gauge-Based Analysis of Global Daily Precipitation, 0.5°-grid box), as supplied by NOAA. GSMaP_MVK integrates passive microwave radiometer data with infrared radiometer data. It is produced with a Kalman filter model, which refines the precipitation rate propagated based on the atmospheric moving vector derived from two successive infrared images. GSMaP_RNL, on the other hand, is a reanalysis product based on Japanese 55-year reanalysis data (six-hourly, model grid (TL319L60)) as ancillary data to produce a continuous and homogeneous dataset for the past. The adjustment in GSMaP-G is applied only to the estimation over land and the rain rate over the ocean. The rain rate of GSMaP-G is calculated based on optimal theory, which adjusts the GSMaP-G hourly rain rate so that the sum of the 24-h GSMaP-G rain rate remains roughly the same as the gauge measurement for each period. The GSMaP-G data are freely available on the daily temporal scale and with 0.1° spatial resolution. For more information on GSMaP-G, refer to Ushio et al. (2009, 2014).

TRMM-3B42 Version 7 (termed TMPA-G), which has been released by NASA's Goddard Space Flight Center, is a merged product of satellite-based rainfall estimates and gauge data (Huffman et al., 2007). The algorithm first combines microwave precipitation estimates from multiple low-Earth-orbiting satellites and then calibrates them to both the TRMM Microwave Imager precipitation (TRMM-2A12) and the TRMM Combined Instrument precipitation (TRMM-2B31). These are merged to produce a microwave-only best estimate for every 3 h. The infrared precipitation estimates from multiple geosynchronous satellites are then calibrated to the microwave estimates and used to fill in the regional gaps in the merged microwave field, thus producing a combined satellite-based rainfall estimate for every 3 h (Kummerow et al., 2000; Huffman et al., 2007). These combined satellite estimates are then summed at the monthly scale and recalibrated

with monthly rain-gauge analysis from the GPCC (Rudolf, 1993) and from the CPC’s Climate Assessment and Monitoring System monthly rain-gauge analysis (Xie and Arkin, 1996), thus providing the final satellite-and-gauge merged precipitation estimates. These monthly estimates are then disaggregated to three-hourly and daily estimates to provide TMPA-G data at 0.25° spatial-resolution. The product is updated 10–15 days after the end of each month. For more information on TMPA-G, refer to Huffman et al. (2007).

MSWEP takes advantage of the complementary strengths of gauge-, satellite-, and reanalysis-based data to provide reliable precipitation estimates for the entire globe (Beck et al., 2017a). MSWEP has been validated at a global scale through observations from ~70,000 gauges and through hydrological modelling for ~9000 catchments (Beck et al., 2017b). Daily gauge observations have been used to determine the merging weights and wet-day biases for the individual precipitation dataset and to improve the rainfall estimates near the gauge stations. The observation database comprises worldwide in situ measurements compiled from the GHCN-D database (Menne et al., 2012), the Global Summary of the Day database, and many other public, private data library. MSWEP data are freely available from 1979–2016 with a three-hourly and daily temporal, and 0.1° and 0.5° spatial-resolution. For more information on MSWEP, refer to Beck et al. (2017a, b). A brief summary of the GSRPs is presented in Table 3.2.

Table 3.2: Salient features of the GSRPs used in the study for the period of 2009–2016.

GSRP Name	Resolution		Coverage		Latency	Main Reference	Data Links
	Spatial	Temporal	Spatial	Temporal			
CHIRPS	0.25°	daily	Global 50°N–S	1981– present	1–3 weeks	Funk et al. (2015)	ftp://ftp.chg.ucsb.edu/pub/org/chg/
GSMaP-G	0.1°	daily	Global 60°N–S	2000– present	2–3 days	Ushio et al. (2014)	http://sharaku.eorc.jaxa.jp/GSMaP/
TMPA-G	0.25°	daily	Global 50°N–S	1998– present	10–15 days	Huffman et al. (2007)	ftp://trmmopen.nascom.nasa.gov/pub/
MSWEP	0.1°	daily	Global 60°N–S	1979– 2016	-	Beck et al. (2017a)	http://www.gloh2o.org/

Figure 3.2 shows some of the global gauge stations and CPC grid centres that, along with other observed datasets, were used to produce GSRP rainfall estimates in and around the Meghna basin. The stations and grid centres are shown for the dates of 25 July 2010, and 17 May 2016. The network of stations is collected from the GHCN-D database provided by NOAA (<ftp://ftp.ncdc.noaa.gov/>), and the grid centres are derived from the CPC's unified 0.5° -grid boxes, which are also provided by NOAA (http://ftp.cpc.ncep.noaa.gov/precip/CPC_UNI_PRCIP/). Each CPC box ($0.5^\circ \times 0.5^\circ$) consists of global gauges located within that box; the number differs for each box (and the minimum number can be 0, as shown in the figure). The average rainfall of the gauges inside a CPC box is considered as the rainfall amount for that box. Based on the figure, the number of GHCN-D stations and the number of gauges inside a CPC box vary by the day according to the gauges' availability.

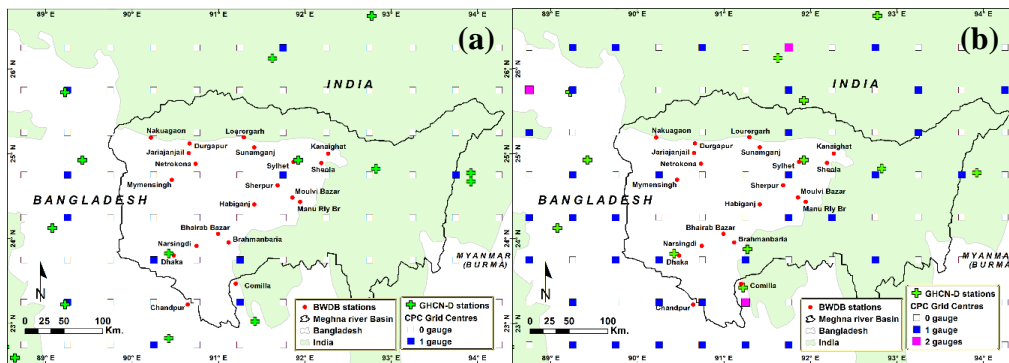


Figure 3.2: Meghna basin showing GHCN-D global gauges and CPC unified 0.5° -grid centres that—along with other observed datasets—were used to produce the GSRP rainfall estimates on (a) 25 July 2010, and (b) 17 May 2016. The local rainfall stations are also shown (red dots).

3.4.2.2 Water Level and Streamflow

Bangladesh Water Development Board provides observed water level and streamflow data for all hydrological stations located in Bangladesh. While the water-level data are regularly measured five times per day (at 0600, 0900, 1200, 1500, and 1800), the frequency-of-discharge data (measured using the velocity-area method) varies from daily

to fortnightly or even monthly. Therefore, in the Meghna basin, rating equations are prepared using observed streamflows and respective water levels so as to generate daily observed streamflows for the entire study period (2009–2016) at two critical hydrological stations: Bhairab Bazar (located at the outlet of the Meghna basin) and Amalshid (located near the Bangladesh-India border at the Kushiya River) (Figure 3.1, green bubbles).

3.5 Methods

Figure 3.3 demonstrates the flowchart of the method used for evaluating the GSRPs, the creation of an improved rainfall dataset, and the investigation of that dataset's applicability when simulating hydrological responses of the Meghna basin. First, the performance of the GSRPs is evaluated by comparing them to ground rainfall observations from the local gauges to identify the GSRPs' further biases. Then, a number of bias-correction techniques are applied to re-correct the GSRP estimates. In addition to bias correction, three merging techniques are also investigated to improve the GSRPs' performance. In addition, a combination of merging and bias correction is also explored. Among the bias-corrected and merged products, the product that provides the best results is selected as a reference rainfall dataset. Finally, the applicability of such dataset is investigated to the simulated streamflows using a distributed hydrological model.

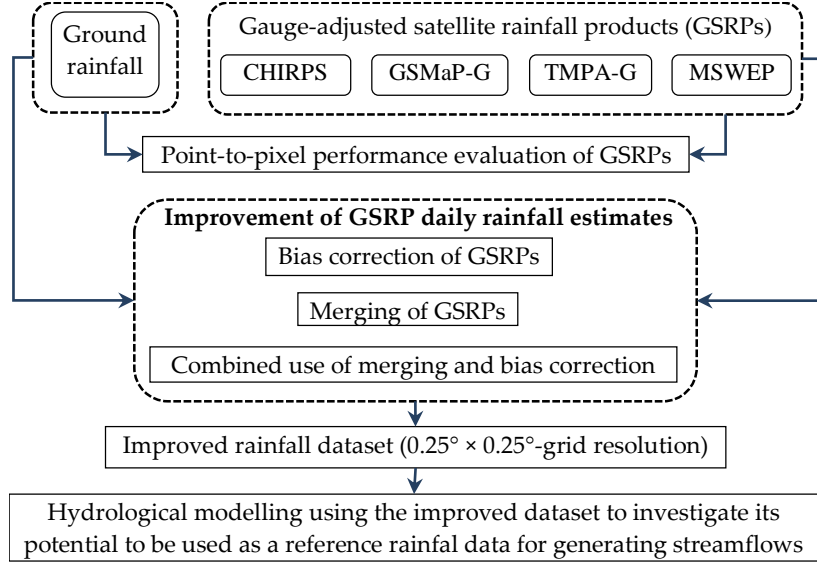


Figure 3.3: Flow chart of the method used for comparing four GSRPs, creating a reference rainfall dataset, and investigating that dataset's applicability when simulating streamflows in the Meghna basin.

3.5.1 Performance Evaluation of GSRPs

The daily GSRP rainfall estimates for the wet seasons (March–October) across the entire study period (2009–2016) are validated by comparing with daily ground rainfall records from the 20 rain-gauge stations inside Bangladesh on a point-to-pixel basis. The daily pixel data closest to each gauge location are extracted from the GSRPs before performing the comparison. The statistical metrics used for this comparison include normalised-mean-squared error (*NMSE*), relative bias (*RB*), root-mean-squared error (*RMSE*), and correlation coefficient (*CC*). These metrics are defined as follows:

$$NMSE = \frac{1}{N} \sum \frac{(P_s - P_g)^2}{\frac{1}{N} \sum P_s \frac{1}{N} \sum P_g} \quad 3.1$$

$$RB = \frac{\sum(P_s - P_g)}{\sum P_g} \times 100 \quad 3.2$$

$$RMSE = \sqrt{\frac{\sum(P_s - P_g)^2}{N}} \quad 3.3$$

$$CC = \frac{Cov(P_s P_g)}{\sigma_{P_s} \sigma_{P_g}} \quad 3.4$$

where P_s is the rainfall estimate from GSRPs (CHIRPS/GSMaP-G/TMPA-G/MSWEP), P_g is the ground rainfall record, and N is the sample size; Cov and σ in Equation 3.4 refer to the covariance and the standard deviation, respectively. NMSE is a dimensionless estimator of the overall deviations between P_s and P_g . RB, which measures systematic differences, is measured as a percentage. Accumulated error is measured using RMSE in mm/day for the daily scale, mm/month for the monthly scale, and so on. The agreement between P_s and P_g is measured using CC, which is dimensionless. A perfect validation should have a CC of 1. The lower RMSE, RB, and NMSE, the better the estimation. These comparison indices for validating various satellite-based rainfall products have been used in many prior studies (Ebert et al., 2007; Wang et al., 2011; Yong et al., 2012; Jiang et al., 2012; Haile et al., 2013; Guo et al., 2015; Salio et al., 2015; Qi et al., 2016).

This study uses categorical statistics, such as probability of detection (POD), strike ratio (SR), false-alarm ratio (FAR), and threat score (TS), which have been used in many studies (Ebert et al., 2007; Su et al., 2008; Guo et al., 2015; Salio et al., 2015; Qi et al., 2016), for evaluating the rainfall-detection abilities of the GSRPs relative to the ground rainfall measurements. These statistics are computed using Equations 3.5–3.8.

$$POD = \frac{\sum A}{\sum(A + B)} \quad 3.5$$

$$SR = \frac{\sum(A + D)}{\sum(A + B + C + D)} \quad 3.6$$

$$FAR = \frac{\sum C}{\sum(A + C)} \quad 3.7$$

$$TS = \frac{\Sigma A}{\Sigma(A + B + C)} \quad 3.8$$

where A is the number of rainfall events detected both by the gauges and the GSRPs; B and C , respectively, are the number of rainfall events detected by the gauges and the number detected by the GSRPs; and D is the number of non-rainfall events detected both by the gauges and the GSRPs. POD , SR , FAR , and TS range from 0 to 1. Perfect detection of rainfall events by the GSRPs relative to the gauges would mean POD , SR , and TS values of 1 and a FAR value of 0.

3.5.2 Bias Correction of GSRPs

Prior to their use for hydrological applications, the GSRPs are further bias-corrected against the ground rainfall measurements to better represent their rainfall estimates for the Meghna basin. Among the many existing bias-correction techniques that have been proposed for correcting satellite data, two widely-used techniques—linear correction and quantile mapping—are implemented and evaluated in this study. In addition, a modified linear correction (MLC) technique is also applied. As with the comparison technique, all of the correction methods are conducted at the available gauge stations inside Bangladesh, and the station-based correction factors are interpolated to each grid cell in the basin for each GSRP (interpolation is performed based on GSRPs' original spatial resolution) to obtain basin-wide corrected rainfall estimates.

3.5.2.1 Linear Correction Method

This method is applied to correct the GSRPs in a dynamic form, with the correction factors calculated based on two varying time periods (i.e., windows). In the former approach, the correction factors are calculated using mean monthly time window, whereas in the latter approach, a length of sequential time window across the entire study

period is used. The linear correction with mean monthly window (LCMW) technique is very simple and has been used in many studies (Hay et al., 2000; Lenderink et al., 2007; Teutschbein and Seibert, 2012; Lafon et al., 2013; Arias-Hidalgo et al., 2013; Fang et al. 2015). In this technique, the mean monthly correction factors for the 12 calendar months and for each gauge station are calculated in the first step as follows:

$$f_{m,k} = P_{g,m,k}/P_{s,m,k} \quad 3.9$$

where $f_{m,k}$ is the correction factor for month m at station k ; and where $P_{g,m,k}$ and $P_{s,m,k}$, respectively, are the mean monthly gauge and satellite estimates for month m at station k . In the second step, the spatial distribution of the correction factors from the gauge locations to the grid cells is obtained by adopting the IDW interpolation method (Shepard, 1968; Dirks et al., 1998; Heistermann and Kneis, 2011). Finally, the corrected GSRPs are calculated as follows:

$$P_{scor,m,d(i,j)} = f_m(i,j) * P_{s,m,d(i,j)} \quad 3.10$$

where $P_{scor,m,d(i,j)}$ are the corrected estimates of the original GSRPs ($P_{s,m,d(i,j)}$) on the d th day of the m th month at grid cell $\sim i,j$; and where $f_m(i,j)$ represents the interpolated correction factors at grid cell $\sim i,j$ for month m .

The latter approach—linear correction with sequential window (LCSW)—has been used in studies, such as Habib et al. (2014) and Bhatti et al. (2016). Sequential time windows of varying lengths (e.g., 3, 5, 7, 10, 15, 20, 25, 30, 40, and 50 days) are tested first, and the 15-day length is found to be the most appropriate for bias correction. Therefore, the correction factors for each 15-day sequential time window throughout the study period are calculated at each gauge station as follows:

$$f_{l,k} = P_{g,l,k}/P_{s,l,k} \quad 3.11$$

where $f_{l,k}$ is the correction factor for 15-day sequential time window l at station k ; and where $P_{g,l,k}$ and $P_{s,l,k}$, respectively, are the accumulated rainfall amounts for the gauge and satellite in time window l at station k . After calculating the correction factors at the gauge locations, their spatial distribution over the grid cells at each sequential time window l is obtained by applying IDW interpolation. Finally, the corrected GSRPs are calculated in a temporally and spatially coherent manner, as follows:

$$P_{scor,l,d}(i,j) = f_l(i,j) * P_{s,l,d}(i,j) \quad 3.12$$

where $P_{scor,l,d}(i,j)$ represent the corrected estimates of the original GSRPs ($P_{s,l,d}(i,j)$) on the d th day of the l th time window at grid cell $\sim i,j$; and where $f_l(i,j)$ represent the interpolated correction factors at grid cell $\sim i,j$ for time window l .

3.5.2.2 Modified Linear Correction (MLC) Method

This method is based on the linear correction method; the correction factors at each gauge station are computed at a daily time step (instead of based on the length of the time window) using arithmetic differences rather than the ratio of the gauges to the GSRPs. Vila et al. (2009) also used this method to correct TRMM 3B42RT satellite estimates for continental South America. That study featured cell-by-cell bias correction with the interpolated gauge observations, but this study's interpolation is conducted with the correction factors (arithmetic differences) calculated at the gauge stations; accordingly, the correction equations are modified as follows:

$$D_{d,k} = P_{g,d,k} - P_{s,d,k} \quad 3.13$$

where $D_{d,k}$ is the correction factor for day d at station k ; and where $P_{g,d,k}$ and $P_{s,d,k}$ are, respectively, the gauge and GSRP estimates for day d at station k . After calculating the values for each day and each station, the correction factors are spatially distributed using

the IDW interpolation method, and the bias-corrected GSRPs are finally calculated as follows:

$$P_{scor,d}(i,j) = D_d(i,j) + P_{s,d}(i,j) \quad 3.14$$

where $P_{scor,d}(i,j)$ represent the corrected estimates of the original GSRPs ($P_{s,d}(i,j)$) on the d th day at grid cell $\sim i,j$; and where $D_d(i,j)$ represent the interpolated correction factors at grid cell $\sim i,j$ for day d .

3.5.2.3 Quantile Mapping (QM) Method

The QM is a non-parametric bias-correction method that corrects errors in the shape of the distribution and that is therefore also capable of correcting errors in variability (Thiemeßl et al., 2011). QM originates from empirical transformation (Thiemeßl et al., 2011) and has been successfully implemented in various hydrological applications (Thiemeßl et al., 2011 & 2012; Sun et al., 2011; Chen et al., 2013; Wilcke et al., 2013). The GSRPs at the gauge stations are adjusted using this method based on a monthly-grouped, daily-constructed empirical cumulative distribution function (*ECDF*). Specifically, the *ECDF* of each GSRP is adjusted to match with the *ECDF* of the gauge rainfall (Wood et al., 2004). This adjustment at the gauge stations can be expressed in terms of *ECDF* and its inverse ($ECDF^{-1}$) as follows:

$$P_{scor,m,d,k} = ECDF^{-1}_{g,m,k}[ECDF_{s,m,k}(P_{s,m,d,k})] \quad 3.15$$

where $ECDF_{s,m,k}$ is the *ECDF* of the GSRP estimates ($P_{s,m,d,k}$) at station k on the d th day of the m th month; and where $ECDF^{-1}_{g,m,k}$ is the inverse *ECDF*, corresponding to $P_{scor,m,d,k}$, which is the corrected rainfall for $P_{s,m,d,k}$ on the d th day of the m th month at station k . Rather than interpolating the QM-corrected GSRP estimates from the gauge stations to the grid cells, these estimates are instead employed with the MLC method to obtain a spatially distributed rainfall for each grid cell. In the first step, at each gauge

station, the difference between gauge- and QM-corrected GSRPs is calculated for each time step (daily) and then distributed them spatially to each grid cell by applying the IDW interpolation. In the end, the gridded differences are added to the original GSRPs to produce the final version of the bias-corrected rainfall for each grid cell.

3.5.3 Merging of GSRPs

Hasan et al. (2016) showed that merging different satellite rainfall products can reduce errors and increase performance, compared to the use of a single product. Given this finding, in this study, a number of merging techniques are applied to the GSRPs to examine whether merging various products can produce a new reference dataset with increased accuracy, which could, in turn, lead to long-term hydrological applications. To capture the spatial and temporal variations in the performance of the GSRPs, this merging is performed dynamically in this study. The final merged product for each grid cell is calculated as follows:

$$P_{mrgd,d(i,j)} = \sum_{s=1}^n w_{s,m,(i,j)} * P_{s,m,d(i,j)} \quad 3.16$$

where $P_{mrgd,d(i,j)}$ is the merged rainfall estimate on the d th day at grid cell $\sim i,j$, n is the number of GSRPs; $w_{s,m,(i,j)}$ is the weight calculated for the GSRP s in month m at grid cell $\sim i,j$; and $P_{s,m,d(i,j)}$ is the rainfall estimate of the GSRP s on the d th day of the m th month at grid cell $\sim i,j$.

Three merging techniques—simple average (SA), error variance (EV), and inverse error variance weighting (IEVW)—are used in this study to calculate the weights of the individual GSRPs at each gauge location. In the first step, the GSMaP-G and MSWEP products (which have 0.1° spatial resolution) are aggregated into the 0.25° resolution (which is what the other two products, CHIRPS and TMPA-G, use) to ensure a common

resolution for the merged product. The 0.25° resolution is selected because it is coarser resolution over which two of the GSRPs (CHIRPS and TMPA-G) are distributed, meaning that an aggregation of the GSMaP-G and MSWEP products from 0.1° resolution to 0.25°—does not produce uncertainty. In the second step, as with the bias-correction techniques, the merging weights of the individual GSRP are calculated at the gauge stations and then interpolated (using the IDW method) to each grid cell of the basin to obtain a spatially distributed merged product. A brief description of the three merging techniques is detailed below.

3.5.3.1 Simple Average (SA) Merging

Satellite rainfall products often show varying performance due to overestimation or underestimation of rainfall. However, researchers have found that using simple averaging for various forecasts in a microeconomic time series can outperform more complicated weighting schemes involving the individual datasets (Stock and Watson, 1999, 2003 & 2004). Therefore, simple averaging of the GSRPs can produce an improved dataset. The merging weights of the individual GSRPs are calculated in this method as follows:

$$w_{s,m,(i,j)} = 1/n \quad 3.17$$

where $w_{s,m,(i,j)}$ is the weight of satellite product s in month m at grid cell $\sim i,j$; and where n is the number of GSRPs. This method is the simplest, as it is static, with the weights being equal for each GSRP and for each month depending only on the number of products.

3.5.3.2 Error Variance (EV) Merging

Following the techniques that Hasan et al. (2016) and Woldemeskel et al. (2013) implemented in their studies, the EV method used in this study is extended to be used for multiple products in a dynamic form. More specifically, to capture the spatiotemporal

variation of the satellite products, the daily rainfall values for both the gauges and the GSRPs are grouped monthly. Then, the variance of the errors between the gauges and the satellite products are estimated for each month at each gauge station and then spatially distributed to each grid cell using the IDW interpolation method. The weight for each product is finally calculated as follows:

$$w_{s,m,(i,j)} = \frac{1}{n-1} * \frac{\sum_{s=1}^n var_{s,m,(i,j)} - var_{s,m,(i,j)}}{\sum_{s=1}^n var_{s,m,(i,j)}} \quad 3.18$$

where n is the number of GSRPs; $var_{s,m,(i,j)}$ is the error variance of the GSRP s for which the weight $w_{s,m,(i,j)}$ is calculated in the m th month at grid cell $\sim i,j$; and $\sum_{s=1}^n var_{s,m,(i,j)}$ is the summation of the error variances for all GSRPs in month m at grid cell $\sim i,j$.

3.5.3.3 Inverse Error Variance Weighting (IEVW) Merging

Shen et al. (2014) implemented this method to evaluate the performance of various satellite datasets on the Tibetan Plateau. The formula is slightly modified in our study, with the sum of the weights of each product set to unity so that the merged product remains unbiased. As with the EV method, this is also dynamic; the monthly weights are calculated as follows:

$$w_{s,m,(i,j)} = \frac{1/var_{s,m,(i,j)}^2}{\sum_{s=1}^n 1/var_{s,m,(i,j)}^2} \quad 3.19$$

where the symbols in this equation are the same as those in Equation 3.19.

3.5.4 Combination of Merging and Bias Correction

In this study, a combination of merging and bias correction is also applied to the GSRPs to examine whether a more accurate rainfall dataset can be generated for the Meghna basin to be used in long-term hydrological applications. Among the merged products produced from the three merging techniques, the product that provides the best

results is then further corrected using the best-performing bias-correction method of those discussed above.

3.5.5 Performance Evaluation of the Bias-Corrected and Merged Products

The overall performance of the improved products (both bias-corrected and merged) is evaluated using Taylor's diagram (Taylor, 2001), which summarizes the statistical differences between the time series of ground rainfall and the satellite estimate. The diagram concludes how fair the satellite-based rainfall estimates relate to the gauge estimates in terms of three statistical indicators: normalized root mean square difference (NRMSD), series normalized standard deviation (NSD), and correlation coefficient (CC). This diagram is useful for summarizing the statistical-error performances in a single 2D plot.

3.5.6 Streamflow Simulations

In this study, a distributed hydrological model called the rainfall-runoff-inundation (RRI) is used to perform streamflow simulations. RRI is a 2D model capable of simulating rainfall-runoff and flood inundation simultaneously (Sayama et al., 2012, 2015a & 2015b). The model deals with slopes and river channels separately. At a grid cell where a river channel is located, the model assumes that both the slope and river are positioned within the same grid cell. The channel is discretized as a single line along the centre line of the overlying slope grid cell. The flow for the slope grid cells is calculated using a 2D diffusive-wave model, and the channel flow is calculated using a 1D diffusive-wave model. For better representations of RRI processes, the model also simulates lateral subsurface flow, vertical infiltration flow, and surface flow. The lateral subsurface flow, which is typically most important in mountainous regions, is treated in terms of the discharge-hydraulic gradient relationship, which takes into account both the saturated

subsurface flow and the surface flow. On the other hand, the vertical infiltration flow is estimated using the Green-Ampt model. The flow interaction between the river channel and the slope is estimated based on various overflowing formulae, which depend on water-level and levee-height conditions.

To investigate its potential for use as a reference rainfall data in streamflow simulation for the Meghna basin, the improved rainfall dataset (created by this study) is used to calibrate the RRI model parameters for the first half of the study period (from 2009 to 2012). The observed streamflows at Bhairab Bazar station are used to fit the model simulations for the calibration period. The calibration is first performed with the default parameters of the model, and the parameters are then finalized according to the best-fit hydrographs and several performance indicators. The parameters for the RRI model's calibration are mainly grouped into two kinds: (1) river-channel parameters and (2) surface- and subsurface-flow parameters. The former type incorporate aspects of river geometry such as river width, river depth, bank height, and channel roughness. The latter type consist of the properties of the land surface layer (roughness), subsurface layer (soil depth, porosity), vertical infiltration (vertical hydraulic conductivity, etc.), and lateral subsurface flow (lateral hydraulic conductivity, porosity, etc.).

Using the calibrated model parameters, the validation of the RRI model is also performed by generating streamflows with the improved dataset for the latter half of the study period (from 2013 to 2016). The results are then compared with the observed streamflows at Bhairab Bazar station. In addition, an additional validation of the RRI model is also conducted by comparing the observed streamflows with those of the model for the Amalshid stream gauge station (the Meghna River's prime entrance point into Bangladesh from India) for the entire study period (2009–2016). This allows for a further

check of the model's performance and of the potential for the rainfall dataset to be used when simulating flood flows inbound from India.

3.6 Results and Discussion

To carry out the performance evaluation of the GSRPs and to investigate their potential for use as a reference rainfall dataset in the Meghna basin, this study compares each of the GSRPs with the ground rainfall measurements at the gauge locations on a point-to-pixel basis. However, rain gauges are available only at 20 locations within the Bangladesh portion of the basin. Therefore, the performance of the GSRPs is evaluated at only these 20 gauge stations. The evaluation is conducted for the wet season at the daily and monthly temporal scales throughout the study period (2009–2016). After the performance check, several bias-correction and merging techniques are applied to the GSRPs to create a set of improved rainfall datasets. In addition, a combined use of merging and bias correction is also explored. Finally, of the bias-corrected and/or merged products, the product that provides the best results, is used to run the RRI hydrological model, which simulates streamflows at two critical locations in the basin. The results of the analyses and the related discussion are as follows.

3.6.1 Performance Evaluation of GSRPs on the Daily Scale

The rainfall-detection ability of the GSRPs (compared to the gauge records) is estimated based on the categorical statistics described in Section 3.5.1. The estimation is collectively conducted for all of the 20 rain-gauge stations, and the results are summarized in Table 3.3. Relative to the gauge records, GSMaP-G and MSWEP outperformed CHIRPS and TMPA-G by detecting more rainy days (Table 3.3, differences measured using POD). However, the former two products detected more non-rainy days as well

(Table 3.3, differences measured using FAR). As shown in Table 3.3, SR and TS indicate no significant disparities among the GSRPs.

Table 3.3: Categorical statistics calculated for daily GSRP rainfall estimates relative to daily ground rainfall in the wet season throughout the study period (2009–2016).

Categorical Statistic	Scores				Perfect Score
	CHIRPS	GSMaP-G	TMPA-G	MSWEP	
Probability of Detection (POD)	0.69	0.98	0.79	0.98	1
Strike Ratio (SR)	0.71	0.62	0.75	0.65	1
False alarm ratio (FAR)	0.35	0.47	0.33	0.45	0
Threat score (TS)	0.50	0.52	0.57	0.54	1

Figure 3.4a–t compares the cumulative rainfall of the ground gauges, CHIRPS, GSMaP-G, TMPA-G, and MSWEP daily estimates at each gauge station calculated for the wet season throughout the study period (2009–2016). The plotting order is based on the varied (extreme- to low-) intensity of the mean annual gauge rainfall (Table 3.1). The results show varying performance, with the GSRPs either over- or under-estimating cumulative rainfall relative to the gauge rainfall at most of the stations—although nearly accurate estimates are also observed at some of the stations. CHIRPS tends to overestimate cumulative rainfall relative to gauge rainfall at most (16) of the stations (Figure 3.4c,e–h,j–t), regardless of gauge rainfall intensity, whereas GSMaP-G underestimates at nine stations (Figure 3.4a–f,i,j,p) and overestimates at six others (Figure 3.4k–n,q,t]). TMPA-G and MSWEP, on the other hand, both underestimate (Figure 3.4a–f,i for TMPA-G and Figure 3.4b,d,f,g,i for MSWEP) and overestimate (Figure 3.4g–h,j–o,q–t for TMPA-G and Figure 3.4a,e,h,k,l,n,o,q–t for MSWEP) the cumulative rainfall at the stations of both high- and low-intensity of gauge rainfall.

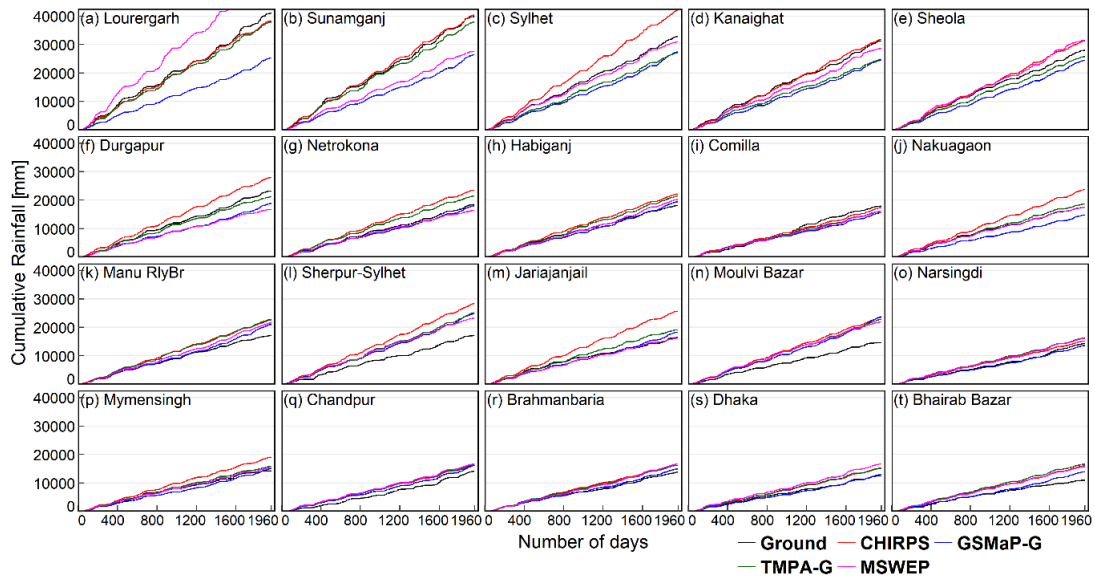


Figure 3.4: Cumulative rainfall of daily estimates calculated for the ground gauges and GSRPs throughout the wet season (March–October) of the study period (2009–2016), at the 20 rain-gauge stations (a–t) located within the Bangladesh portion of the Meghna basin.

Using the indices based on Equations 3.1–3.4, Figure 3.5a–t compare daily CHIRPS, GSMaP-G, TMPA-G, and MSWEP estimates for the wet seasons during the entire study period against the daily ground rainfall measurements at the 20 rain-gauge stations. The results once again show varying performance for daily estimates of each product. According to the calculated statistics, each product performs differently, resulting in both positive and negative relative biases (RB) in extreme- as well as low-rainfall areas. The accumulated errors (i.e., NMSE and RMSE) for each product result in high magnitudes at all stations and indicate no significant disparities among the products. The errors of agreement (the calculated CCs) show very low coherence for CHIRPS and slightly better (but still low) coherence for the other three products at all gauge stations.

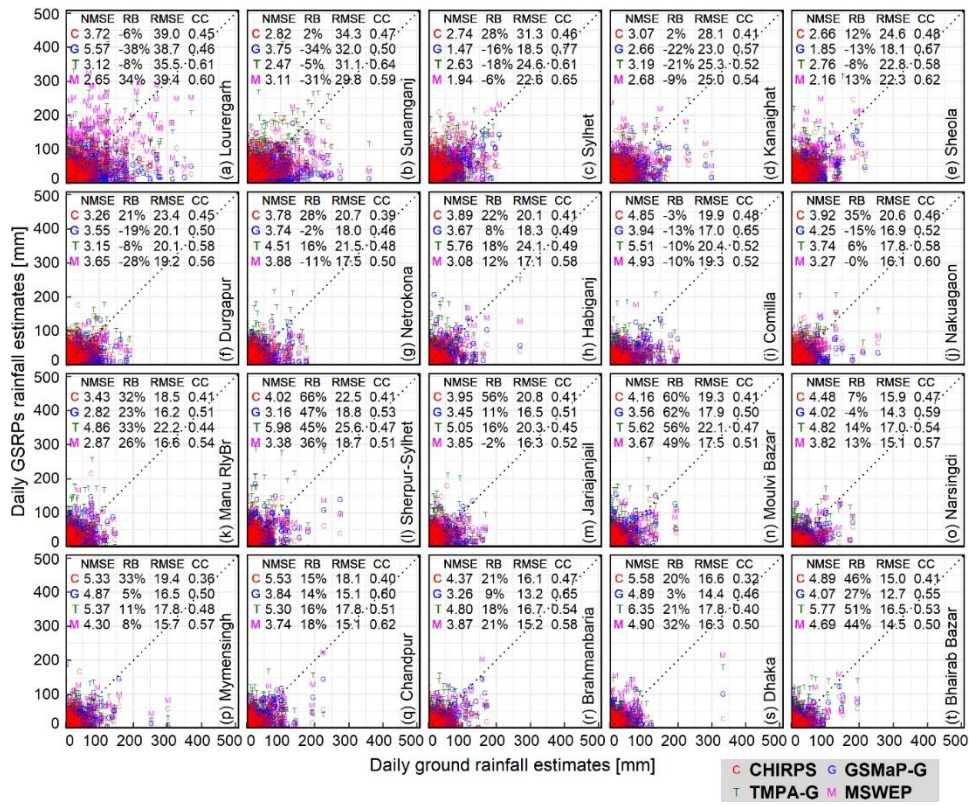


Figure 3.5: Scatterplots of daily GSRP estimates against daily ground rainfall for the wet seasons during the entire study period (2009–2016) at the 20 rain-gauge stations (a–t). Comparison indices are included inside the plot for each station.

3.6.2 Performance Evaluation of GSRPs on the Monthly Scale

Figure 3.6a–t present a comparison of mean monthly accumulated estimates for CHIRPS, GSMaP-G, TMPA-G, and MSWEP relative to the ground rainfall records at each gauge station. Unlike with the daily rainfall accumulations, the monthly accumulations of all products have lower NMSE and show greater coherence (measured using CC) relative to the ground rainfall. This indicates that the GSRPs accurately estimate the mean monthly accumulated rainfall. On the other hand, the monthly accumulations of all the products follow the daily trend and show insignificant disparities in calculating RMSE. The relative bias (RB) results for the monthly accumulations, are the same as for the daily accumulations, as RB is calculated for the entire study period (2009–2016) in both cases.

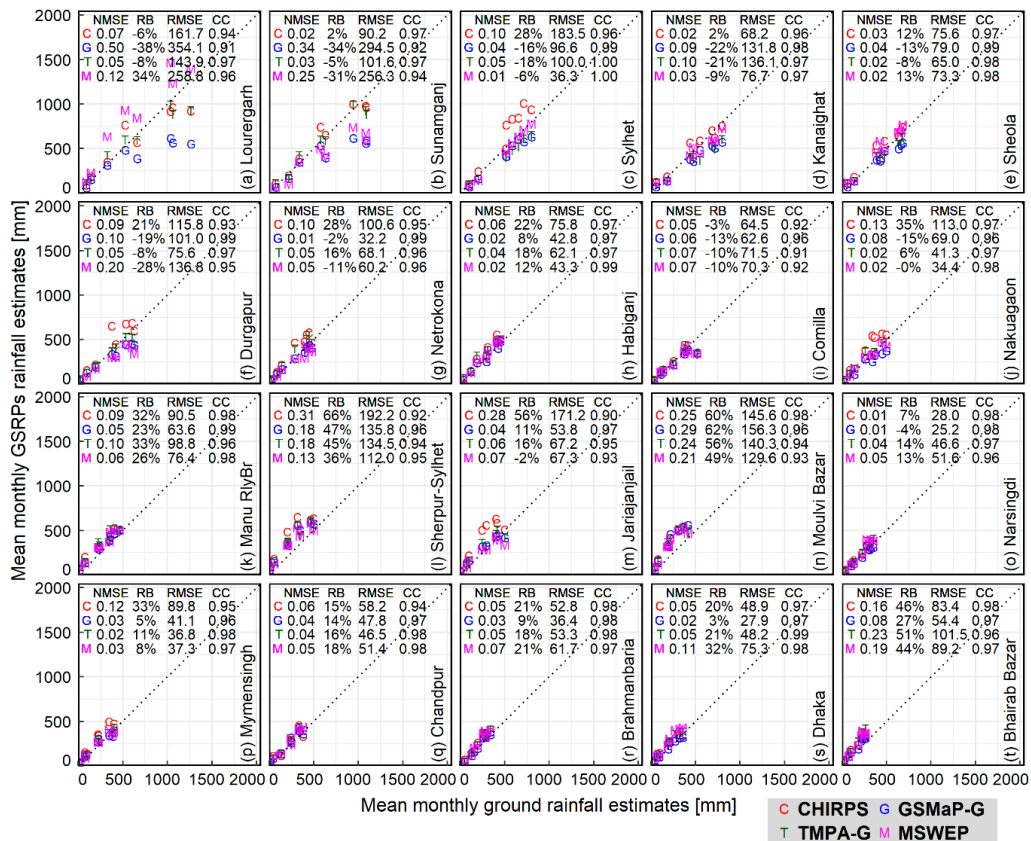


Figure 3.6: Scatterplots of mean monthly accumulated GSRP estimates against the ground rainfall for the wet seasons during the entire study period (2009–2016) at the 20 rain-gauge stations (a–t). Statistical indices are included inside the plot for each station.

Figure 3.7a–t compare mean monthly ground rainfall to the GSRP estimates at the 20 rain-gauge stations for the months of rainy season (March–October) during the study period (2009–2016). The results, which show that the mean monthly rainfall of the gauge stations, that experienced medium to low rainfall intensity (Figure 3.7g–t), fit with the mean monthly accumulated rainfall of the GSRPs reasonably well for almost all of the rainy months. On the other hand, at nearly all the gauge stations that experienced extreme rainfall (Figure 3.7a–f), CHIRPS overestimates the monthly rainfall, GSMaP-G underestimates it, and TMPA-G and MSWEP both over- and underestimates it. The results also show that the stations located in the farthest northeastern part of Bangladesh experienced extreme rainfall (Figure 3.7a–f).

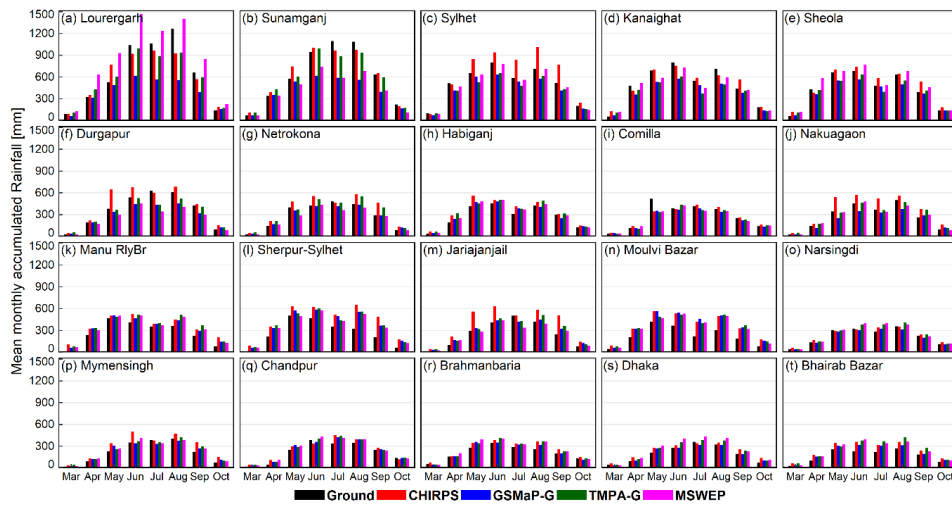


Figure 3.7: Mean monthly accumulated rainfall of the ground gauges and CHIRPS, GSMaP-G, TMPA-G, and MSWEP for the months of the rainy season (March–October) during the study period (2009–2016) at 20 gauge stations (a–t).

Until now, it is observed that all of the GSRPs show a significant amount of bias (either positive or negative), as compared to the ground rainfall measurements, on both the daily and the monthly temporal scales and at each gauge station (regardless of station’s topographical location or rainfall intensity). In addition, all the GSRPs largely detected the non-rainfall events. It is, thus, rational to correct the bias of the GSRPs so that they can be used as reference rainfall datasets for long-term hydrological applications in the Meghna basin. For this purpose, local rain-gauge data from 20 stations are used.

3.6.3 Evaluation of Bias-Corrected GSRPs

Each bias-correction technique described in Section 3.5.2 is applied to the original GSRPs to produce a set of bias-corrected rainfall datasets for the Meghna basin. Fifteen out of the 20 rain gauge stations are used to implement the bias correction techniques, and the remaining five stations are taken out for the validation of the correction techniques. Four experiments are conducted to select the five validation stations randomly, and these are conducted to make sure that every station is taken out once in all the experiments. However, the performance of the correction methods does not vary much

in any of the combination of the validation stations. As a result, to keep the manuscript concise, one experiment with five randomly-selected validation stations (that include Sunamganj, Sheola, Nakuagaon, Brahmanbaria, and Bhairab Bazar) is presented in this study. Figure 3.8a–e shows Taylor diagrams (Taylor, 2001) with a comparison of the original and bias-corrected daily estimates for the GSRPs with those of the ground gauges at the five validation stations for the rainy seasons of 2009–2016. The purpose of this diagram is to show the temporal variability of the satellite estimates (both the original and corrected GSRPs) relative to the ground-based observed rainfall, in terms of NRMSD, CC, and NSD. According to Taylor (2001), the grey straight lines in Figure 3.8a–e display the CC of the satellite estimates; the blue dotted arcs are the NRMSD; the green dotted arcs display the NSD of the satellite estimates; the black dashed arc line denotes the NSD of the observed fields; satellite estimate patterns which agree well with the observed field's pattern lie close to a point marked obs on the x -axis, indicating a relatively high correlation and a low NRMSD; and the NSD of satellite estimates, matching the observed-based NSD, have patterns with the right amplitude. The results indicate that the linear correction method based on the mean monthly time window (LCMW) mostly fails to correct the satellite estimates (blue symbols), relative to the original GSRPs (red symbols); this method, thus, shows no significant improvements in terms of the performance indicators (CC, NRMSD, and NSD). Likewise, the linear correction method based on the sequential time window (LCSW) cannot correct the bias of the GSRPs (green symbols), compared to the original GSRPs (red symbols), although LCSW performed slightly better than LCMW in terms of removing systematic biases from the original GSRPs. The quantile mapping (QM) correction method adopted in this study outperforms the linear correction methods and leads to improved indices (orange symbols) compared

to the original GSRPs (red symbols). Higher correlations (in CC), lower NRMSD, and lower variability (in NSD) are observed at all five validation stations for all of the GSRPs after correction with the QM method. However, the modified linear correction (MLC) method shows significant improvements in removing systematic biases from the GSRPs (black symbols) and outperforms both the linear and QM correction methods. The NRMSD and NSD errors for the validation set decrease with the MLC method, and the CCs indicate greater coherence than in the original GSRPs. Although all of the GSRPs are corrected comparatively well in the MLC method, the TMPA-G provides better results than the other three products (GSMaP-G, CHIRPS, and MSWEP).

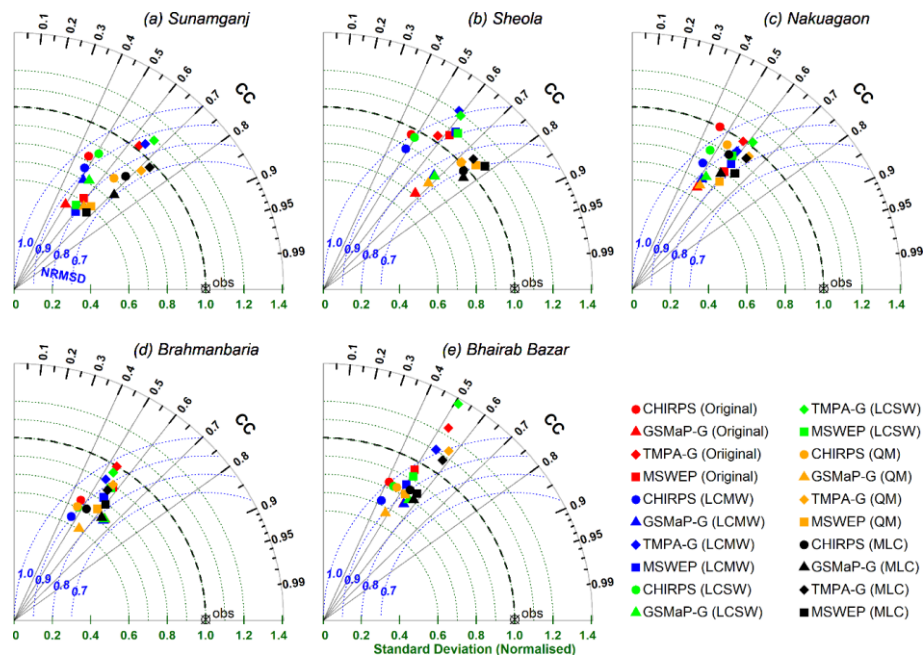


Figure 3.8: Taylor diagram illustrating statistical comparison between original, bias-corrected GSRP estimates and gauge rainfall (obs mark), as calculated for the wet seasons of 2009–2016 at five validation stations (a–e). The CCs are related to the azimuthal angle (grey lines), which denote a similarity in pattern between the satellite and gauge fields. NSDs (green contours) indicate the amount of variance between the satellites and the gauge time series, and is proportional to the radial distance from the origin. The NRMSD (blue contours) between the satellite products and the rain-gauge fields is proportional to the distance from the point on the x -axis identified as obs. For details, refer to Taylor (2001).

3.6.4 Evaluation of Merged Products

Researchers have shown that merging satellite rainfall products can reduce errors and increase performance relative to any individual product. Hence, three merging techniques—SA, EV, and IEVW, laid out in Section 3.5.3—are applied to the original GSRPs to see if merging alone can produce an improved dataset relative to both the original and the bias-corrected GSRPs. The daily estimates of the three merged products are compared with those of the gauges at the 20 gauge stations for the rainy season throughout the study period. Figure 3.9a–t show Taylor diagrams with statistical comparisons between satellite estimates (both original GSRPs and merged products) and observed rainfall at the gauge stations. As shown in the figures, the results indicate that merging the GSRPs can significantly reduce the biases of the individual product relative to the ground rainfall. Compared to the original GSRPs (bubbles), the products of all three merging methods (triangles) result in improved statistical indices at each gauge station. Even the SA method, which does not use any ground rainfall records, provides better results (magenta triangle) than any individual GSRP provides. This may be due to the fact that combining the GSRPs leverages the mutual strengths of each product to create a more representative product. Although all three merging methods perform well in reducing errors from the original GSRPs relative to the ground rainfall, the IEVW (black triangle) performs better than the SA and EV methods.

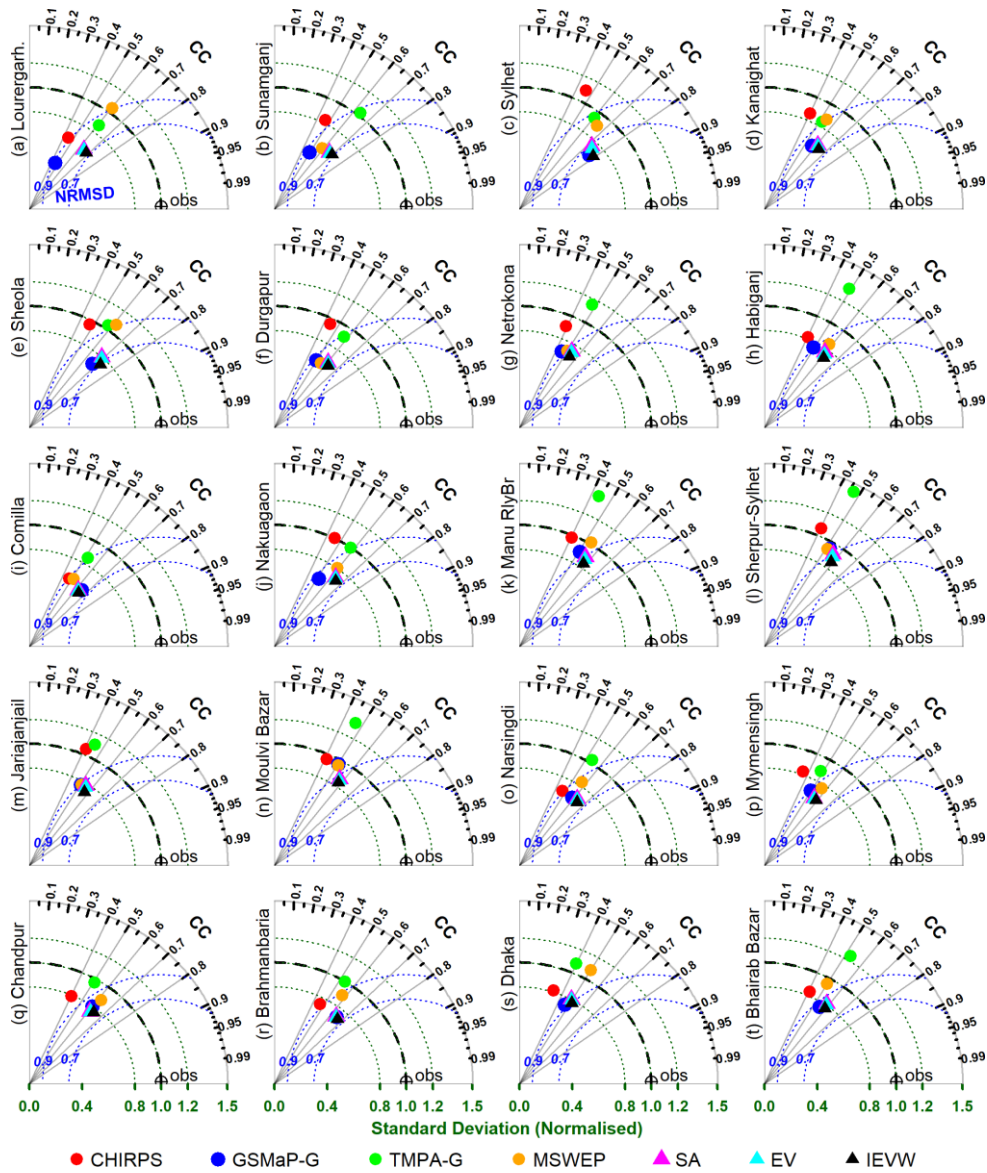


Figure 3.9: Taylor diagram illustrating a statistical comparison between satellite products (original and merged) and ground rainfall (obs mark) for the wet seasons of 2009–2016 at the 20 rain-gauge stations (a–t). Instructions for reading a Taylor diagram are given in Figure 3.8.

3.6.5 Combined Use of Merging and Bias Correction

As discussed in Section 3.6.4, the merging of the GSRPs improves the data and performs better (with increased indices) than any individual product does. All three of the merging techniques produce representative datasets, with IEVW outperforming SA and EV. On the other hand, as discussed in Section 3.6.3, the original GSRPs are best corrected using the MLC bias-correction method. This method improves the accuracy of

the products and reduces errors significantly. However, among the five validation stations, Sunamganj and Sheola, which both experienced extreme rainfall, show better results (higher CC and lower NRMSD) for the MLC-corrected GSRPs than for the IEVW-based merged product (Figures 3.8a,b and 3.9b,e). On the other hand, the IEVW-based merged product produces improved indices (higher CC and lower NRMSD) at the remaining three stations (Figures 3.8c,d,e and 3.9j,r,t)—those that experienced medium to low intensity of rainfall. Therefore, the IEVW merging technique followed by the MLC bias-correction method is explored to examine whether the combined use of merging and bias correction can produce an improved dataset with increased performance and applicability. Figure 3.10a–e show Taylor diagrams with statistical comparisons between time series for the satellite products (original GSRPs; MLC corrected GSRPs; and IEVW-based merged products (both without and with the MLC bias correction)) and ground rainfall at the five validation stations for the rainy seasons of 2009–2016. The results show improvements for the combined product that are employed with both merging (IEVW) and bias-correction (MLC) techniques. Compared to the errors (CC, NRMSD, and NSD) produced with the original GSRPs (red symbols), the MLC-corrected GSRPs (blue symbols), and the IEVW-merged product of the original GSRPs (magenta symbol), the combined product (black symbol) results with improved indices (higher CC, lower NRMSD, and relatively lower NSD) at each of the five validation stations, which indicates that the combined use of merging and bias correction can produce an improved dataset for various hydrological applications in the Meghna basin.

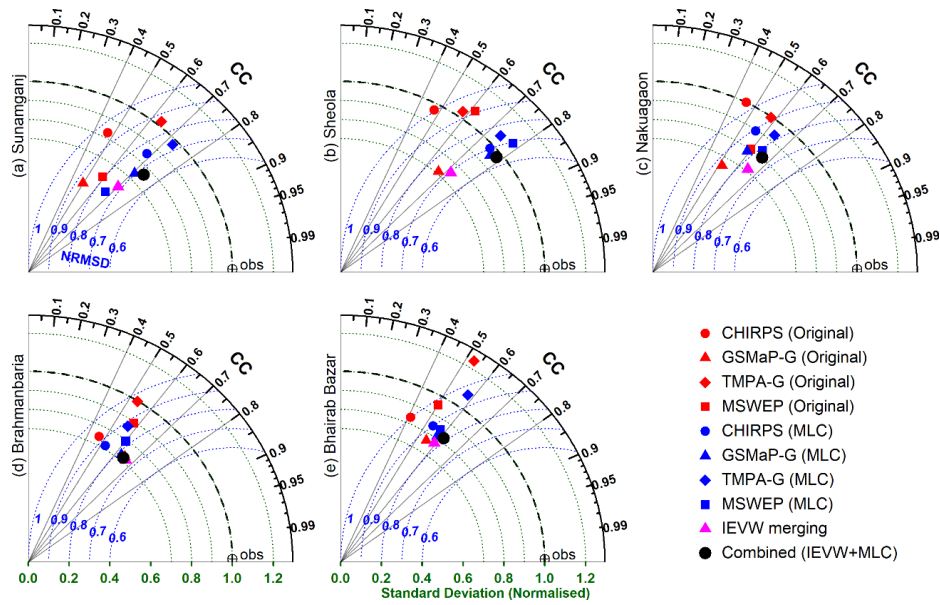


Figure 3.10: Taylor diagram with the statistical comparison of the original GSRPs, the MLC-corrected GSRPs, and the IEVW-based merged product of the original GSRPs (both without and with the MLC bias correction) against ground rainfall for the wet seasons of 2009–2016 at the five validation stations (a–e). Instructions for reading a Taylor diagram are given in Figure 3.8.

The improved dataset, which is created in this study by combining the IEVW merging technique and the MLC bias-correction method (the dataset hereafter called IMLC), is finally compared with the original GSRPs relative to the ground rainfall measurements for daily, monthly, and annual time series; this is done to evaluate the overall temporal representation and variability of the satellite rainfall estimates. Figure 3.11a–c show Taylor diagrams with a statistical comparison of the original GSRPs and the IMLC product relative to the ground rainfall, collectively calculated for the five validation stations—in terms of (a) daily, (b) monthly, and (c) annual accumulated rainfall—for the entire study period of 2009–2016. As with the original GSRPs, the best agreement for the IMLC product in terms of correlation, is in monthly accumulated rainfall. All the original GSRPs capture the monthly rainfall amount reasonably well, and have CCs ranging from 0.89 to 0.97; by comparison, the monthly rainfall of the IMLC product alone shows a CC of around 0.97. On the other hand, the daily correlations for

the GSRPs are found considerably lower, with no dataset showing a CC greater than 0.6, whereas the daily rainfall of the IMLC product shows a higher CC of about 0.75. The annual accumulated rainfall has lower correlations for the GSRPs, with the exception of CHIRPS and TMPA-G, leading to a CC at the same level as the IMLC product: about 0.95. All the GSRPs and the IMLC product underestimate the inter-daily, -monthly, and -annual variability—in other words, the NSD of the daily, monthly, and annual rainfall—except for the daily variability, which TMPA-G overestimates. However, in all three time scales, IMLC shows lower variability than the GSMaP-G and MSWEP products; it also produces minimal variation that is nearly the same as what is found in the CHIRPS and TMPA-G products. The ranking of NRMSD for the GSRPs varies depending on the time scale; however, compared to GSMaP-G and MSWEP, CHIRPS, and TMPA-G show relatively low NRMSD errors for the monthly and annual estimates, and relatively high errors for the daily estimates. On the other hand, the improved product, IMLC, shows considerably lower NRMSD errors than all of the GSRPs on the daily time scale, and also lower NRMSD errors than the GSMaP-G and the MSWEP products at the monthly and annual time scales, just as the TMPA-G and CHIRPS products do. Overall, the three statistics plotted in the Taylor diagram show lower NRMSDs and lower variability (in NSD), as well as higher coherence (measured with CC) for the IMLC product than any individual GSRP at all three time scales, when compared to the gauge rainfall. In particular, the daily rainfall of the IMLC product produces better indices than do the daily GSRPs, indicating IMLC's potential for use as a reference rainfall dataset in any hydrological model to simulate daily hydrological responses of the Meghna basin.

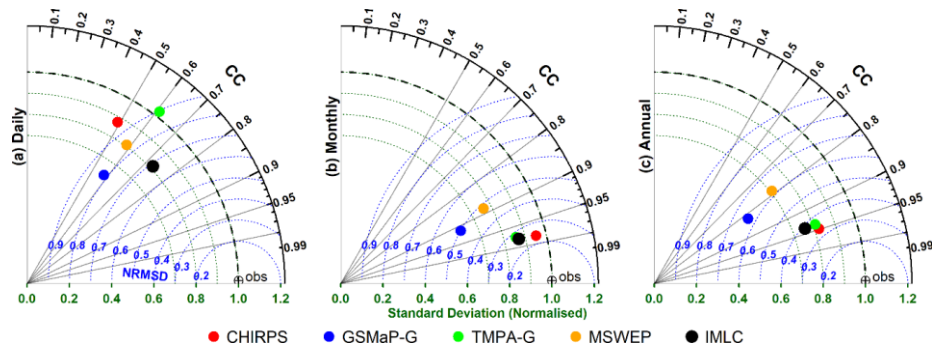


Figure 3.11: Taylor diagrams plotted for the (a) daily, (b) monthly, and (c) annual time series of the original GSRPs and the IMLC product vs. the ground rainfall collectively calculated for the five validation stations for the period of 2009–2016. Instructions for reading a Taylor diagram are given in Figure 3.8.

Figure 3.12a–e show the gridded (0.25° resolution) annual average rainfall, as calculated from the four GSRPs and the IMLC product, for the study period of 2009–2016. The purposes of this figure are to understand the spatial distribution of the rainfall pattern by each of the GSRP products and to check the performance of the IMLC product relative to the GSRPs. The results indicate that the IMLC product has used the respective strengths of the individual GSRPs to offset their respective weaknesses, resulting in a representative rainfall product for the basin.

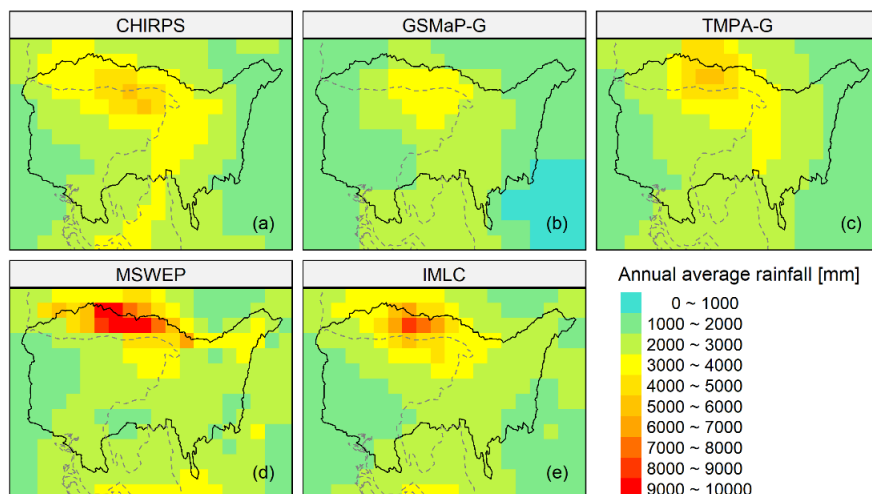


Figure 3.12: Annual average rainfall distribution at 0.25° grid resolution for (a) CHIRPS, (b) GSMaP-G, (c) TMPA-G, (d) MSWEP, and (e) IMLC product during the study period (2009–2016).

3.6.6 Validation of the IMLC product outside Bangladesh

As discussed earlier, India does not share any kind of hydro-meteorological data with Bangladesh, officially. Therefore, we could not validate the satellite time series (either the GSRPs or the IMLC product) at either spatial or temporal scale outside the Bangladesh portion of the Meghna basin. However, the India Meteorological Department shares some customized rainfall information on its website (<http://www.imd.gov.in/>); for example, it shares the district-wise monthly average rainfall, and the district-, subdivision-, and state-wise weekly accumulated rainfall. The monthly average rainfall figures are available for the last five years, whereas the weekly rainfall for the past week is given online only for the current time. The district-wise monthly average rainfall figures are calculated based on the arithmetic averages of the monthly accumulated rainfall values for the stations located in that district. Among the 26 districts that lie fully or partially within the Indian part of the Meghna basin, the monthly average rainfall of nine districts (e.g., South Garo Hills, West Khasi Hills, East Khasi Hills, Jaintia Hills, Cachar, Karimganj, Hailakandi, North Tripura, and Dhalai; Figure 2.1a) is compared with the corresponding district-average monthly rainfall figures derived from the GSRPs and from the IMLC product for the period of 2012–2016 (five years). Figure 3.13a–i show Taylor diagrams that compare the district-average monthly time series of the satellite products (both the original GSRPs and IMLC) against that of the observed rainfall for the aforementioned nine Indian districts. Of the three indices (NRMSD, NSD, and CC) shown in the Taylor diagrams, NRMSD and NSD errors are lower and CC is higher for the IMLC product than for each of the GSRPs in every district, which indicates IMLC's strength in detecting the magnitude and spatio-temporal distribution of monthly rainfall in the Indian portion of the basin.

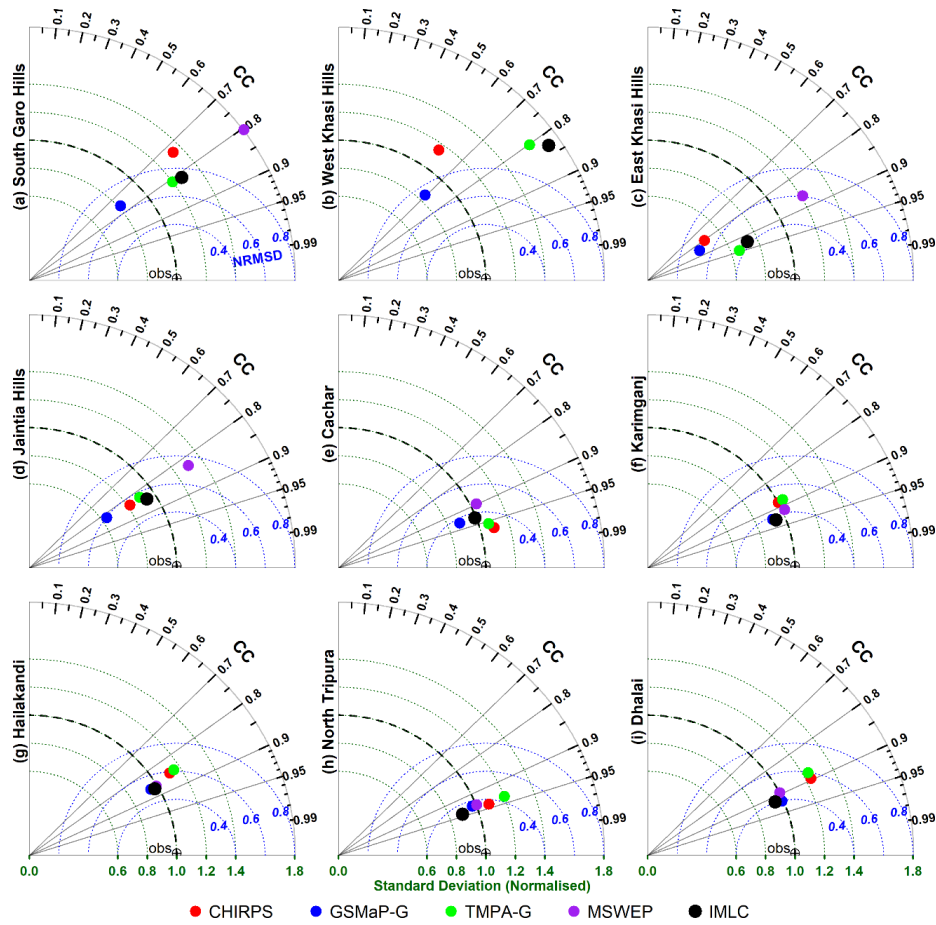


Figure 3.13: Taylor diagram with a comparison of the monthly accumulated district-average rainfall estimates (calculated from the original GSRPs) and IMLC product (the improved dataset created in this study) relative to the observed rainfall of nine districts (a–i) located inside the Indian portion of the Meghna basin for the period of 2012–2016. Instructions for reading a Taylor diagram are given in Figure 3.8.

The IMLC dataset, which is created in this study by merging the GSRPs using the IEVW technique and applying the MLC bias-correction method, showed better spatio-temporal representation of rainfall estimates than did the individual GSRPs at all the gauge stations, including the five validation stations located inside the Bangladesh portion of the Meghna basin. In particular, the three validation stations (Sunamganj, Sheola, and Nakuagaon) that experienced heavy rainfall in the basin, all of which are located near or on the Bangladesh-India border (Figure 3.1), resulted in better estimations of rainfall for the IMLC product (Figure 3.10a–c). The IMLC product also showed improved results for

monthly average rainfall estimates relative to those of observed rainfall for the nine districts in the Indian portion of the basin (Figure 3.13a–i). Therefore, it can be assumed that this IMLC product (which has a grid resolution of 0.25°) can provide better estimation of rainfall in all the grid cells in the basin, both inside and outside of Bangladesh. Given this assumption, the IMLC product is hereafter treated as the improved rainfall dataset for streamflow simulations in the basin.

3.6.7 Streamflow simulations with the improved dataset (IMLC product)

The applicability of the improved rainfall dataset is investigated by simulating streamflows at two critical stream-gauge stations in the Meghna basin using the RRI hydrological model. To produce more reliable streamflows, the parameters of the RRI model are needed to be calibrated and validated for the Meghna basin. Thus, the model is first calibrated with the improved rainfall dataset for the period of 2009–2012 at the basin's outlet, Bhairab Bazar station (Figure 3.1). The model validation is also performed at this station using the improved dataset for the period of 2013–2016. Similarly, an additional validation of the model is also carried out at the Amalshid stream-gauge station (one of the Meghna River's prime entrance point into Bangladesh) for the entire period of the study (2009–2016).

Figure 3.14a,b show daily hydrographs of the observed and simulated streamflows at Bhairab Bazar station for the period of model's calibration and validation. Figure 3.15 shows the daily hydrographs of the observed and simulated streamflows at Amalshid station, which are plotted for the purpose of providing additional model validation and for checking the performance of the improved rainfall dataset when simulating incoming streamflows from the Indian part of the basin. The calculated model-performance indices are presented in Table 3.4 for the calibration, validation, and additional-validation

periods. The calculated NSE is 0.93, 0.93, and 0.75, while the CC is 0.98, 0.97, and 0.86 for the calibration, validation, and additional-validation periods, respectively. The other three statistics in Table 4: RMSE, VB, and NMSE show overall satisfactory indices in all three phases. These statistical indices (Table 3.4), together with the hydrographs (Figures 3.14 and 3.15), reveal that the RRI model simulations using the improved rainfall dataset reproduce the timing and volume of the streamflows, as well as the seasonal, annual, peak, and low flows very well, which indicates that the improved dataset has the potential to provide accurate streamflow estimates across the basin. This improved dataset can, thus, be used as a reference rainfall dataset for long-term hydrological applications, damage assessments, and other climatic applications in the Meghna basin.

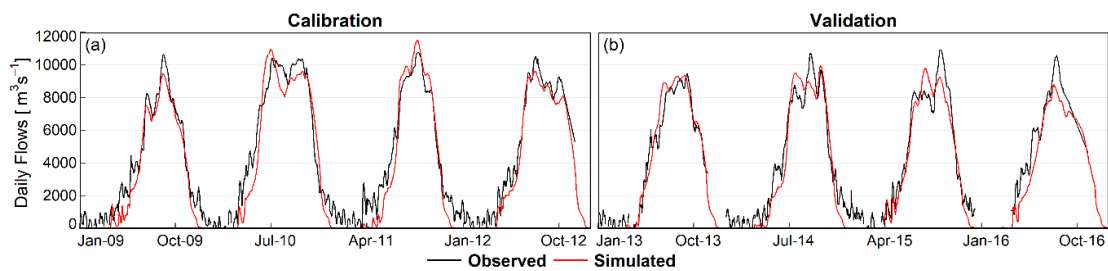


Figure 3.14: Daily observed streamflows (black) and simulated streamflows (red) produced by the improved rainfall dataset (the IMLC product) for the periods of (a) calibration (2009–2012) and (b) validation (2013–2016) using the RRI model at the Bhairab Bazar stream gauge. See Table 3.4 for the statistical metrics used to evaluate the simulated streamflows.

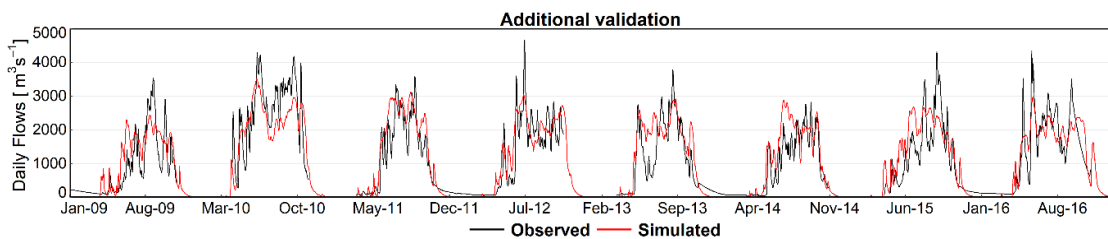


Figure 3.15: Daily observed streamflows (black) and simulated streamflows (red) produced by the improved rainfall dataset for additional validation of the RRI model at the Amalshid stream gauge during the entire study period (2009–2016). See Table 3.4 for the statistical metrics used to evaluate the simulated streamflows.

Table 3.4: Statistical indices used to measure the performance of the RRI model simulations in the calibration, validation, and additional-validation phases.

Rainfall Product	Errors (Units)	Bhairab Bazar Station		Amalshid Station
		Calibration (2009–2012)	Validation (2013–2016)	Additional Validation (2009–2016)
Improved rainfall dataset (IMLC product)	Nash-Sutcliffe Efficiency (NSE) (-)	0.93	0.93	0.75
	CC (-)	0.98	0.97	0.86
	RMSE ($\text{m}^3 \text{s}^{-1}$)	994	939	537
	Volume Bias (VB) (%)	-10	-8	8
	NMSE (-)	0.04	0.04	0.22

3.7 Conclusions

The lack of upstream, basin-wide hydro-meteorological data for the Meghna basin makes flood risk and water resource management challenging for Bangladesh. Moreover, the ground rainfall data inside Bangladesh are sparse in both the time and scale. To overcome such limitations, four GSRPs (CHIRPS, GSMaP-G, TMPA-G, and MSWEP), all of which are freely available at near-present (1–3 week latency), are evaluated to create a reference dataset for hydrological applications in the basin. The applicability of the dataset is investigated by simulating streamflows of the basin.

The performance of the GSRPs is evaluated against the ground rainfall records at the 20 rain-gauge stations inside Bangladesh. The evaluation is conducted at the daily and monthly temporal scales and on a point-to-pixel basis for the rainy seasons of the entire study period (2009–2016). The analyses reveal that all the products have significant weaknesses in detecting the magnitude and spatio-temporal distribution of rainfall. CHIRPS mostly overestimates the rainfall, GSMaP-G mostly underestimates it, and both TMPA-G and MSWEP show varying performance, with both over- and underestimation at the rain-gauge locations. The biases are higher at the daily scale than at the monthly

scale. In the case of capturing rainfall events, the GSRPs perform considerably well, but they come up with many false alarms, too.

Several bias-correction techniques (LCMW, LCSW, MLC, and QM) are applied to improve the GSRPs' daily estimates with respect to the locally-available ground rainfall. Fifteen out of the 20 rain-gauge stations are used to implement the correction techniques, and the other five are used for validating the techniques. The correction factors are calculated at the gauge stations first; then, these station-based factors are distributed using IDW interpolation to yield grid-based factor maps for each time step. Finally, bias-corrected satellite estimates are obtained by combining the original GSRPs with the grid-based correction-factor maps. The first two correction techniques (LCMW and LCSW) show difficulties in correcting the daily GSRP estimates, which might be due to the limitations of GSRPs and to the low correlations existing between the gauges and the GSRPs. The QM method, on the other hand, outperforms both LCMW and LCSW, resulting in high performance indices. However, the MLC correction method is found better than the other three methods and considerably improves upon the daily GSRP estimates by reducing their systematic errors.

Merging of the GSRPs is investigated using three merging techniques (SA, EV, and IEVW) to check whether merging alone can produce a representative rainfall dataset with improved performance than both the original and the bias-corrected GSRPs. Merging improves the data and provides better results than the individual GSRPs. At the daily temporal scale, for which some GSRPs show overestimation of rainfall while others show underestimation, merging these products brings significant improvements. However, although the merged products show improved statistical indicators at three of the five validation stations, the corrected GSRPs (with the best-performing bias-correction

method, MLC) provide better results at the remaining two stations (those that experienced extreme rainfall). Therefore, a combination of merging and bias-correction technique is explored, and the use of the IEVW merging technique followed by the MLC bias-correction method produces the best results and, thus, creates an improved dataset.

Using the improved dataset, the RRI model is then run to generate streamflows for the basin. The generated daily streamflows are compared to the daily streamflows, as measured by two critical stream gauges (Bhairab Bazar and Amalshid; Figure 3.1). The simulated streamflows using the improved rainfall dataset match the observed streamflows well in both pattern and magnitude. The data reproduces the timing and volume of streamflows, as well as the seasonal, annual, peak, and low flows, reasonably well for the whole basin at the outlet (Bhairab Bazar) and for the Indian part of the basin at Amalshid point. This finding indicates that the developed dataset has the potential of generating accurate streamflows for the entire Meghna basin.

Since Bangladesh does not receive any reliable river flow and rainfall information from India in the Meghna basin, the accurate daily streamflow generation performed with the developed rainfall dataset, allows us to overcome the issues of poor data availability and data sharing in the basin which, in turn, helps us to quantify flood flows into Bangladesh. This dataset can also serve as reference rainfall for a wide range of applications in the basin (e.g., flood modelling and forecasting, irrigation planning, damage, and risk assessments, construction of hydraulic structures, and climate-change adaptation planning). In this study, the methodology is also used create rainfall for the 2017 flood, and accordingly a hazard map for the flood in terms of depth, duration, and extent, was generated using the RRI model.

Chapter 4: Establishment of flood damage functions

4.1 Introduction

Under this study's research framework, two of the five key objectives are the assessment of flood damage and risk for both present and future climate. Flood damage and risk assessment in an area provide better flood disaster risk reduction strategies to the policy-makers (Merz et al., 2010; Emanuelsson et al., 2014; Hasanzadeh Nafari et al., 2017; Win et al., 2018). However, they involve three main components: assessment of flood hazard, flood vulnerability, and flood exposure (Messner et al., 2007; Foudi et al., 2015, Kefi et al., 2018). Flood hazard, which is mostly related to inundation depth, duration, and extent, is described in the previous chapter. This chapter of the dissertation is focused on the estimation of flood vulnerability for flood damage and risk assessment in the study area.

4.2 Flood vulnerability and literature review

Flood vulnerability is usually represented by flood damage functions that are derived by correlating flood hazard characteristics with damage (Okazumi et al., 2014a, b; Shrestha et al., 2016). More specifically, flood damage functions define a relationship between inundation depth and economic damage for a particular type of land use (e.g., agriculture) or structure (e.g., house); hence they are also called stage-damage functions (Messner et al., 2007; Merz et al., 2010; Jongman et al., 2014; Hasanzadeh Nafari et al., 2017). These stage-damage functions can be of two types as empirical and synthetic. Empirical damage functions are developed using actual damage data collected after flood events, whereas the synthetic damage functions are developed based on damage data collected by questionnaire survey (Merz et al., 2010; Win et al., 2018). Whether they are empirical or synthetic, damage functions can also be characterised as absolute and relative

functions. Functions which are drawn with monetary damage value are called absolute damage functions, whereas those represented by the percent damage of the total exposed value are called relative damage functions (Kreibich et al., 2010; Hasanzadeh Nafari et al., 2017). As relative damage functions are characterized by damage ratios, they are thus more flexible than absolute functions to be transferred for different time and space since the percent damage is independent of the changes in market values (Merz et al., 2010; Hasanzadeh Nafari et al., 2017; Win et al., 2018).

In Bangladesh, several government agencies are individually responsible for collecting relevant flood damage data after flood events. However, the flood damage data and information recorded by these agencies are limited, inconsistent, and fragmented. Therefore, unlike many developed countries, the empirical type of flood damage functions using actual flood damage data are yet to be established in Bangladesh. The synthetic approach of developing flood damage functions is thus the best alternative in Bangladesh. However, such synthetic damage functions to assess flood vulnerability for flood risk assessment in Bangladesh have not yet been established. Only a few researchers attempted to calculate potential flood risk in the urban areas of Bangladesh (mainly in Dhaka city) by assuming vulnerability as proportional to the population density or by calculating vulnerability as indices assuming several weight factors according to land use classes (Tingsanchali and Karim, 2005; Khan et al., 2012; Masood and Takeuchi, 2012). Two recent studies (Gain and Hoque, 2013; Gain et al., 2015) that were conducted for flood risk assessment in the eastern part of Dhaka also estimated vulnerability either by assuming land use-based weight factors or by using stage-damage relationships or equations that were obtained from several other studies.

Many other researchers and government agencies worldwide attempted to establish flood damage functions via questionnaire surveys for the areas with different content characteristics and established stage-damage relationships through survey results of various damage categories (e.g., agricultural or residential damage) (MOC, 1996; MLIT, 2005; Zhai et al. 2005; Shrestha et al. 2016; Velasco et al. 2016; Hasanzadeh Nafari et al. 2017; Kefi et al. 2018; Win et al. 2018). Other researchers also used depth-damage functions obtained from other countries due to the fact of bearing similar regional content characteristics (Shrestha et al., 2016a & 2016b). The fact is that for north-eastern region of Bangladesh (study area), there is no regional-scale damage functions with identical content characteristics exist, and thus establishing of such functions on a local scale is necessary. To the best of the authors' knowledge, this is the first study that used questionnaire surveys to develop flood damage functions for vulnerability assessment in Bangladesh. Accordingly, this chapter of the dissertation developed reliable flood damage functions for agriculture, house building and household property damage using the data of a structured questionnaire survey that was conducted in two pilot sub-districts of the northeastern Bangladesh. The established damage functions are to be used for flood damage and risk assessment in the mentioned area.

4.3 Study area

The area studied for the component of this chapter is the northeastern part of Bangladesh located downstream of the Meghna river basin, which is described in detail under Chapter 2.

4.4 Methods

Figure 4.1 shows the flowchart of the methodology used in this chapter for developing reliable flood damage curves through the data of a questionnaire survey

conducted in the two sub-districts (Dhakkhin Sunamganj and Balaganj) of the study area in order to assess flood vulnerability for agriculture and households.

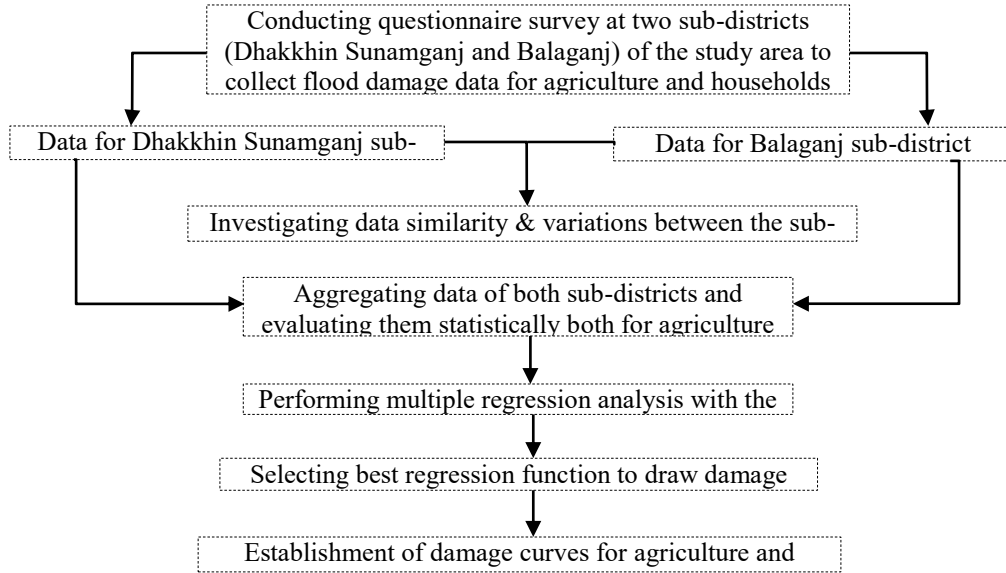


Figure 4.1: Flow chart of the methodology used for establishing reliable damage curves for agriculture and household damage in the northeastern part of Bangladesh.

4.4.1 Outline of questionnaire survey

During flood time, the people of the study area mainly worry about their nearly-ready-for-harvesting Boro rice and their houses with household properties. According to the daily disaster reports of April 28, 2017 (published on May 4, 2017), by the Department of Disaster Management (DDM, 2017), Boro rice damage, number of affected and destroyed houses, and loss of livestock were reported for the 2017 flood. Any other types of private and public property damage (such as local road damage, embankment damage, etc.) were not stated in the report. No casualties were reported as well. Also, during the past floods of 2004, 2010 and 2016, damage to Boro rice and households were only reported by Bangladesh Bureau of Statistics (BBS, 2011 & 2017). Given such previous reports, Boro rice and household damage were found as major concern for the government and policy makers to draw roadmap for sustainable development. Therefore, based on the

available reported data, Boro rice, house building and in-house property damage classes were considered for this study to conduct the survey work discussed in this chapter, and accordingly estimated and verified their flood damage for 2017 flood in the next chapter. However, other damage classes, such as road damage, livestock damage, etc. are recommended to be included in a future study to collect their damage data through field survey and estimate their damage due to floods.

A questionnaire survey was conducted to collect primary data on Boro rice damage, house building damage, and in-house property damage against flood depths and duration at the aforesaid pilot sub-districts of the study area from November 25th to December 6th, 2018 (12 days). The reasons for selecting Dhakkin Sunamganj and Balaganj as pilot area for conducting the questionnaire survey are: (1) Boro rice and households of these two sub-districts were affected and damaged in larger quantity during the recent 2017 flood (DDM, 2017); (2) As described in Section 2.2, northeastern Bangladesh is mainly surrounded by two river systems, the Surma and Kushiya, and each of the pilot sub-districts was chosen from these two independent river systems; and (3) Both sub-districts consist of three different types of households (BBS, 2011). However, about 81 percent of the households of Dakkin Sunamganj sub-district are of one type whereas the Balaganj sub-district consists of all three types of households. Therefore, to get more generalized results, these two sub-districts were selected; (4) Access to the selected sub-districts from the district headquarters were easy that made possible to complete the survey work within the stipulated time.

To calculate the minimum representative sample size of the target damage categories (i.e., samples of farmers for Boro rice damage and of households for house and property damage), a probability sampling technique was used. For doing so, population

size of farmers having more than 0.05 acre of operating land and households comprising of at least two members were obtained from the Bangladesh Bureau of Statistics for the aforesaid sub-districts. The obtained population size were 39941 and 86279 for farmers and households, respectively (BBS, 2011). Using a confidence level of 90 percent, a margin of error of 6 percent for farmers and 6.5 percent for households, and considering a response rate of 50 percent, the target minimum sample size was calculated, and that for farmers and households were 188 and 160, respectively. The actual number of samples collected at the field during the questionnaire survey were 196 and 165 for farmers and households, respectively. Therefore, the surveyed dataset for this study can be considered sufficient and reliable. Table 4.1 shows the population size, minimum and collected number of sample size by sub-district. The designed sample questionnaires for Boro rice and households are presented in Appendix A1 and Appendix A2, respectively. Some of the pictures taken during the survey activities are presented in Appendix B.

Table 4.1: Total population size, standard minimum sample size, and collected number of actual sample size by sub-district

Item	Sample class	Sub-districts	
		Dakkhin Sunamganj	Balaganj
Population size	Farmers	39941	
	Households	86279	
Calculated minimum sample size	Farmers	188	
	Households	160	
Collected sample Size (% of total)	Farmers	131 (66.8)	65 (33.2)
	Households	67 (40.6)	98 (59.4)

As mentioned above, the survey work was conducted for 12 days, and that for seven days in Dhakkhin Sunamganj sub-district under Sunamganj district and for five days in Balaganj sub-district under Sylhet district. As depicted in Table 4.1, total number

of samples collected in Dhakkhain Sunamganj sub-district were 131 farmers for rice damage data collection and 67 households for building and property damage data collection. On the other hand, the total samples collected in Balaganj sub-district for Boro rice and household damage were 65 and 98, respectively. An average of 30 samples were collected each day from dawn to dusk spending an average of 15–20 minutes per sample. An average of 5 minutes was spend to make the questionnaire understandable for the respondent and the remaining time was used to get the answers to the questions. Three employees (sub-assistant engineers, surveyors) from BWDB constantly supported conducting the survey. Every day in the morning, Boro rice damage survey was conducted in a local village bazar (market place) by gathering 5–10 farmers. The farmers were notified beforehand to gather in such a place with the help of the BWDB staffs. An average of 30 percent Boro damage sample were collected from this kind of gathering. After collecting Boro damage data in such a way, remaining samples were collected from each individual farmer by moving one village to another. While collecting Boro damage data from individual farmer/household in village/paddy field, household damage data (includes both building and in-house property damage) were also collected at the same time. Sometimes the same individual was the respondent to answer for the Boro rice as well as household damage. All of the respondents who answered the questionnaires of Boro damage were male; only about 5 percent of the respondents who answered the household damage questionnaires were female. Almost all of the respondents were of 30–50 years of age.

To avoid subjectivity of a questionnaire survey, following points are usually needed to keep in mind while designing the questionnaires (Gopikrishnan and Vinay, 2016):

- Making short and clear questions
- Avoiding hypothetical questions
- Breaking down difficult questions
- Keeping the time period short and relevant
- Providing simple and exhaustive set of answer options
- Using precise, simple language

The questionnaires of this study's survey work (presented in Appendix A1 and Appendix A2) were designed considering the above points to avoid the subjectivity of the respondents. Avoiding respondent's subjectivity during the interview process improves the accuracy of the survey. Usually subjectivity of a respondent in a questionnaire survey is produced by an inability or lack of desire to answer questions correctly, which are further caused by a lack of experience or knowledge, lack of ability to recall information, unfamiliarity with the item questioned for, respondent fatigue, etc. (Gopikrishnan and Topkar, 2014). This can also take place when the questionnaires are not written correctly.

It is noteworthy to be mentioned that 1–2 months prior to the actual survey work, draft questionnaires were prepared by the author and sent them to the BWDB employees (the author's colleagues) to carry out discussions with the farmers/households whether the question set in the draft questionnaires are understandable to the respondents. The BWDB colleagues went to the sample areas, randomly selected 60 potential farmers/households (30 for each sub-district), and directly asked and discussed the draft questions to get real responses. From such discussions, the recommendations and corrections made by the respondents over the draft questionnaires were collected by the BWDB colleagues and sent back to the author to consider them for finalizing the questionnaires. Based on these obtained feedbacks, the design of the sample

questionnaires were finalized to make them easily understandable for the respondents and accordingly used them in the actual questionnaire survey. During the actual survey, all the questions under the questionnaires were asked to the respondents by the author himself with the help of the BWDB colleagues, and the answers were written down by the author. No questionnaire was given to the respondents to answer the questions by themselves. In such a way, the subjectivity of the respondents was significantly avoided in the questionnaire survey, which increased the accuracy of such survey. However, it is recommended to undertake such questionnaire survey again in future study for another flood to make an objective evaluation of such questionnaire survey.

In this study, the questionnaire survey was mainly conducted considering the recent pre-monsoon flood (flash flood) of 2017. However, the sample questionnaires also included some comprehensive questions for other floods as well, such as floods in 2004, 2010, and 2016. Refer to Appendix A.1 for questions a4, a5, and a6 about Boro rice damage. For household damage, on the other hand, refer to Appendix A.2 for questions a5, a6, a7, and a8. During the survey, the real reaction to these thorough questions related to flood depths, duration, and damage for the flood years of 2004, 2010, and 2016, seemed difficult to response by the respondents. Due to their forgotten memory, most of the respondents were not able to provide adequate information on flood depths, duration, and damage of Boro rice and households for the 2004, 2010, and 2016 floods. However, the respondents were able to recall such information for the 2017 flood and answer the questions for this recent past flood. Therefore, the damage data collected against flood depths and duration via the questionnaire survey in this study for each damage class were based on the 2017 flood.

4.4.1.1 Boro rice damage survey

Boro rice is the major crop of northeastern Bangladesh planted usually in mid-December to early January and harvested by late April. The damage of Boro rice mainly takes place 20-30 days before its harvesting time due to flash floods that are likely to occur almost every year due to heavy rainfall in the mountains of the upper Meghna basin in India. Therefore, although rice damage due to flood varies with its growing stages, that of the Boro rice mainly takes place in its flowering through maturity stage, and thus, considering this stage of Boro rice, a total number of 196 flood affected farmers were interviewed during the field survey. Each target interviewee was asked to reply to the reduced amount of rice yield in terms of varying flood depths and duration while conducting the questionnaire survey. The length of the Boro paddy, its average expected yield per unit area, its value per unit weight, its production damage per unit area during the recent flood years, and many other data were also collected from the Boro damage survey.

4.4.1.2 Household damage survey

Several steps are required for developing household damage functions. The major step of these is the classification of houses by type, age, and social status (Messner and Meyer, 2005). During the field survey, three types of houses were noticed according to their building materials. They are shown in Figure 4.2(a-c) and called as (a) Mud (locally called as Kaccha), (b) Brick (locally called as Semi-Packa), and (c) Concrete (locally called as Packa) houses. It is to be noted that the houses observed in the surveyed area were all one-story building structure, and the house type that was mostly seen in the area is Mud. Two kinds of household damage were considered while the questionnaire survey was conducted. They are the house building damage (termed as house damage hereafter)

and household property damage (termed as property damage hereafter). House damage mainly included the repair cost of a damaged house or the reconstruction cost of a destroyed house. On the other hand, the damage to in-house stored Boro rice, furniture, kitchen items, appliances, clothes, radio, television, and other household goods were considered as property damage. A total number of 165 flood affected households, as said before, were interviewed to gather information on house and its property damage according to varying flood inundation depths. Several other questions, such as the value and plinth level (floor height from the ground level) of the target houses, the inventory of household properties and their total value, and the depth of inundation the houses experienced during the recent flood events, were also asked at the time of household damage survey.



Figure 4.2: Different types of houses according to building materials. (a) Mud: made of mud/soil, straws, bamboo sticks, jute sticks, and corrugated iron sheet; (b) Brick: made of mud/cement, bricks, and corrugated iron sheet; (c) Concrete: made of bricks, cement, brick/stone chips, and steel rods.

4.4.2 Development of flood damage functions

In this study, three flood damage functions, i.e., depth-duration-damage function for Boro rice, depth-damage function for the three house types, and depth-damage function of household properties for each house type, were developed through the data of the above described questionnaire survey. During the survey, the reduced yield of Boro rice in terms of varying inundation depths and duration was collected as per a local measurement unit called Maund per Bigha (equivalent to 330 kilogram per hectare). To

make it clear for all readers, this local unit of measuring rice yield was converted to its equivalent of metric ton (MT) per hectare for this study. The house and its property damage, on the other hand, were collected in Bangladesh currency (Taka), and for this study, to make it independent of the changes in market values and to transfer for different time and area, the damage of the houses and their properties was normalized and expressed as percent damage using the following equations:

$$PHD_{i,j} = 100 * HDV_{i,j}/HV_{i,j} \quad 4.1$$

$$PHPD_{i,j} = 100 * HPDV_{i,j}/HPV_{i,j} \quad 4.2$$

where, $PHD_{i,j}$ is the house damage in percentage for the house type i and sample j , $HDV_{i,j}$ and $HV_{i,j}$ are the house damage value and house building value, respectively, for the house type i and sample j ; $PHPD_{i,j}$ is the property damage in percentage for the house type i and sample j , $HPDV_{i,j}$ and $HPV_{i,j}$ are the property damage value and household total property value, respectively, for the house type i and sample j .

In order to develop a relationship between flood damage and inundation parameters (depths and duration) using the primary data of a questionnaire survey, many previous researchers suggested to perform multiple regression analysis (Zhai et al., 2005; Grahn and Nyberg, 2017; Kefi et al., 2018; Win et al., 2018). Thus, using five models, this study also performed regression analysis with the surveyed data to generate depth-damage relationships for each target damage category. The function names and their equations of the five regression models are listed out in Table 4.2.

Table 4.2: Name and equations of the regression models used in this study.

Regression Models	Equation of function
Linear	$y = a + bx$
Logistic	$y = a/(1 + be^{-cx})$
Natural Logarithm	$y = a + b \ln(x)$
Polynomial (3rd order)	$y = ax^3 + bx^2 + cx + d$
Power	$y = ax^b$

y = dependent variable = Damage of Boro rice, house, and property;

x = Independent variable = Depth of inundation; a, b, c and d are parameters of the functions

To evaluate the performance of the models, four indicators, the Coefficient of Determination (CD), Correlation Coefficient (CC), Standard Error (SE), and Akaike's Information Criterion (AICC), were used. A perfect model should have the CC and CD indices of 1. In addition, the lower the SE and AICC indices, the better the model performance.

4.5 Results and discussion

For this study, a questionnaire survey, emphasizing the flood damage to agriculture and households, was conducted in the study area to construct their synthetic type of reliable flood damage functions. Agricultural damage survey was explicitly conducted for Boro rice, which is the major crop cultivated in the study area and frequently suffers from the pre-monsoon flash floods just before its harvesting. The household survey, on the other hand, was mainly focused on the house building damage and in-house property damage. By using five regression models, statistical analyses with the surveyed data were performed to develop reliable damage functions for the target damage classes. The model that performed the best according to the performance indices described in the previous chapter was selected to draw the damage curves for the respective damage class.

4.5.1 Development of agricultural damage curves

Flood damage to Boro rice was considered as agriculture damage in this study. Damage to rice is mainly governed by flood depths, duration, and growing stages of rice. However, damage to Boro rice takes place in its flowering through maturity stage because of the flash floods that hit the study area 20-30 days before harvesting the rice. Therefore, during the questionnaire survey, each target farmer was asked about the flood damage to Boro rice in terms of varying inundation depths and duration considering only the flowering through maturity stage of the rice. The target farmers were also asked to reply to several other questions such as the length of the Boro paddy, its average expected yield per unit area, its value per unit weight, and etc. The data collected for 196 target samples indicated that the average length of the Boro paddy is about 85 cm and its initial flood damage usually starts after 2-3 days of inundation at a depth of about 30 cm. Some of the characteristics of the Boro rice revealed from the surveyed data are shown in Table 4.3.

Table 4.3: Characteristics of Boro rice in the sample area

Rice type	Average length (cm)	Average yield (MT/hectare)	Depth at which flood damage starts (cm)	Duration at which flood damage starts (day)
Boro	85	4.95	30	2-3

While conducting the survey in two selected sub-districts of the study area, flood damage to Boro rice was collected in terms of its yield damage considering the varying depths of 30, 45, 60, 75, and 90 cm and varying range of duration of 1–3, 4–7, and above 7 days. To see its variation between the sub-districts, the surveyed dataset collected for each sub-district was compared using four statistical indices (mean, median, mode and standard deviation). This comparison was performed for each set of flood duration and shown in Figure 4.3a–c. The results showed slight variability within the dataset of the sub-districts considering all four statistics. This might be due to the fact that the

topography, land use, households, and people’s livelihoods in the northeastern part of Bangladesh are very similar. It is thus expected that the damage curves that are to be developed by this study can not only be used for flood damage assessment in the pilot sub-districts but the entire area of northeastern Bangladesh as well.

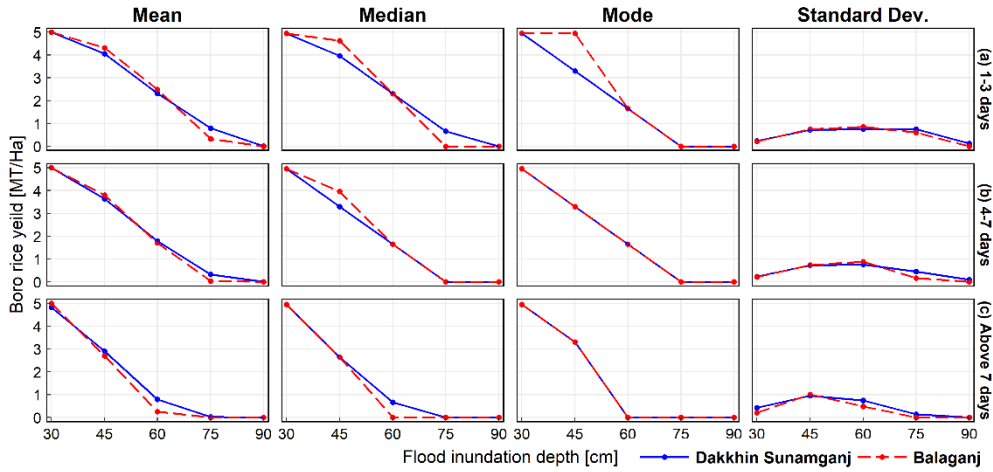


Figure 4.3: Comparison between the collected dataset of two sub-districts using four statistical indices, and performed for the flood duration of (a) 1–3 days, (b) 4–7 days, and (c) above 7 days.

Given the collected data of the two sub-districts a whole for each set of flood duration, box and whisker plots of the dataset were plotted to depict the relationship between the yield loss of the Boro rice and flood depths. The plots are shown in Figure 4.4a–c. Several statistics of the dataset, such as the mean, median, mode and standard deviation, are also drawn in the figure.

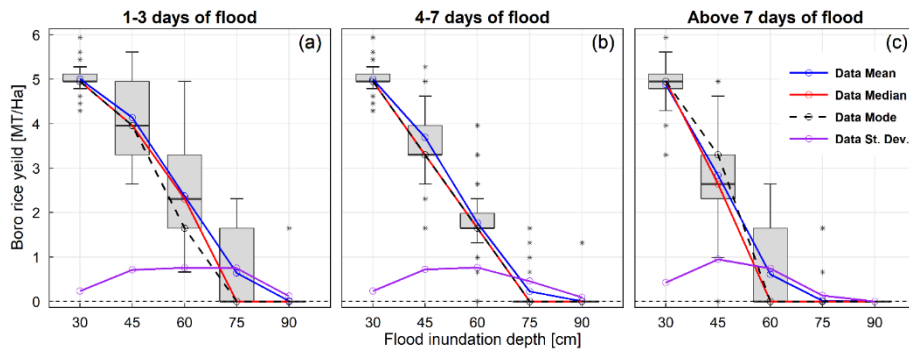


Figure 4.4: Distribution of rice yield loss against selected flood heights, plotted in box and whisker plots with the collected 196 target samples for the flood duration of (a) 1–3 days, (b) 4–7 days, and (c) above 7 days.

For 1–3 days of flood, the yield loss at flood heights of 45, 60, and 75 cm showed larger variability in the dataset (Figure 4.4a). A moderate variability for the depths of 45 and 60 cm was shown in the case of the flood that lasted more than 7 days (Figure 4.4c). However, the data for 4–7 days of flood, on the other hand, showed slight variations in yield loss at all depths of inundation (Figure 4.4b). The variability in the dataset might be due to the effect of selecting several days on a single set of flood duration. This might also be caused by the interviewee’s responses that are subject to their individual experiences and memories related to flood damage. Although variability and inconsistency were somewhat observed in the collected data of Boro rice damage, the standard deviation of the dataset was obtained reasonably small in quantity for each selected depths and duration, which indicates sufficient reliability of the collected data. Using these reliable data, regression analyses with five models were performed to establish a best fit relationship between rice damage and flood depths for each range of selected flood duration. The results of the regressions are provided in Table 4.4.

Table 4.4: Results of five regression models performed with 196 target samples collected for Boro rice damage due to flood

Regression Models	No. of samples	Flood duration	Value of parameters				SE	CC	CD	AICC
			a	b	c	d				
Linear	196	1-3 days	7.826556	-0.0899	-	-	0.65	0.95	0.90	-835.24
		4-7 days	7.518275	-0.0896	-	-	0.67	0.94	0.89	-794.51
		Above 7 days	6.702198	-0.0838	-	-	0.91	0.89	0.79	-183.81
Logistic	196	1-3 days	0.000194	-1.0000	0.000002	-	1.07	0.85	0.72	138.99
		4-7 days	0.000267	-1.0000	0.000004	-	0.98	0.87	0.76	-37.353
		Above 7 days	0.000755	-1.0001	0.000006	-	0.84	0.90	0.81	-304.25
Natural Logarithm	196	1-3 days	21.97742	-4.8574	-	-	0.72	0.93	0.87	-653.06
		4-7 days	22.03312	-4.9442	-	-	0.62	0.95	0.91	-939.55
		Above 7 days	20.96035	-4.7942	-	-	0.73	0.93	0.87	-611.68
Polynomial (3 rd order)	196	1-3 days	0.000049	-0.0087	0.387006	-0.0781	0.59	0.96	0.92	-1046.25
		4-7 days	0.000047	-0.0078	0.293776	1.9257	0.53	0.97	0.93	-1260.42
		Above 7 days	0.000019	-0.0016	-0.110532	9.1686	0.59	0.95	0.91	-1024.53
Power	196	1-3 days	946.2634	-1.5166	-	-	1.01	0.87	0.75	21.916
		4-7 days	2300.416	-1.7837	-	-	0.89	0.90	0.80	-223.88
		Above 7 days	15824.16	-2.3661	-	-	0.79	0.92	0.85	-470.05

Following the equations of their individual function, each regression model could predict a relationship of rice yield loss with respect to inundation depths for the three duration ranges. Figure 4.5a–c show the depth-damage relationships of Boro rice predicted by the five regression models for each set of duration. The calculated performance indicators are also shown in the figure.

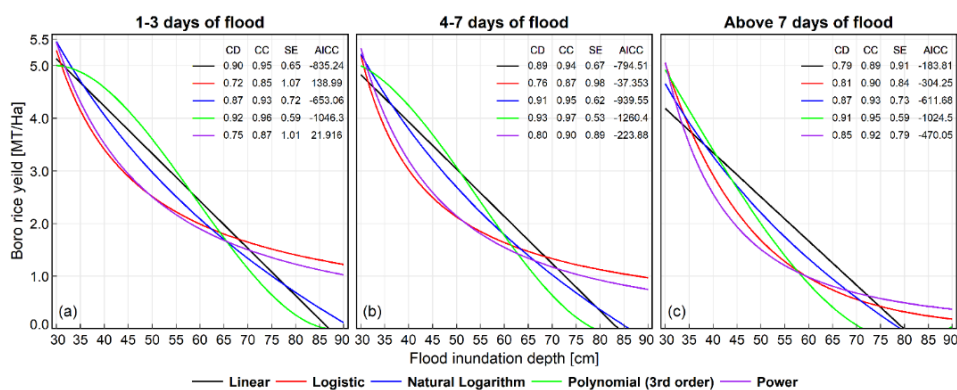


Figure 4.5: Damage curves predicted by five regression models for each set of flood duration of (a) 1–3 days, (b) 4–7 days, and (c) above 7 days.

The results depicted in Table 4.4 and in Figure 4.5a–c indicate that the performance of each regression model for each range of duration agrees reasonably well with satisfactory indices. Even the simplest linear type model showed good performance with a CC and CD values ranging from 0.89 to 0.94 and from 0.79 to 0.89, respectively. However, of the five regression models, the model that performed the best for each range of flood duration was the polynomial type. Compared to the other four models, it showed the higher magnitude of CC and CD values (ranging between 0.95 and 0.97 and between 0.91 and 0.93, respectively) together with the lower values of SE and AICC indices (ranging from 0.53 to 0.59 and from -1260.42 to -1024.53, respectively). Considering its best performance among all regression models, the polynomial type (3rd order) was chosen to establish the damage function of the Boro rice for this study. Figure 4.6a–c show the damage curves of Boro rice drawn for the different range of flood duration using the best selected regression model performed with the data of the questionnaire survey. To avoid the differences between the actual and collected damage, an uncertainty band of standard deviation ($\pm 1\sigma$) was integrated to the established damage curves. The curves revealed that the rice yield becomes near zero when the flood height exceeds 75 cm (the depth at which grains start to flourish), regardless of the inundation duration. One important finding revealed from the developed Boro damage curves was that Boro paddy can allow water with no damage up to an average of 25 cm depth (at which tiller of rice evolves). However, allowing water up to such a depth usually delay the maturity of rice by about 15-20 days.

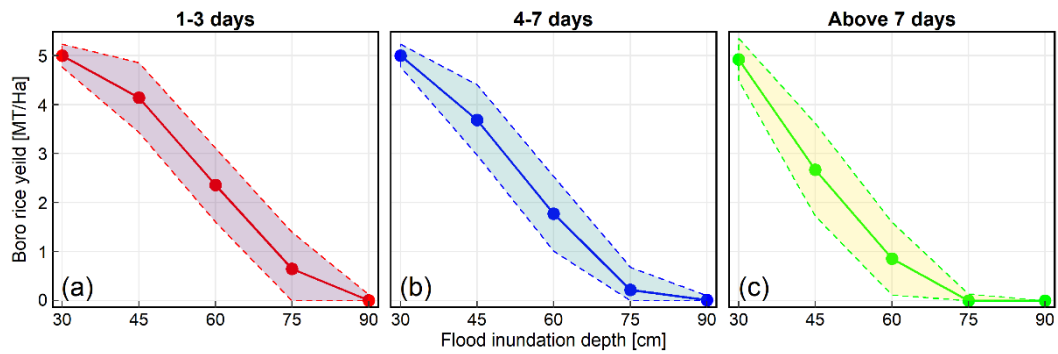


Figure 4.6: Flood damage curves of Boro rice developed via the data of a questionnaire survey conducted in the study area for the duration range of (a) 1–3 days, (b) 4–7 days, and (c) above 7 days. Standard deviation ($\pm 1\sigma$) is added to show the uncertainty bands.

4.5.2 Development of household damage curves

During the questionnaire survey, a total number of 165 flood affected households under the selected sub-districts were interviewed; out of which, 91 were categorized as Mud, 41 as Brick, and 33 as Concrete. The household survey produced a wide range of useful information that help develop damage functions for the three types of houses and their in-house properties.

4.5.2.1 House building damage curves

House building damage is mainly dominated by flood inundation depths. Therefore, in the field, each target household was asked to estimate the repair or the reconstruction cost of their houses according to the varying inundation depths. Several other questions were also asked; for example, the average value of each type of houses (excluding in-house property value) and the average floor level of the houses from the ground (plinth level). The type of houses, together with their average value, their average plinth level, and their distribution in the sample area, are provided in Table 4.5.

Table 4.5: Characteristics of different house types observed in the study area

House type	Proportion (percent)	Average plinth level (m)	Average value (Thousand BDT/\$US)
Mud	55	1.5	276/3246
Brick	25	1.8	685/8057
Concrete	20	1.8	1436/16890

During the survey in both sub-districts, the flood damage to house buildings was collected in terms of varying flood heights above plinth level of 30, 60, 90, 120, 150, 180, and 215 cm. The collected data was in monetary value expressed in Thousand BDT. To be used for different time and space, the data was normalized and expressed in percent damage using Equation 4.1. Similarly to Boro rice damage, the variability in house damage within the sub-districts was also investigated by four statistical indices and shown in Figure 4.7a–c.

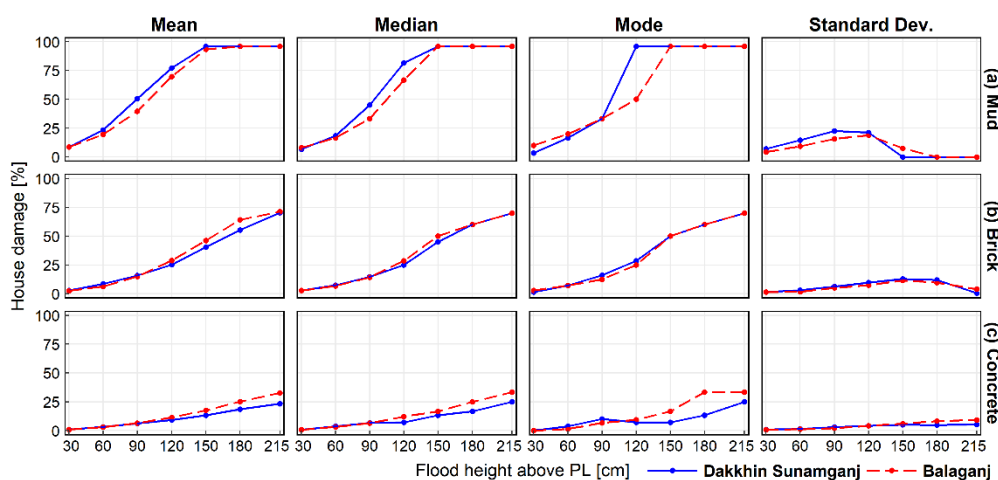


Figure 4.7: Comparison between the collected datasets of two sub-districts using four statistical indices for (a) Mud, (b) Brick, and (c) Concrete houses.

Because of similar topography, land use, households, and people’s livelihoods in the study area, an insignificant variation within the house damage data of each sub-district was observed (Figure 4.7a–c). Therefore, the damage data collected for each sub-districts was considered as a whole and plotted against the selected flood heights for all three types

of houses in box and whisker plots to see the depth-damage relationship. The plots are shown in Figure 4.8a-c. The mean, median, mode and standard deviation of the dataset are also shown in the Figure.

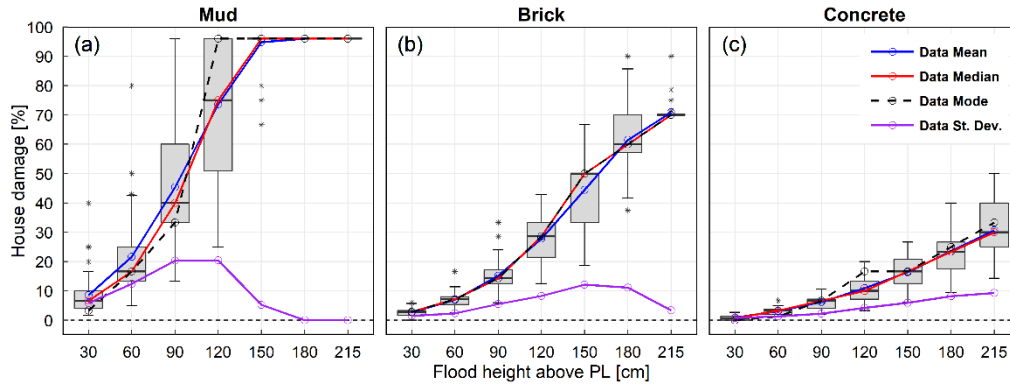


Figure 4.8: Distribution of house building damage against selected flood heights, plotted in box and whisker plots with the collected 165 target samples for the house types of (a) Mud, (b) Brick, and (c) Concrete.

Larger house damage variation was observed within the dataset for the Mud house type, particularly for the 90, and 120 cm of flood heights. This might be due to the effect of household responses that are dependent on both the experiences and memories of the respondent. Another reason could be the variety of building materials the Mud houses are constructed of. The roof of some Mud houses are made of iron sheets, whereas some are of straws. The wall, on the other hand, are sometimes built with straws and sometimes with jute sticks or bamboo sticks. The Brick and Concrete houses showed a mild variability within the damage data indicating consistency of the dataset. Although the house damage data resulted in larger to mild variability for all three types of houses, the standard deviation of the dataset for each type of house was found satisfactorily low for almost all flood heights, which indicated that the dataset is entirely reliable. Using these house damage data, regression analyses were performed to identify the best depth-damage

relationships for the three types of houses. The regression results are provided in Table 4.6.

Table 4.6: Results of five regression models performed with 165 target samples collected for flood damage to three types of houses.

Regression Models	No. of samples	House type	Value of parameters				SE	CC	CD	AICC
			a	B	c	d				
Linear	91	Mud	-2.308075	0.5351	-	-	16.27	0.89	0.80	3553.63
	41	Brick	-15.62295	0.4010	-	-	8.55	0.94	0.89	1231.80
	33	Concrete	-6.782667	0.1649	-	-	5.85	0.87	0.75	815.95
Logistic	91	Mud	99.00861	44.638	0.041039	-	12.46	0.94	0.88	3215.06
	41	Brick	79.30398	62.377	0.029431	-	7.54	0.96	0.92	1160.66
	33	Concrete	39.41865	47.180	0.023697	-	5.60	0.88	0.77	797.24
Natural Logarithm	91	Mud	-177.9507	51.972	-	-	15.30	0.91	0.82	3474.91
	41	Brick	-131.2998	35.499	-	-	12.70	0.87	0.76	1458.76
	33	Concrete	-53.69458	14.456	-	-	7.13	0.79	0.63	907.54
Polynomial (3 rd order)	91	Mud	-0.000033	0.0097	-0.118620	3.0656	12.53	0.94	0.88	3222.89
	41	Brick	-0.000018	0.0073	-0.476719	11.582	7.60	0.96	0.92	1165.95
	33	Concrete	-0.000002	0.0013	-0.043291	1.1611	5.61	0.88	0.77	798.68
Power	91	Mud	0.058441	1.4348	-	-	16.24	0.89	0.80	3551.03
	41	Brick	0.011702	1.6321	-	-	8.14	0.95	0.90	1203.81
	33	Concrete	0.002243	1.7762	-	-	5.59	0.88	0.77	795.46

Using the regression results, the function of each regression model was able to estimate the house damage with respect to the flood inundation depths. The estimated house damage for all three types of houses were plotted against the flood heights above plinth level in Figure 4.9a–c. The calculated performance indicators are also shown in the figure.

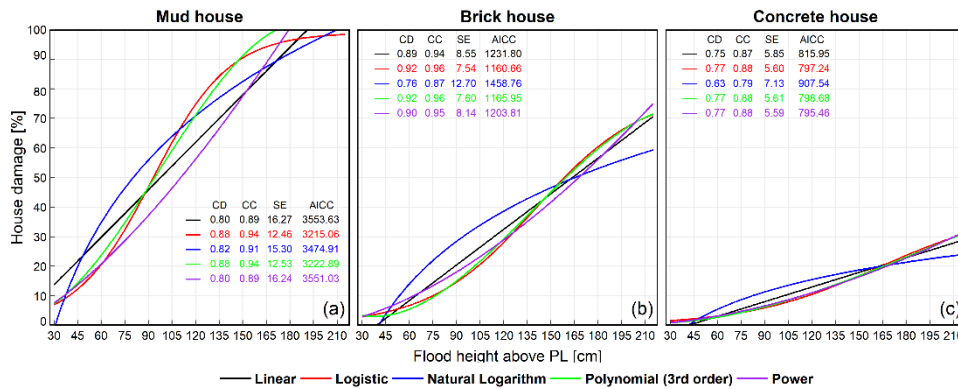


Figure 4.9: Depth-damage relationships predicted by five regression models for the house types of (a) Mud, (b) Brick, and (c) Concrete.

According to the performance indicators shown in Table 4.6 and Figure 4.9a–c, although each of the models showed satisfactory performance for all three types of houses, the logistic model performed the best for the Mud and Brick houses producing the larger CC and CD values with smaller SE and AICC values. For the Concrete house type, on the other hand, the power regression model produced the best indicators. Although the logistic, polynomial and power models produced identical CC and CD indices for the Concrete house type, the other two indices, however, were generated with better indices for power model than the two other models. Therefore, the less complicated power model was selected instead of the more complicated polynomial and logistic model for the Concrete type of house. Figure 4.10a–c show the flood damage curves developed for the Mud and Brick houses using the results of logistic regression model, and for the Concrete houses using the regression results of power type model. To avoid the differences between the actual and collected damage, an uncertainty band of standard deviation ($\pm 1\sigma$) was incorporated to each of the established damage curves. The curves revealed that the flood damage to Brick and Concrete houses never reaches one hundred percent irrespective of the flood heights, because of their building materials. The

construction method and materials of the Mud houses make them most vulnerable to flood, compared to the other two types of houses.

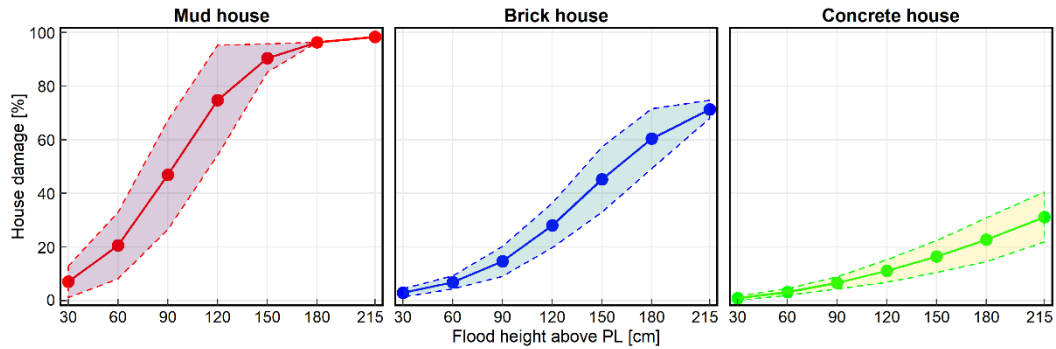


Figure 4.10: Flood damage curves developed through the data of the questionnaire survey conducted in the study area for (a) Mud, (b) Brick, and (c) Concrete type of houses. Standard deviation ($\pm 1\sigma$) is added to show the uncertainty bands.

4.5.2.2 Household property damage curves

The damage to household properties in each sub-district for the total 165 households were collected in monetary value with a currency of Thousand BDT, and for this study, they were converted into percent damage using Equation 4.1. The distribution of the data collected for each sub-district was compared, and no significant variability was found according to four statistical indices shown in Figure 4.11a–c. Hence, considering the entire 165 samples, the property damage to all three types of houses were plotted in box and whisker plots against the selected flood heights. The plots, together with the data’s mean, median, mode and standard deviation, are shown in Figure 4.12a–c.

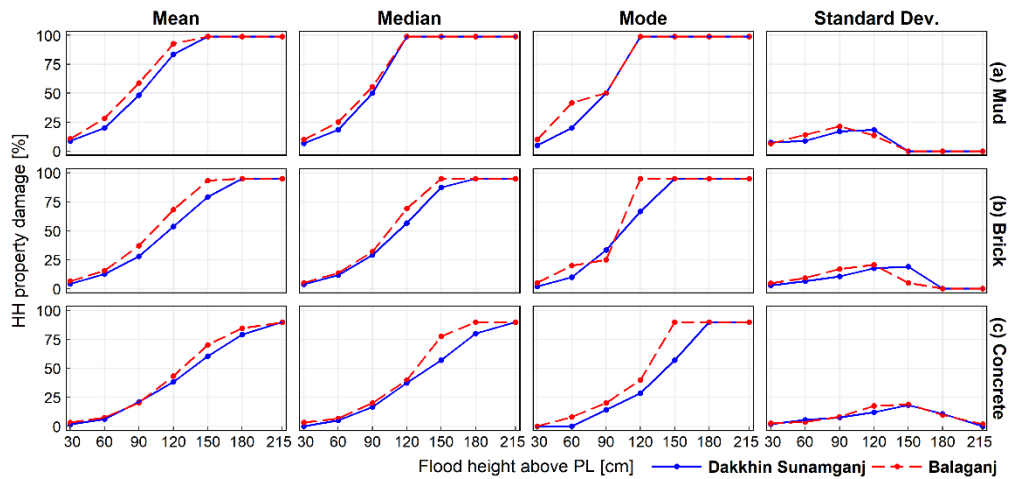


Figure 4.11: Comparison between the in-house property damage data of the two sub-districts performed with four statistical indices and for the house type of (a) Mud, (b) Brick, and (c) Concrete.

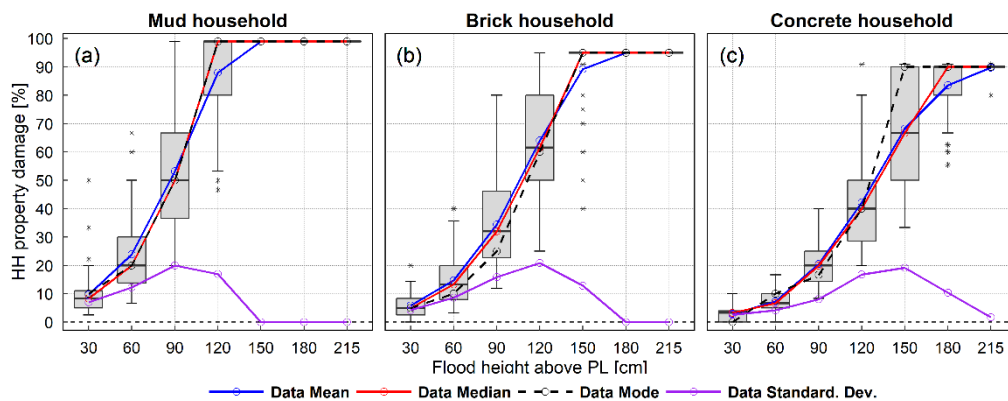


Figure 4.12: Distribution of the damage to household properties against selected flood heights, plotted in box and whisker plots with the collected 165 target samples for the house types of (a) Mud, (b) Brick, and (c) Concrete.

Although an inconsistency and variability in the property damage dataset were observed maybe due to the same reasons stated for the house damage, the dataset was investigated to identify depth-damage relationships by conducting the five regression models which were also performed for the rice and house damage. The model results are depicted in Table 4.7, and the damage curves predicted by each model for the three types of households are shown in Figure 4.13a–c.

Table 4.7: Results of different regression models performed with the household property damage data collected for 165 samples.

Regression Models	No. of samples	Household type	Value of parameters				SE	CC	CD	AICC
			a	b	c	d				
Linear	91	Mud	2.338476	0.5389	-	-	17.52	0.88	0.78	3647.89
	41	Brick	-10.90645	0.5616	-	-	15.13	0.92	0.84	1559.52
	33	Concrete	-19.97812	0.5375	-	-	12.73	0.93	0.87	1175.30
Logistic	91	Mud	101.1704	60.144	0.048048	-	11.50	0.95	0.91	3112.44
	41	Brick	98.02995	98.029	0.042513	-	11.83	0.95	0.90	1419.41
	33	Concrete	92.86422	114.31	0.038246	-	11.09	0.95	0.90	1112.76
Natural Logarithm	91	Mud	-180.1408	53.550	-	-	14.95	0.92	0.84	3445.67
	41	Brick	-188.6330	53.116	-	-	16.07	0.90	0.82	1594.08
	33	Concrete	-179.4930	48.546	-	-	16.80	0.88	0.77	1303.46
Polynomial (3 rd order)	91	Mud	-0.000027	0.0067	0.323612	-8.1503	12.08	0.94	0.89	3176.80
	41	Brick	-0.000043	0.0143	-0.685676	14.1977	11.88	0.95	0.90	1422.68
	33	Concrete	-0.000037	0.0139	-0.937985	19.9961	11.14	0.95	0.90	1115.94
Power	91	Mud	0.079741	1.3896	-	-	17.05	0.91	0.82	3469.94
	41	Brick	0.270495	1.1164	-	-	15.68	0.91	0.83	1579.81
	33	Concrete	0.034920	1.4796	-	-	13.17	0.93	0.86	1190.88

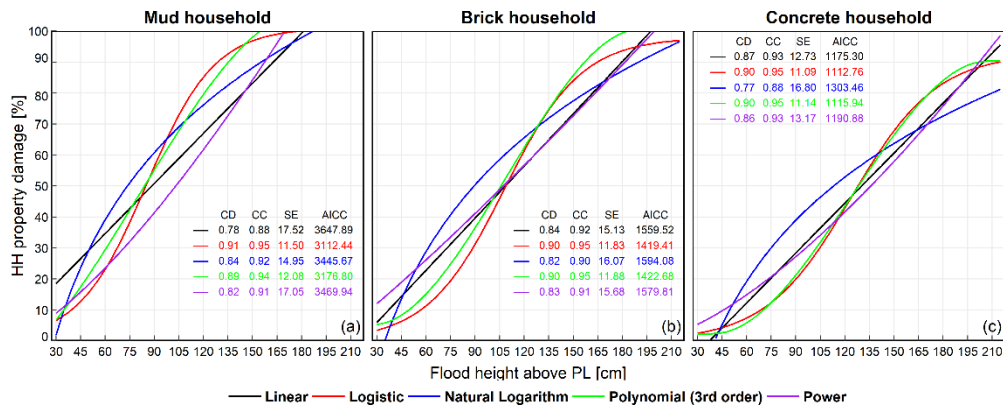


Figure 4.13: Household property damage and depth relationships predicted by five regression models for the house types of (a) Mud, (b) Brick, and (c) Concrete.

Although both the logistic and polynomial models performed better than the other three models, producing the same CC and CD indices, the less complicated logistic model was selected as the best model over the more complicated polynomial model through the SE- and AICC-Test for all three types of households. Figure 4.14a–c show the flood

damage curves developed for the in-house properties of three types of households, using the results of the best performing logistic regression model. To avoid the differences between the actual and collected damage, an uncertainty band of standard deviation ($\pm 1\sigma$) was incorporated to each of the established damage curves. Since most of the Brick houses are constructed with attic, and Concrete houses are with half ceiling at lintel height, it is thus observed that the owner of the Mud houses cannot save some household goods that the owner of the Concrete and Brick houses can save, when flood height exceeds 150 cm. It is evident that the construction method and materials of the Mud houses make such houses most vulnerable to flood, compared to the other two types of houses.

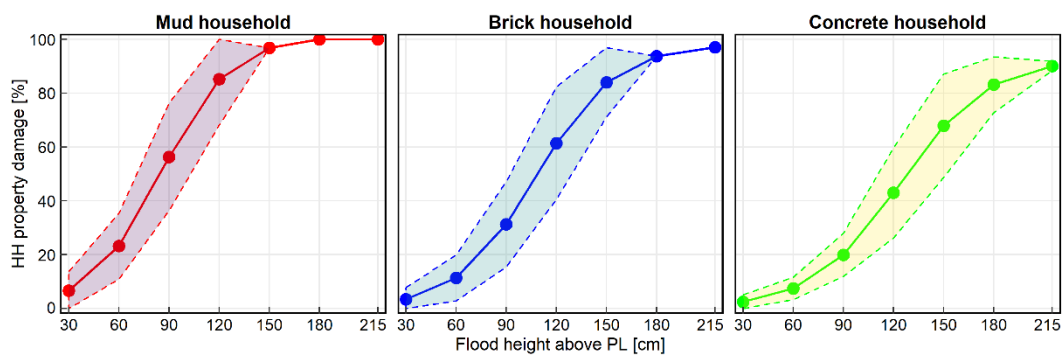


Figure 4.14: Flood damage curves developed for in-house properties through the data of the questionnaire survey for (a) Mud, (b) Brick, and (c) Concrete type of houses. Standard deviation ($\pm 1\sigma$) is added to show the uncertainty bands.

4.6 Conclusions

Northeastern Bangladesh is frequently affected by flood disasters. To effectively reduce flood disasters, flood risk assessment is an important tool for the policy makers to identify effective counter-measures and formulate future adaptation plans. Of the three main components of flood risk assessment, the estimation of flood vulnerability, which is often represented by flood damage curves, has not been drawn much attention in

Bangladesh. Flood damage curves can be developed either empirically or synthetically. However, empirical type of flood damage curves are yet to be developed in Bangladesh due to the lack of integrated and consistent damage data bank. Therefore, synthetic type of flood damage curves usually developed through the data of questionnaire surveys are the alternative for Bangladesh.

In this study, a questionnaire survey with sufficient sample size was conducted in two pilot sub-districts of northeastern Bangladesh in order to establish reliable flood damage curves for agriculture and household damage. Boro rice, the main crop of the area, was considered for agricultural damage, whereas the household damage included house building and in-house property damage. The damage to Boro rice mainly takes place in its flowering through maturity stage due to flash floods that occur 20–30 days before harvesting the rice. Therefore, considering this stage, data on flood damage to Boro rice was collected in terms of varying flood depths and duration for 196 samples. The house and its property damage data, on the other hand, were collected from 165 samples for three types of houses (Mud, Brick, and Concrete) according to varying flood heights above plinth level.

The data of the collected samples belonged to each sub-district were compared for all three of the damage classes, and no significant variations were found between the sub-districts. This might be due to the fact that the topography, land use, households, and people's livelihoods in the northeastern part of Bangladesh are greatly similar. Therefore, two sub-district's data were aggregated together and investigated to see the depth-damage relationships for each of the three damage classes. Although variability and inconsistency were somewhat observed in the collected data, their standard deviation was obtained

reasonably small in quantity for each damage class, which indicates that the collected dataset were sufficiently reliable.

To establish reliable depth-damage relationships for each damage class, regression analyses with five models were performed with the surveyed data. Although each of the five models showed satisfactory performance, the model that performed the best according to four performance indices was chosen to draw damage curves for each three of the damage classes. In such a way, the Boro rice damage curves for three sets of flood duration and the house and in-house property damage curves for three house types were developed. The Boro damage function showed that its damage is mainly governed by flood depth and duration. Yield of Boro rice becomes zero at a flood depth of about 70–75 cm (the depth at which grains start to grow) and a flood duration of seven and/or more days. The household damage, on the other hand, is mainly dependent on inundation height above plinth level and the type of houses, such as Mud, Brick, and Concrete. Compared to the other houses, the Mud houses were found the most vulnerable to flood due to their construction method and building materials. For the very same reason, some percentage of the household properties of the Concrete and Brick houses are being saved, and those of Mud houses are not, when flood height exceeds 150 cm.

The established damage curves can be of useful for post disaster flood damage assessment, near-real-time flood damage assessment, or future potential flood damage assessment in the northeastern part of Bangladesh for practicing an effective and timely management of flood risk disasters. The applicability of the damage curves is investigated to assess flood damage and risk for present and future climate in the following chapters.

Chapter 5: Flood damage assessment

5.1 Introduction

Flood damage and risk assessment is an important tool that provides benefits evaluation to mitigate floods and often used to evaluate potential consequences of a flood (Romali et al., 2015; Olesen et al., 2017). It thus can play an essential role for mitigating flood disaster as well as allotting resources for restoration and reconstruction (Dutta et al., 2003). A flood damage assessment model mainly consists of three main components: estimation of flood hazard, flood vulnerability, and flood exposure (Messner et al., 2007; Foudi et al., 2015, Kefi et al., 2018). Flood hazard is defined as the function of flood inundation parameters, i.e., flood depths and duration. These hazard parameters are usually estimated by hydrological modelling. Flood vulnerability is represented by flood damage curves that are derived by correlating hazard parameters with damage (Okazumi et al., 2014a, b; Shrestha et al., 2016). For a particular type of land use (e.g., agriculture) or structure (e.g., house), the damage curves define the relationships between flood depth and economic damage (Messner et al., 2007; Merz et al., 2010; Jongman et al., 2014; Hasanzadeh Nafari et al., 2017). The third component of the flood damage assessment model is the flood exposure that are usually derived using land-use land-cover maps and population distribution maps. This chapter of the dissertation describes a flood and risk assessment methodology, assesses flood damage to agriculture and household for the 2017 flood in the study area, and accordingly verifies with the recorded damage to support the damage assessment methodology.

5.2 Literature review

Flood damage and risk assessment in Bangladesh has not yet received much scientific attention and still remains a challenge. Some researchers, however, attempted

to assess potential flood risk mainly for two areas of Bangladesh: the south-west region and the capital city, Dhaka. For the south-western part of Bangladesh, Tingsanchali and Karim (2005) prepared a risk map demonstrating low, medium, and high risk areas considering 100-year potential flood hazard map. Rather than developing flood damage curves in their study, vulnerability for different unit area was assumed as proportional to the area's population density. Masood and Takeuchi (2012) attempted to prepare a risk map for the mid-eastern part of Dhaka city, considering risk as a function of hazard and vulnerability index. Hazard index was assigned according to inundation depth generated for a 100-year potential flood, whereas vulnerability index was calculated by assuming several weight factors based on land use classes. Accordingly, a risk map was prepared classifying three risk zones (low, medium, and high) according to some assigned risk indices. Considering a 100-year potential flood, Gain and Hoque (2013) calculated expected damage for the eastern part of Dhaka city. Their study covered the estimation of economic damage for several land use classes, rather than different aspects of damage categories. Vulnerability to different land use classes in their study was estimated using an empirical depth-duration-damage relationship developed for Dhaka city by Japan International Cooperation Agency (JICA, 1991). Incorporating social dimensions to vulnerability, flood risk maps considering a 100-year potential flood for the eastern Dhaka were produced by Gain et al. (2015). In their study, expected economic flood damage for several damage categories was calculated. However, vulnerability in their study for calculating economic flood damage was assessed either by assuming land use-based weight factors or by using stage-damage relationships that were obtained from several other studies.

Flood damage and risk assessment in Bangladesh conducted by the previous studies were mostly in the context of urban potential floods. To the best of the author's knowledge, none of the previous researchers attempted to assess flood damage for an actual flood event and/or for the rural Bangladesh. In addition, previous studies were limited to estimating vulnerability either by assuming land use-based weight factors or by using stage-damage relationships or equations that were obtained from several other studies, rather than using empirically or synthetically established damage curves. Furthermore, the calculated economic damage in the previous studies was nowhere validated with any historical flood event. Therefore, this chapter of the dissertation attempts to estimate economic flood damage for agriculture and households that was caused by the 2017 flood in the study area. The calculated damage was subsequently validated with the actual recorded damage.

5.3 Study area

The study area for the component of this chapter is the six districts of north-eastern Bangladesh located downstream of the Meghna river basin, which is described in detail under Chapter 2.

5.4 Methods

In the study area, Boro rice is the main crop for people's livelihood, and their houses with household properties are the only assets they worry about during the flood time. This study thus emphasized Boro rice, house building, and household properties as three damage classes to perform flood damage assessment for the 2017 flood. Flood hazard, vulnerability, and exposure are the three main components of a flood damage and risk assessment model (Messner et al., 2007; Foudi et al., 2015, Kefi et al., 2018). In this research, a flood hazard map at a 500-m grid was generated using the RRI model forced

with a rainfall data prepared using the methodology described in Chapter 3. Flood vulnerability for the three target damage classes was estimated using the synthetic damage curves that were constructed in this study, details of which are described in Chapter 4. Flood exposure to the Boro rice was extracted using a land cover map provided by IRRI (IRRI, 2010), and flood exposed households were obtained from a household distribution map prepared in this study using the global population map provided by ORNL, household proportion, and household size collected from Bangladesh Bureau of Statistics (BBS, 2011). Finally, potential flood damage to each damage class on a 500-m resolution was calculated and subsequently validated with the actual damage data. Figure 5.1 shows the flowchart of the methodology used for flood damage assessment in this study.

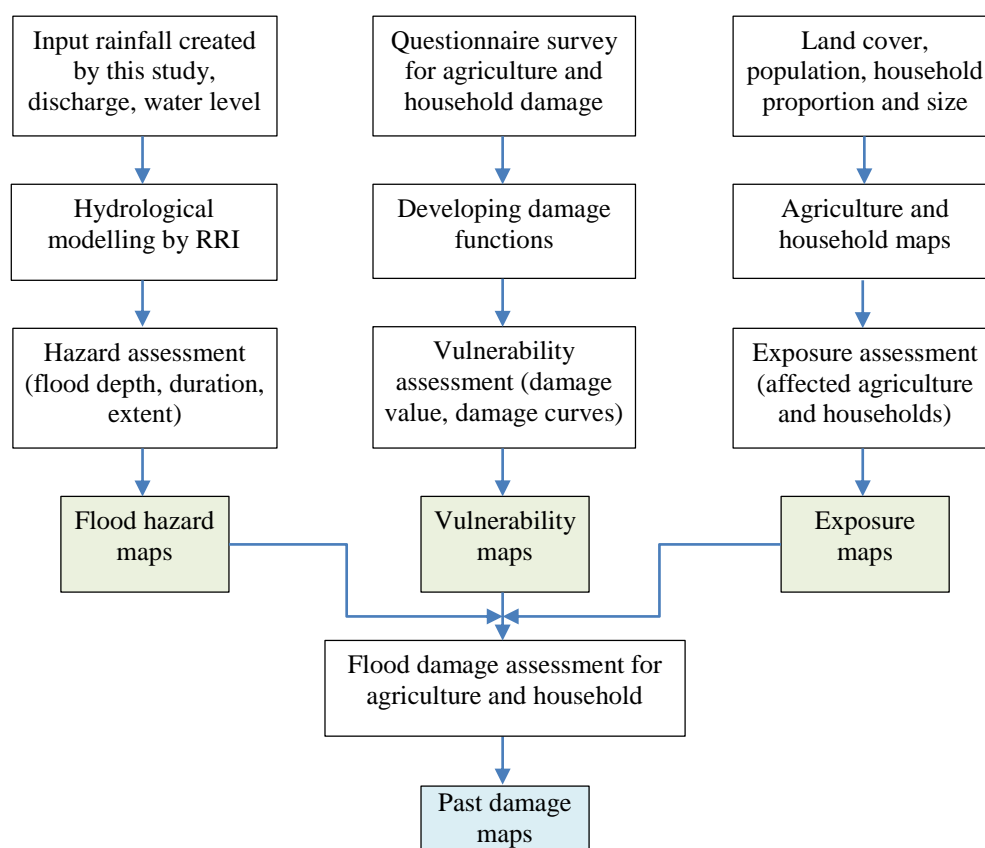


Figure 5.1: Flow chart of the research structure used in this research for flood damage assessment in the northeastern part of Bangladesh.

5.4.1 Generation of hazard maps

In this study, the Rainfall-Runoff-Inundation (RRI) model, a 2D hydrological model, was used to simulate the flood hazard parameters (depths and duration) at 500-m grid resolution in the northeastern part of Bangladesh, located downstream of the Meghna river basin. The details of the RRI model is described in Section 3.5.6 of Chapter 3. To run the RRI model, an input rainfall data for the target flood (the 2017 flood) was prepared for the Meghna river basin at $0.25^\circ \times 0.25^\circ$ resolution by using the methodology described in Chapter 3. The scientific methodology of creating such rainfall data was published in a peer reviewed Journal in 2018 (Khairul et al., 2018)

5.4.2 Estimation of vulnerability

Flood vulnerability is represented by flood damage curves that can be of empirical (developed using real damage data) and synthetic (developed through survey data) types. However, due to the lack of integrated flood damage data, this study established synthetic type of damage curves for the target damage classes (Boro rice, house building, and in-house properties) using the data collected through a structured questionnaire survey that was conducted in two sub-districts of the study area (northeastern Bangladesh). The details of establishing the mentioned damage curves are described in Chapter 4. A depth-damage relationship for Boro rice was developed considering three sets of inundation duration (1–3 days, 4–7 days, and above 7 days). On the other hand, house building and in-house property damage curves in relation to flood depths were developed for three types of houses (Mud, Brick, and Concrete) that were observed in the study area. These developed damage curves were used to estimate vulnerability for flood damage assessment in this chapter of the dissertation.

5.4.3 Exposure assessment

For agricultural flood damage assessment, grid-based land-use land cover (LULC) maps are usually used to extract the area exposed to inundation. However, due to the lack of such observed data, several satellite-based globally available LULC raster maps obtained from different sources (e.g., GLCC, GLCNMO, FAO, and IRRI) were investigated to extract the extent of Boro rice for the study area. Most of these LULC maps showed a greater extent of agricultural area which includes all type of crops cultivated all year around in the study area, and hence it was difficult to separate the extent of Boro rice with that of the other crops. However, the IRRI has provided separate LULC maps for each type of crops cultivated in the study area. Therefore, the extent map of Boro rice provided by IRRI, which has roughly the same spatial resolution of 500 m as the inundation model, was chosen for Boro exposure assessment in this research. The Boro extent by district obtained from the IRRI map was compared with district-based Boro zoning provided by Department of Agricultural Extension, Bangladesh (DAE, 2017), and was found reasonably satisfactory. Figure 5.2 shows the Boro rice extent provided by IRRI for the study area, and Table 5.1 compares the extracted Boro area from IRRI map by district with the Boro zoning area provided by DAE.

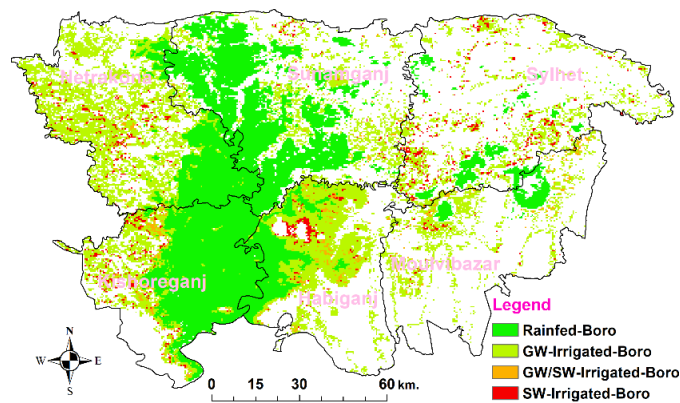


Figure 5.2: Boro extent map for the study area provided by IRRI

Table 5.1: Cultivable extent of Boro rice by district extracted from IRRI map; the extent is compared with the area provided by DAE.

Districts	Boro land cover area (ha)	
	IRRI	DAE
Sunamganj	203, 650	223, 082
Netrakona	185, 140	184, 320
Kishoreganj	186, 965	165, 515
Habiganj	122, 266	116, 510
Moulvibazar	57, 121	53, 426
Sylhet	73, 041	83, 065
NE total:	828, 183	825, 918

The area of one grid was calculated as:
 $= 0.004167^\circ * 0.004167^\circ$
 $= 0.004167^2 * 110.6 * 110.6$ sq. km.
 $= 0.004167^2 * 110.6^2 * 100$ ha
 $= 21.2267$ ha

For household exposure assessment, a household distribution map with the proportion of each type of house in the study area was required. However, neither such map nor such observed data of the study area is available. An attempt to prepare such household map by extracting roof of the houses from the Google Earth map was failed due to the existence of dense vegetation canopy cover over the built up areas. Therefore, in this research, a household distribution map was prepared considering the population distribution, average family size, and proportion of three house types by district. Such methodology of preparing household distribution map was also used by Shrestha et al. (2016) in their study. Population distribution of the study area was obtained from LandScan 2016 global population data with a spatial resolution of 1-km. The data was resampled to 500-m resolution to make it as identical as the inundation model. The average family size and proportion of house type by district was collected from Bangladesh Bureau of Statistics (BBS, 2011). By dividing the number of population with the average family size for each district, the household distribution map for the study area was prepared at 500-m grid resolution. Figure 5.3a–b respectively show the LandScan

population map and the prepared household map, both at 500-m resolution for the study area. Table 5.2 compares the estimated number of population and households by district with that of the figure obtained from the latest Bangladesh census (BBS, 2011). The estimated number reasonably agree with the census data for both cases. The average family size and the proportion of house type obtained from BBS were also depicted in Table 5.2. The number of different types of houses belonging to each grid was obtained using the percent proportion of the house type for each district.

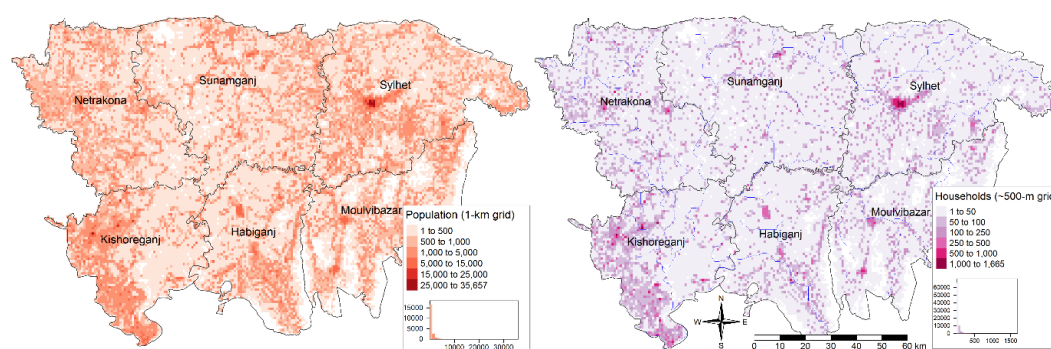


Figure 5.3: 500-m grid distribution maps of the study area for (a) population extracted from 1-km grid LandScan 2016 and (b) houses prepared using LandScan population and the average family size by district.

Table 5.2: Comparison of LandScan (2016) population and the calculated number of houses by district with those of the figure obtained from Bangladesh census data (BBS-2011)

Districts	Population (nos.) (BBS-2011)	Population (nos.) (LandScan-2016)	Household (nos.) (BBS-2011)	Household (nos.) (Calculated-2016)	Average family size (BBS-2011)	Proportion of house type (%) (BBS-2011)		
						Mud	Brick	Concrete
Sunamganj	2,467,968	2,694,047	440,332	490,299	5.6	81	12	7
Netrakona	2,229,642	2,436,228	479,146	537,152	4.6	88	10	2
Kishoreganj	2,911,907	2,780,617	627,322	610,340	4.6	85	12	3
Habiganj	2,089,001	1,955,511	393,302	374,828	5.3	75	19	6
Moulvibazar	1,919,062	2,046,088	361,177	392,799	5.3	59	29	12
Sylhet	3,434,188	3,691,434	596,081	656,582	5.7	47	31	22
NE total	15,051,768	15,603,925	2,897,360	3,062,000	-	-	-	-

5.4.4 Flood damage assessment

Potential flood damage to Boro rice, house buildings, and in-house properties caused by the 2017 flood in the study area were estimated at a 500-m grid resolution. The

following model was used to estimate the damage to Boro rice for each affected grid cell of the study area:

$$EDB_{i,j} = V * Y * A * DF_{h,d}(i,j) \quad 5.1$$

where, $EDB_{i,j}$ is the economic damage to Boro rice for any flood affected grid cell i, j ; V is the average value of rice per unit weight; Y is the average yield of rice per unit area; A is the area of the grid cell, and $DF_{h,d}(i,j)$ is the rice damage factor obtained from the damage curve for the grid cell i, j corresponding to model-simulated flood depth of h and a duration of d . The area of one grid cell is calculated 21.2267 ha, as shown in Table 5.1. The average yield of Boro rice is considered 4.95 MT/ha in this study based on the data collected during the survey period. The unit price of Boro rice, which is USD 386 per MT in 2017, was collected from DAE, Bangladesh.

The potential damage to house buildings and in-house properties were estimated for each grid cell of the study area using the same hazard parameters used for the Boro rice. Flood heights above the plinth level of houses were considered for calculating such damage. The following two models were used to calculate the damage to house buildings and in-house properties, respectively, for each affected grid cell of the study area:

$$EDH_{(i,j)} = \sum_{k=1}^3 VH_k * N_{k(i,j)} * DFH_{k,h}(i,j) \quad 5.2$$

$$EDP_{(i,j)} = \sum_{k=1}^3 VP_k * N_{k(i,j)} * DFP_{k,h}(i,j) \quad 5.3$$

where, $EDH_{i,j}$ and $EDP_{i,j}$ are the economic damage to house buildings and in-house properties, respectively, for any flood affected grid cell i, j ; VH_k and VP_k respectively are the average value of house buildings and in-house properties for the house type k , $N_{k(i,j)}$ is the number of houses for the house type k at the grid cell i, j , and $DFH_{k,h}(i,j)$

and $DFH_{k,h(i,j)}$ are the damage factors obtained from damage functions of house buildings and in-house properties, respectively, for the house type k and grid cell i,j corresponding to a flood depth of h simulated by the hydrological model.

5.5 Results and discussions

Flood damage assessment was conducted in this research for three damage classes (Boro rice, house buildings, and in-house properties) considering the 2017 flood in the study area. In doing so, a 2D hydrological model, RRI, was set up at 500-m resolution with an input rainfall data developed in this study for the Meghna basin, calibrated and validated the model, and subsequently potential inundation maps in terms of hazard parameters (flood depths and duration) for the 2017 flood were generated. The damage curves established by this study were used to assess flood vulnerability for the target damage classes. By combining the hazard and vulnerability maps with the exposure maps, potential flood damage to Boro rice, house buildings and in-house properties was estimated and accordingly verified with the recorded damage.

5.5.1 Calibration and validation of RRI model

The parameters of the RRI model was calibrated for the target event of the 2017 flood, and validated the same for the flood event of 2010. Both calibration and validation were performed by comparing the simulated streamflows with the observed streamflows at the outlet of the Meghna basin, i.e., at the Bhairab Bazar station (Figure 3.1). Figure 5.4a–b compare the hydrographs of simulated and observed streamflows for the period of model calibration and validation. Two indices, Nash–Sutcliffe Efficiency (NSE) and Correlation Coefficient (CC), were used to check the model performance. All together, the hydrographs and the performance indices (shown inside the plot) showed satisfactory efficiency of the model in generating the timing and volume of streamflows.

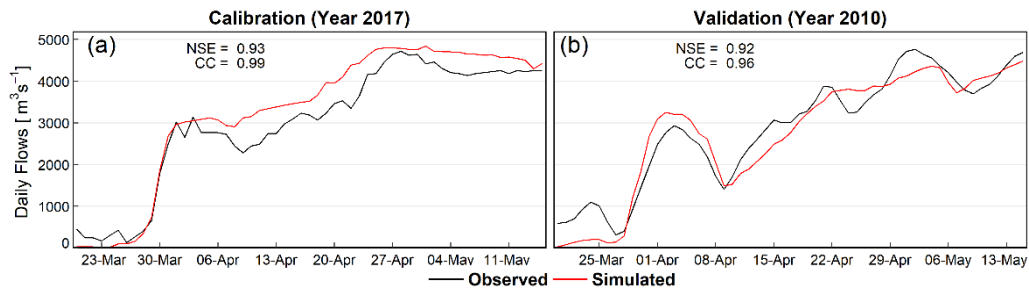


Figure 5.4: Comparison of streamflows simulated by RRI model with the observed streamflows at Bhairab Bazar station for the period of model's (a) calibration and (b) validation.

At the time of the model's calibration, the water levels simulated along the river channels were also verified with the observed river water level measured at 15 gauging stations located inside the Bangladesh part of the Meghna basin. Figure 5.5a compares the simulated river water levels with those recorded at the 15 stations on April 5, 2017. Figure 5.5b, on the other hand, shows a scatter plot that compares simulated and observed river water levels measured at the 15 stations for a flood period of 30 days, 2017 (30th March to 28th April). All together, the results indicated that the RRI model was able to calculate the inundation depths reasonably well along the river channel.

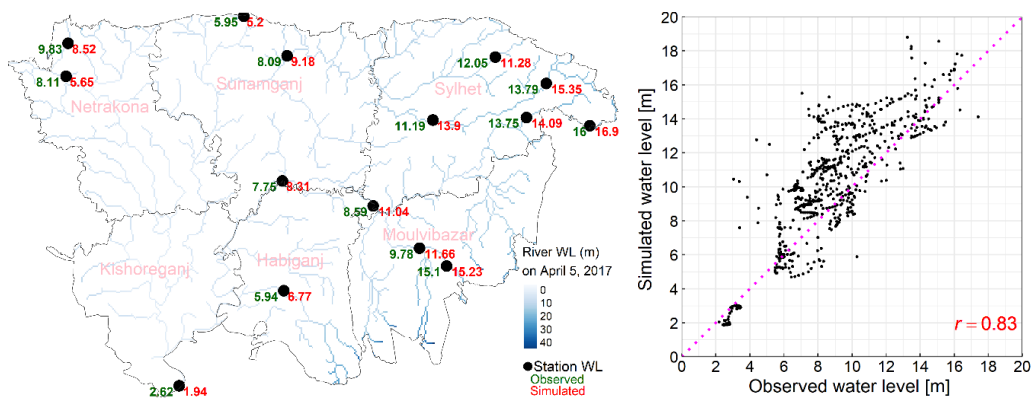


Figure 5.5: Validation of water levels simulated by RRI model along the river channel with the observed water levels measured at 15 stations (a) on 5th April 2017 and (b) for 30 days of the 2017 flood (30th March to 28th April).

5.5.2 Generation of hazard parameters

The calibrated and validated RRI model was used to generate potential inundation maps in terms of hazard parameters (flood depths, duration, and extent) for the target flood event of 2017. Figure 5.6a–b show the potential flood inundation depths and inundation duration generated by the RRI model for each grid cell (500-m) of the study area. The results indicate that the inundation depths that the study area mostly experienced in the 2017 flood range between 0.5m and 4m.

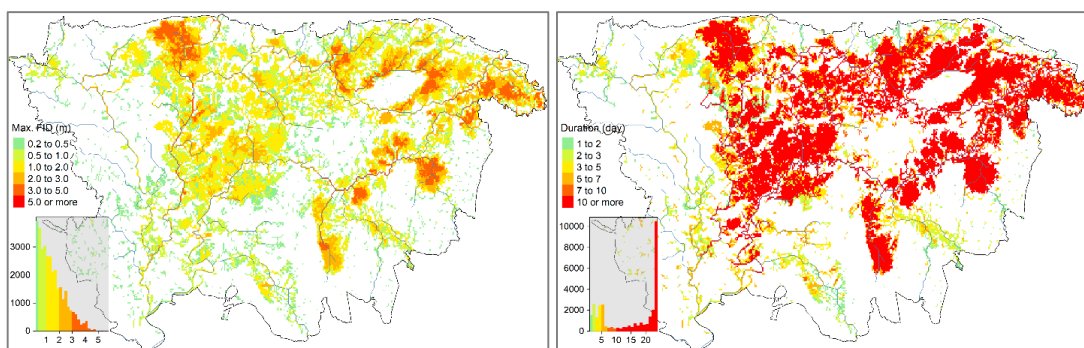


Figure 5.6: Potential inundation maps at 500-m grid generated by RRI model in terms of (a) flood depths and (b) flood duration across the study area during the 2017 flood event (30th March to 28th April).

5.5.3 Flood damage curves to estimate vulnerability

In this research, flood damage curves for the Boro rice, house buildings, and in-house properties were developed using the data of a structured questionnaire survey conducted in the study area. The details of the questionnaire survey and developing the damage curves are described in Chapter 4 of this dissertation. Figure 5.7a–c show the developed damage curves for the mentioned damage classes.

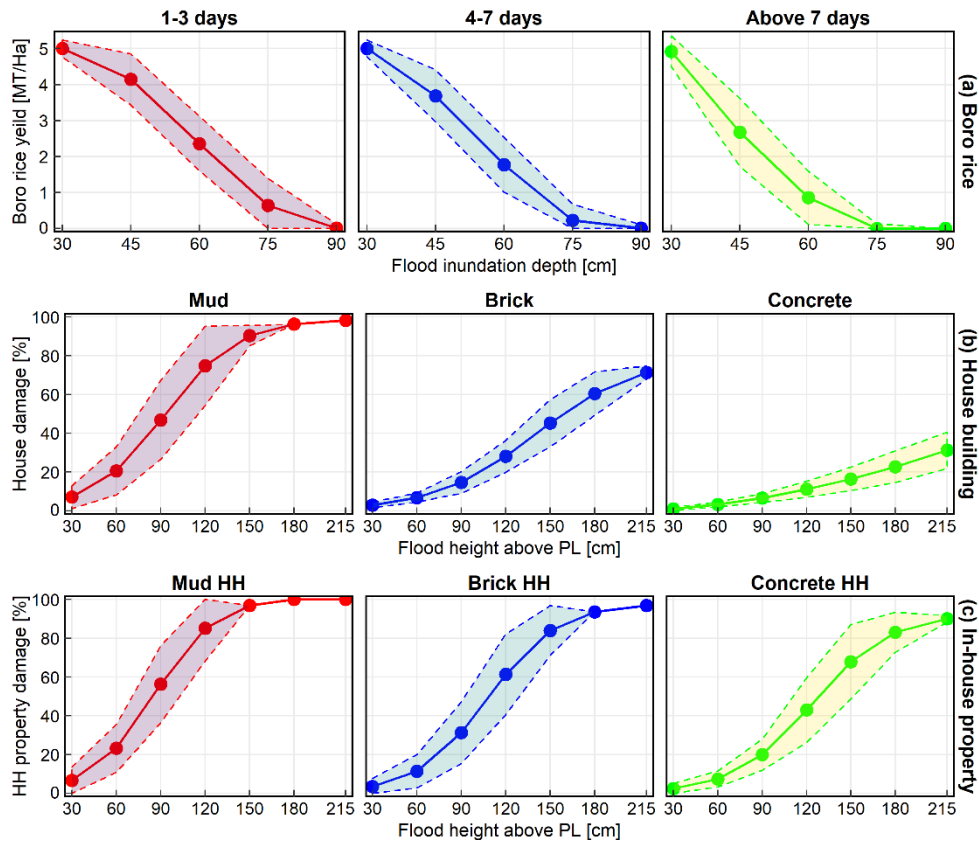


Figure 5.7: Synthetic type of damage curves developed through the data of a questionnaire survey conducted in the study area for (a) Boro rice, (b) house buildings, and (c) in-house properties. Standard deviation ($\pm 1\sigma$) is included as uncertainty bands to avoid the differences between actual and collected damage.

5.5.4 Flood damage to Boro rice

The model described in Equation 5.1 was used to estimate the potential damage to Boro rice caused by the 2017 flood in the study area. By combining the flood depths and duration map simulated by the RRI model, depth-duration-damage relationship obtained from the Boro damage curve, and Boro extent provided by the IRR map, a distributed flood damage map for Boro rice at 500-m grid resolution was produced for the study area. Figure 5.8 shows the map produced for the Boro rice damage caused by the 2017 flood in the study area consisting of six administrative districts. The map was produced considering the average yield of Boro rice.

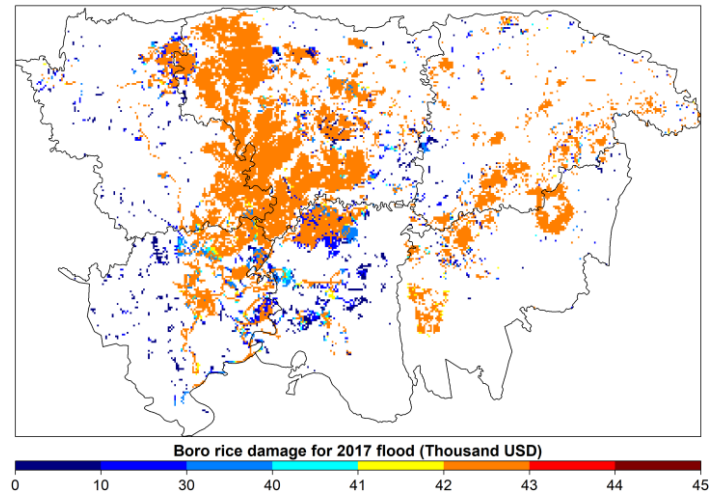


Figure 5.8: Distributed damage map produced for the Boro rice considering its average yield for the 2017 flash flood in the study area.

The area with damage to Boro rice by district, which was reported by the Department of Disaster Management, Bangladesh, on its daily disaster reports of April 28, 2017 (DDM, 2017), is compared with the estimated area by district in Figure 5.9. Overall, the estimated area with damage to Boro rice reasonably agree with the reported affected area for each administrative district. It is observed that Sunamganj and Kishoreganj districts were severely affected by the flood according to both estimated and reported statistics.

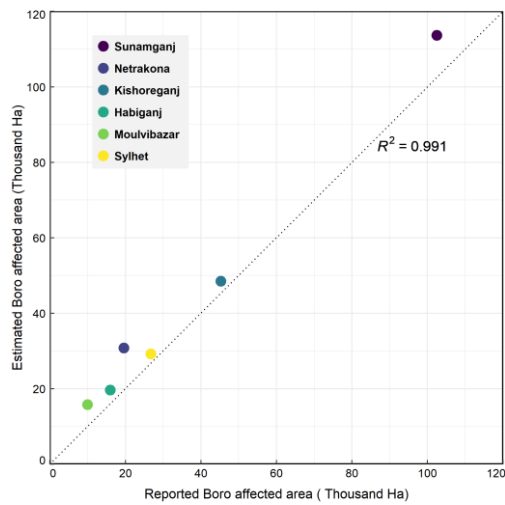


Figure 5.9: Estimated and reported area with Boro rice damage caused by the 2017 flood for each administrative district of the study area.

The damage to Boro rice was estimated to 468 million USD for a combined total of the six districts considering the average yield of Boro rice (Figure 5.8). Boro rice damage was also estimated considering maximum and minimum rice yield, based on the established damage curves. The reported Boro rice damage was collected from three different sources. Department of Disaster Management (DDM), Department of Agricultural Extension (DAE), and Kamal et al. (2018) reported Boro rice damage caused by the 2017 flood as 356, 612, and 450 million USD, respectively, and those are calculated considering minimum, maximum, and average yield of Boro rice. Table 5.3 compares the Boro rice damage estimated for maximum, minimum, and average yield with those of the reported damage obtained from three different sources. The estimated Boro for each case (maximum, minimum, and average yield) was found to satisfactorily agree with the reported damage.

Table 5.3: Comparison of estimated and reported damage of Boro rice for the 2017 flood.

Boro damage (million USD)	Estimated	Reported
Maximum	589	612 (DAE, 2017)
Minimum	372	356 (DDM, 2017)
Average	468	450 (Kamal et al., 2018)

5.5.5 Household damage assessment

Household damage assessment was performed for house building as well as in-house property damage. The hazard parameters used for estimating Boro damage were also used for calculating household damage. The damage curves developed for house and its properties were used for vulnerability estimation, and the house distribution map prepared in this study was used as exposure component. The questionnaire survey conducted in the study area revealed that house and its occupancy are usually affected by

a flood when the flood height exceeds the plinth level (floor level from the ground; Figure 5.7b–c). Considering average plinth level for each type of house as reference, the number of affected households for each administrative district was estimated and compared with that of the figures reported by the Department of Disaster Management, Bangladesh (DDM, 2017). Figure 5.10 presents this comparison in a scatter plot. It is found that the affected number of households is underestimated in some of the districts. This might be resulted from the household distribution map that was prepared considering population distribution and average household size by district. A precise household distribution map might overcome this issue.

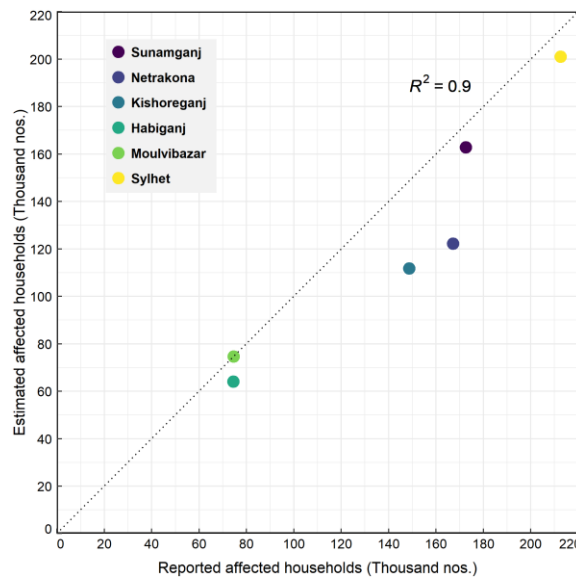


Figure 5.10: Comparison of the estimated and reported number of affected households caused by the 2017 flood for each administrative district of the study area.

5.5.5.1 Damage to house buildings

Potential damage to house buildings for each grid cell of the study area was estimated using the model illustrated in Equation 5.2. The model multiplied the affected number of houses for each house type, respective house damage factors, and the average house value to estimate the house damage for each grid cell. Figure 5.11 shows the

estimated damage to house buildings in the study area for the 2017 flood. The total house damage estimated for 776 579 affected houses in the study area amounted to 322 million USD. This estimated damage couldn't be validated due to lack of reported damage data.

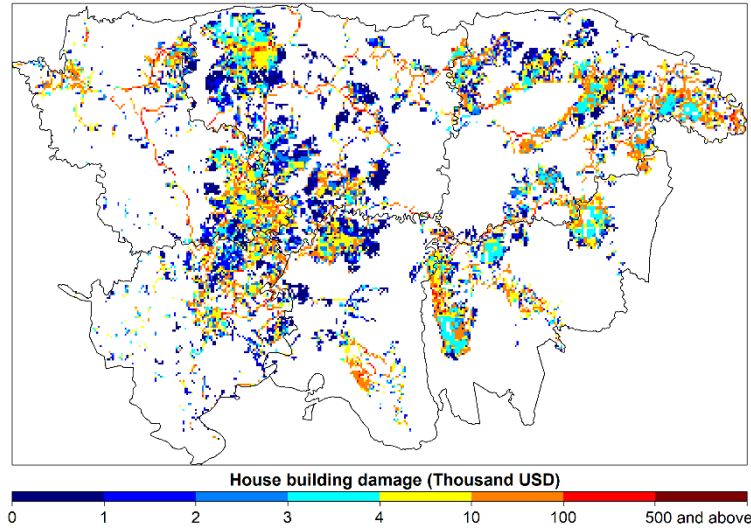


Figure 5.11: Estimated house building damage for each grid cell of the study area considering the flood event of 2017.

5.5.5.2 *Damage to in-house properties*

Following the model explained in Equation 5.3, the potential damage to in-house properties was calculated for each grid cell of the study area by multiplying the affected number of houses with corresponding damage factors and in-house property value considering each type of household. Figure 5.12 shows the estimated damage to in-house property due to the 2017 flood. The total in-house property damage for the study area was estimated to 139 million USD. Due to the lack of reported damage data, the estimated damage to in-house property couldn't be compared and verified as well.

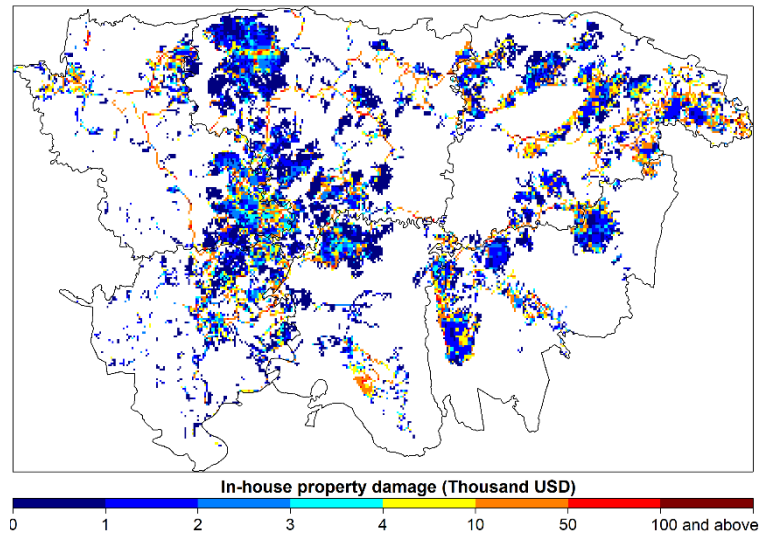


Figure 5.12: In-house property damage for each grid cell of the study area considering the flood event of 2017.

5.6 Conclusions

Flood damage assessment plays an important role in post flood disaster management for the policy makers. This study conducted flood damage assessment in the area downstream of the Meghna river basin, located in the northeastern part of Bangladesh, considering a past flood event of 2017. The main crop of the area, Boro rice, house buildings, and in-house property damage were considered as three damage classes. Flood damage assessment consists of three components: flood hazard, vulnerability, and exposure assessment. Flood hazard consists of inundation depths, duration and extent, which were simulated using RRI model forced with a rainfall data created by using the methodology developed by this study. Flood vulnerability for each damage class was estimated using the damage curves established by this study. For exposure assessment, a land cover map provided by IRRI and a house distribution map prepared by this study were used.

By integrating the hazard, vulnerability and exposure maps, potential damage to Boro rice, house buildings, and in-house property was estimated for the mentioned flood.

The estimated area with Boro rice damage (~237 734 ha) was found to agree with the reported area (225 840 ha). The total damage to Boro rice was estimated to 589, 372 and 468 million USD, considering maximum, minimum, and average rice yield, respectively. The reported damage obtained from three different sources for the same were 612, 356 and 450 million USD, respectively. It was found that the Boro damage estimated for the three cases satisfactorily agrees with that of the reported Boro damage. The total household damage (building plus properties), on the other hand, was estimated to 461 million USD, which couldn't be validated due to lack of reported data. However, the estimated number of affected households (~776 579) was compared with the reported number (850 088), and found that the estimated number is underestimated in some cases, which might result from the household distribution map that was prepared considering population distribution and average household size by district. A precise household distribution map might overcome this issue. The results of this chapter of the dissertation can help strengthen emergency preparedness on a short-term basis. They can also help to introduce or strengthen the flood forecasting and early warning system through constructing an observation network.

Chapter 6: Flood risk assessment under global change

6.1 Introduction

Due to global climate change, the frequency and intensity of flood disasters are expected to increase and that is likely to pose increasing threats to various sectors worldwide (IPCC, 2014). In addition, population and land use change together with changing climate (particularly heavy precipitation) is likely to intensify the damaging effect of flooding. Therefore, quantification of local-scale flood risk to such global changes is essential to transfer the scientific knowledge to local decision makers for improving the efficiency of local adaptation strategies. This chapter of the dissertation describes a methodology to quantify flood risk to agriculture (mainly to Boro rice) due to change in climate and land use in the study area.

6.2 Literature review

Up to date, very few studies have been conducted to quantify flood risk due to global changes (e.g., changes in climate and land use) in Bangladesh. Winsemius et al. (2013) estimated flood discharge and flood inundation globally including the Ganges-Brahmaputra-Meghna (GBM) basins using a distributed hydrological model at 50–km resolution. They estimated flood risk in Bangladesh for present and future climates considering population and land use change by downscaling the inundation model from 50–km to 1–km resolution. However, they did not perform hydrological model calibration with observed river discharges. Gusyev et al. (2015) performed a flood hazard assessment in the GBM basins using a distributed hydrological Block-wise TOP (BTOP) model (Takeuchi et al., 2008) at a grid resolution of 20km. They further performed flood risk assessment in Bangladesh by linearly downscaling the BTOP-produced peak discharges from 20km to 500m resolution to generate inundation depths using a flood inundation

depth (FID) model (Kwak et al., 2012 & 2015). However, they used only one GCM output with SRES, A1B scenario. The uncertainty due to GCMs was not taken into account in their study. Also, they only estimated the number of affected population in changing climate. In addition, the hydrological model was calibrated at a course resolution of 20km with greater uncertainty in producing the inundation depths over Bangladesh. In this study, a 2D hydrological model, RRI, was calibrated and validated for the Meghna river basin with observed river discharges at a finer resolution of 500m. This very same model was used to generate the hazard parameters, such as the flood inundation depths and duration for the study area also at 500m resolution. The inundation depths along the river channel were also verified with the observed river water level. This calibrated and validated model was used to map future hazard due to the effect of climate change. Agricultural exposure map in future was predicted using past land cover maps. Finally, by integrating the future hazard and exposure with the present vulnerability, flood risk to agriculture (for Boro rice) was quantified due to the changes in climate and land use. This chapter of the dissertation describes in detail the methodology of estimating such flood risk in the study area. It also shows the results and discusses the findings. At the end of this chapter, a concluding remark is drawn.

6.3 Study area

The study area for the component of this chapter is the Bangladesh part of the Meghna basin (northeastern Bangladesh), which is described in detail under Chapter 2.

6.4 Methods

Figure 6.1 shows the flowchart of the methodology used in this chapter for quantifying agricultural flood risk (for Boro rice) in the Bangladesh part of the Meghna basin due to the effect of global changes, such as changes in climate and land use.

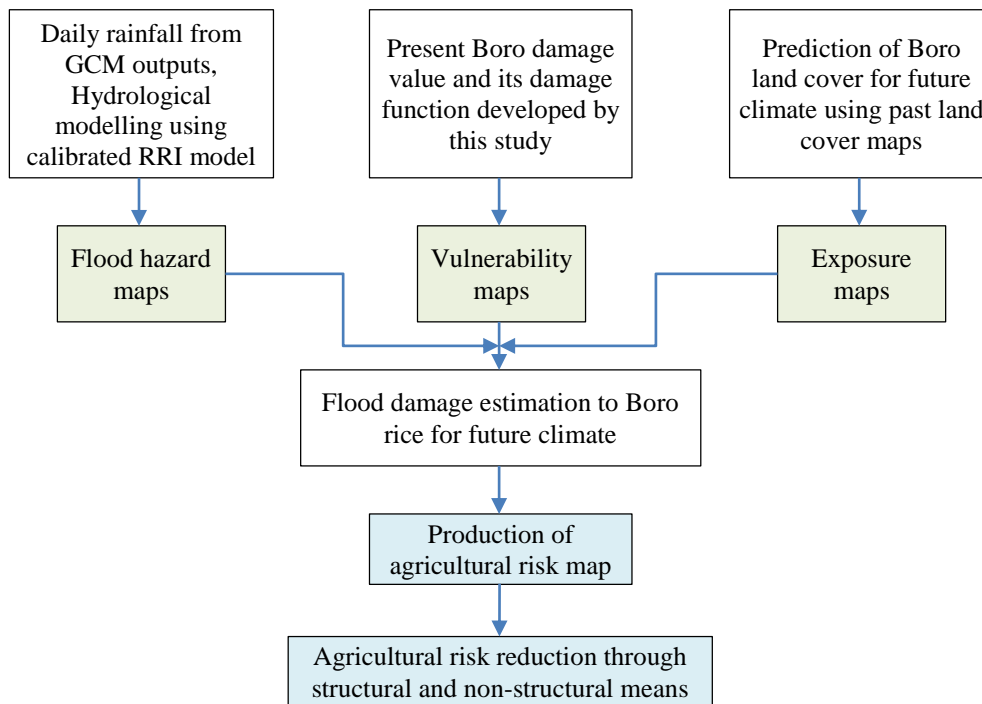


Figure 6.1: Flow chart of the methodology used in this chapter for future flood risk assessment in the northeastern part of Bangladesh due to global changes.

6.4.1 Flood hazard

Flood hazard is the first component of a flood risk assessment model and is represented by flood depth, duration, and extent. These flood hazard parameters can be simulated using hydrological models. The Rainfall-Runoff-Inundation (RRI) model, which has already been calibrated and validated using observed river discharges and water levels, was used for future inundation simulations in this chapter.

To simulate hazard parameters for future climate, reliable future rainfall covering the study area is required. For this purpose, Global Climate Models (GCMs) are developed to produce future rainfall due to global warming. For accurate climate change analysis, different rainfall outputs from the GCMs are necessary to integrate into the hydrological model. In this study, different GCMs were selected from the fifth Coupled Model Inter-comparison Project (CMIP5). CMIP5 consists of total 44 climate models

spanning for the whole globe under the scenario of Representative Concentration Pathways (RCP). The Data Integration and Analysis System (DIAS) of the University of Tokyo provides the CMIP5 database under its ‘CMIP5 data analysis tool’. This analysis tool under CMIP5 (can be accessed at <http://apps.diasjp.net/modelvis/cmip5/>) was used in this study for selecting reliable GCMs for the study area. The tool was also used to correct the biases of the selected GCMs.

The methodology proposed by Nyunt et al. (2016) for selecting reliable GCMs was used in this study as well. Nine climatic variables (precipitation (pr), outgoing long wave radiation (rlut), air temperature (ta), sea level pressure (psl), specific humidity (hus), zonal wind (ua), meridional wind (va), ground temperature (ts), and geopotential height (zg)) at the local and regional scales were considered for GCM selection. Due to the greater spatial variability, a local scale (86°E-98°E, 20°N-30°N) for precipitation was considered, while a regional scale (60°E-140°E, 0°N-40°N) was used for the other eight variables. The monthly time-series of 1981-2000 for the months of March and April (pre-monsoon period) was set for GCMs selection. The GCM-simulated nine climatic variables for all 44 models for the said period were compared and evaluated at monthly scale with those of the global reanalysis and observation data using two performance indicators, such as the spatial correlation (Scorr) and Root Mean Squared Error (RMSE). These indicators for all 44 models and for each variable were transferred to their respective indices following a simple methodology. For example, if Scorr of a model is above the mean Scorr of all models, the Scorr index of that model was set to 1, otherwise set to 0. On the other hand, if RMSE of a model is below the mean RMSE of all models, the RMSE index of that model was set to 1, otherwise set to 0. Then a performance score was calculated for each model and for each climatic variable by subtracting 1 from the

arithmetic sum of the two indices. Finally each model was ranked by the total score obtained from the arithmetic sum of the points for each climatic variable corresponding to that model. Table 1 shows the ten selected models with their ranks that were obtained following the above described methodology.

Table 6.1: Selected GCMs with their performance scores obtained for the nine climatic variables considered in this study.

Model name	pr	rlut	ta	psl	hus	ua	va	ts	zg	Total score
CNRM-CM5	1	1	0	1	0	1	1	1	1	7
CanESM2	1	-1	1	1	1	1	1	0	1	6
CESM1 (CAM5)	1	1	1	1	1	0	-1	1	1	6
MIROC5	0	1	1	1	1	1	-1	1	1	6
MRI-CGCM3	1	0	1	1	1	1	0	1	0	6
MRI-ESM1	1	-1	1	1	0	1	1	1	0	5
CMCC-CMS	0	-1	1	0	1	1	1	1	1	5
CSIRO-Mk3.6.0	1	-1	0	1	1	0	1	1	1	5
GFDL-CM3	0	-1	0	1	0	1	1	1	1	4
GFDL-ESM2G	0	-1	1	1	0	1	0	0	1	4

In this study, rainfall output of the selected GCMs from 2040–2059 for the RCP8.5 scenario was used for climate change analysis for the study area. Before doing so, the bias of the GCMs rainfall was corrected using a statistical method proposed by Nyunt et al. (2016). This correction method has three main steps: 1) the Generalized Pareto Distribution (GPD) for extreme rainfall bias correction, 2) ranking order statistics for wet and dry day frequency errors, and 3) a two-parameter gamma distribution function for monthly rainfall bias correction. This method of bias correction has been built inside CMIP5 data analysis tool under the DIAS system. Thus the correction of the GCMs rainfall was performed using the CMIP5 tool with the reference data of APHRODITE from 1981-2000. For details of the bias correction method, refer to Nyunt et al. (2016). For future hazard simulation, flood events for each of the model were selected by

considering a maximum of sequential 5-day accumulated rainfall obtained from each model's basin average rainfall.

6.4.2 Flood vulnerability

The developed damage curves, details of which are described in Chapter 4, were also used in this part of the dissertation as the vulnerability component for future flood risk assessment in the study area.

6.4.3 Flood exposure

The third component of the flood risk assessment model is the exposure, which is mainly related to land-use land-cover maps. The Boro rice land cover maps for the future climate were predicted based on the previous land use change trend. Previous Boro land cover maps provided by International Rice Research Institute for 2000, 2010, and 2017 were used for this purpose. A land change modeller (LCM) developed by Clark Labs, Clark University (Clark Labs, 2019) was used to predict future land cover. In LCM, a Markov Chain and logistic regression was applied to determine the suitable spatial configuration considering particular driver factors. The driver factors that were used in this study to influence the change allocation were the DEM and slope. The previous land cover maps provided by IRRI were divided into two classes (rainfed and irrigated Boro). Accordingly, the future land cover maps were predicted with these two land cover classes. Figure 6.2 shows the previous and predicted land cover maps for the Boro rice in the study area. Instead of showing all land cover maps predicted for the considered flood years for each GCM, a sample Boro land cover map predicted for a random year of 2056 is shown in the figure.

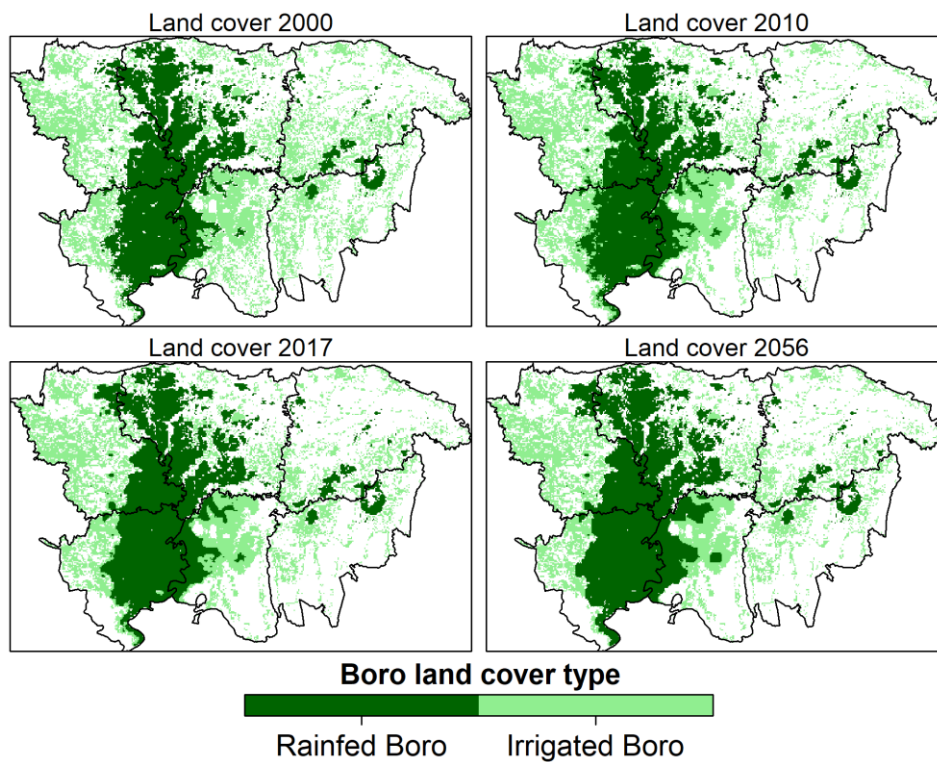


Figure 6.2: Past and predicted land cover maps of Boro rice in the study area

6.5 Results and discussion

To observe agricultural flood risk in the study area, future flood damage to Boro rice was estimated by combining three components of flood risk assessment model: flood hazard, vulnerability, and exposure. Future flood hazard was estimated in terms of inundation depth and duration by simulating the corrected outputs of the selected GCMs using the calibrated and validated RRI model. Present damage curves were used for vulnerability estimation, and flood exposure was assessed using the predicted land cover maps.

6.5.1 Flood hazard estimation for future climate

Corrected rainfall outputs from the each selected GCM were used to estimate future flood hazard in this study. To select extreme flood events in future climate for each GCM, basin averaged 5-day accumulated maximum rainfall was used. Figure 6.3a–b,

respectively, show basin averaged 1-day and 5-day accumulated maximum rainfall for the past (1991-2000) as well as future (2040-2059) climates. The figures are drawn for the months of March and April since flash floods in the study area usually occur during these two months of a year. The results showed significant amount of increase in future rainfall for the later eight models of the ten selected models, which may lead to an increase in inundation depths and areas. Consequently, these eight models were selected to simulate future hazard in terms of inundation depth and duration using the RRI model.



Figure 6.3: Basin averaged extreme rainfall of each selected GCM for the past (1981-2000) and future climate (2040-2059) drawn for the months of March and April considering (a) 1-day and (b) 5-day accumulated maximum rainfall.

Based on the 5-day accumulated maximum rainfall, flood event of each GCM for the future climate was selected. Daily rainfall data of each selected flood event were used to force the calibrated and validated RRI model for generating inundation maps in terms of maximum depths and duration for each grid cell (~ 500m) of the study area. Figure 6.4 shows the flood hazard maps in terms of peak flood depths for each flood event of the each model. The hazard map of the past flood of 2017 was also provided in the figure. The results showed that the 2017 flood was a big flood compared to most of the future floods in terms of flood inundation depths and extent. Only two models (GFDL-ESM2G and MRI-CGCM3) showed increased amount of inundation depths for future floods than the past flood of 2017.

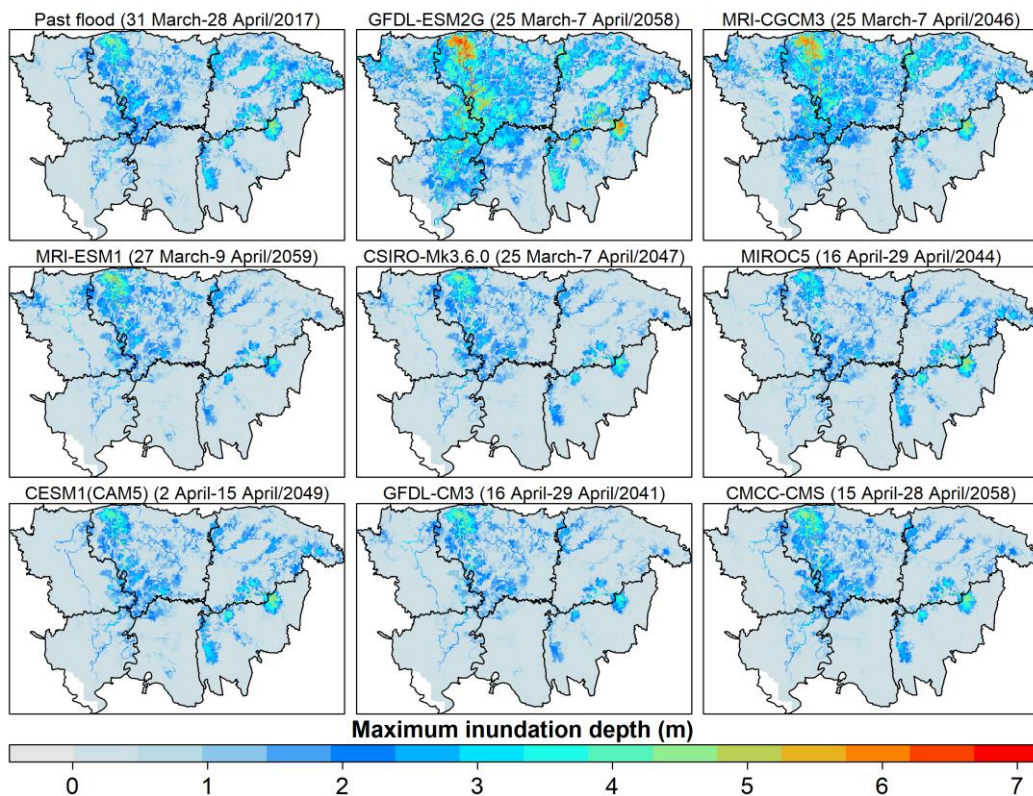


Figure 6.4: Flood inundation maps in terms of maximum depths for the past and future climates.

In line with the maximum inundation depth comparison by Figure 6.4, the area of inundation produced by each model for the future climate was also compared with that of

the past climate. Figure 6.5 compares the area of inundation generated by each selected GCM with that of the past flood (2017) for different sets of inundation depths. It was observed that two of eight models showed an increase in inundation areas, whereas six other models resulted in decrease in total inundation area compared to the past flood. However, almost all models showed an increase in inundation area with a depth of over 75 cm at which approximately 100 percent Boro rice damage occur (refer to Figure 5.7a). It is also found that the Mud house type is likely to be more vulnerable in future since nearly all models showed increased area of inundation with a depth over 1.5 m at which the building and goods of Mud households are completely destroyed (refer to Figure 5.7b, c). Another finding is that the area of inundation with maximum inundation depths will decrease in future, shown by six of eight models, which indicates that the agricultural damage is likely to be larger than the household damage.

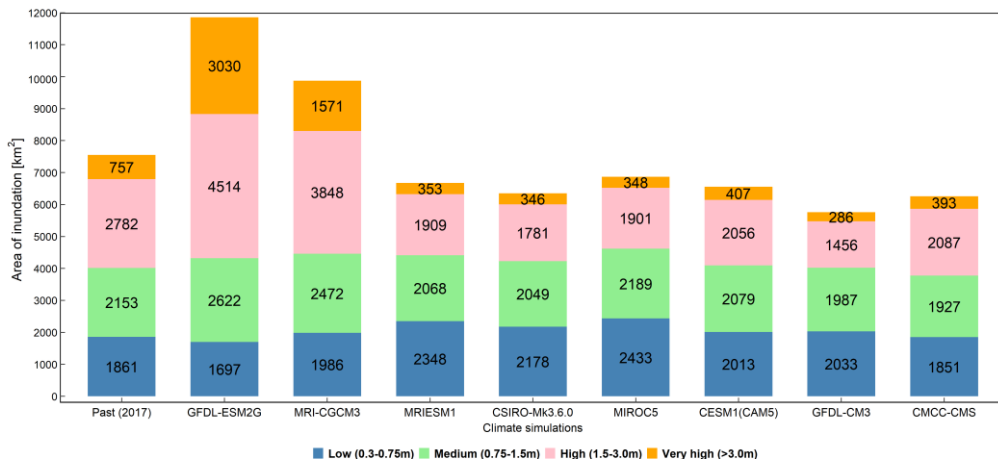


Figure 6.5: Comparison of flood inundation areas for past and future climates considering different sets of flood inundation depths.

All together, the results showed that the inundation depths and area are the main impacts of climate change. Future hazard maps showing flood depths and extent of inundation will help to identify the areas at high risk to be prioritized and thus provide important information for integrated flood risk management in the study area.

6.5.2 Agriculture land cover change

Future land cover change for Boro rice extent was predicted based on past Boro maps, and accordingly a sample Boro land cover map for a random year of 2056 was derived (shown in Figure 6.2) for agricultural risk assessment in the study area due to changes in climate and land use. Figure 6.6 shows the changes in the cultivating area of Boro rice (extent of Boro coverage) of two classes (rainfed and irrigated Boro) from past to future. It is observed that the area of rainfed Boro may increase from 2017 to 2056 by 7%, while the irrigated Boro area may decrease by 13%. The changes in the Boro land cover from 2000 to 2010, 2017, and 2056 (Figure 6.6) showed an increase in rainfed Boro and decrease in irrigated Boro. The fact of increasing adjacent rainfed Boro area is because of the land's lower elevation. These low lying lands are suitable only for agriculture purposes, but not for built-up uses. On the other hand, irrigated Boro land, which consists of high elevation areas, are suitable to extend built-up areas. The use of this kind of land is increasing for buildings and infrastructure constructions, which leads to a decrease in irrigated Boro areas.

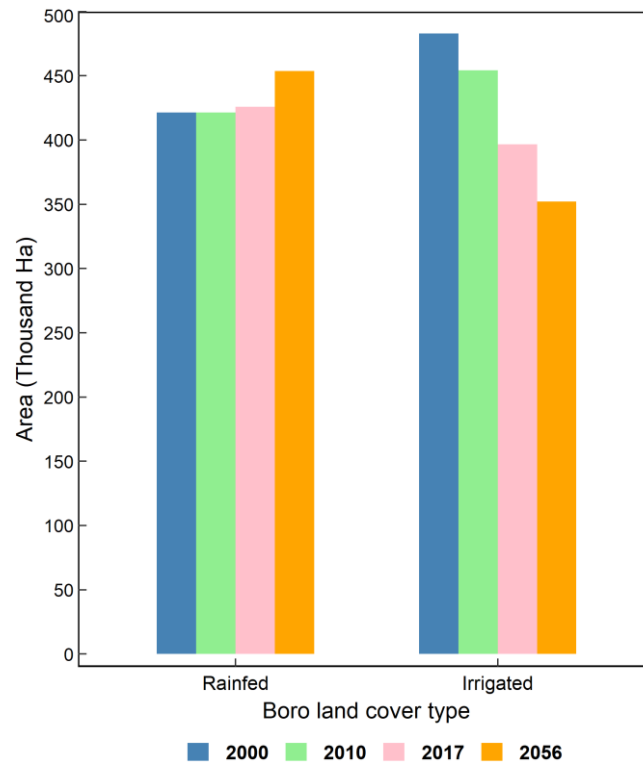


Figure 6.6: Land cover change from past to future for the Boro rice of two classes.

6.5.3 Flood damage functions

To assess agricultural flood risk, vulnerability represented by damage functions is needed to be integrated with hazard and exposure components. In this study, the Boro damage curves developed and described in Chapter 4 were used for agricultural damage assessment in future.

6.5.4 Future damage assessment

In this study, flood damage to Boro rice (agricultural damage) was assessed for future climate. This study has not considered to estimate household damage (that includes both house building and in-house property damage) for future climate to avoid greater uncertainty that might be raised from household distribution map. No methodology has yet been established to predict number of future households in any study area. However, a future household distribution map can be predicted by using predicted future population and predicted household size. All these together will produce more uncertainties in

preparing household distribution map that might lead to erroneous results in future household damage estimation. Another reason for not estimating future household damage in this study is that the agricultural damage is likely to be larger than the household damage in future climate, which has been revealed from future hazard analysis by this study. Therefore, Boro damage estimation was only considered for future climate in this study. Damage estimation was performed for each flood event of the selected GCMs considered for hazard estimation. Predicted Boro land cover maps and the developed damage curves at present value were incorporated in damage estimation as exposure and vulnerability components, respectively. Figure 6.7 shows flood damage to Boro rice estimated for each flood event of the selected GCMs.

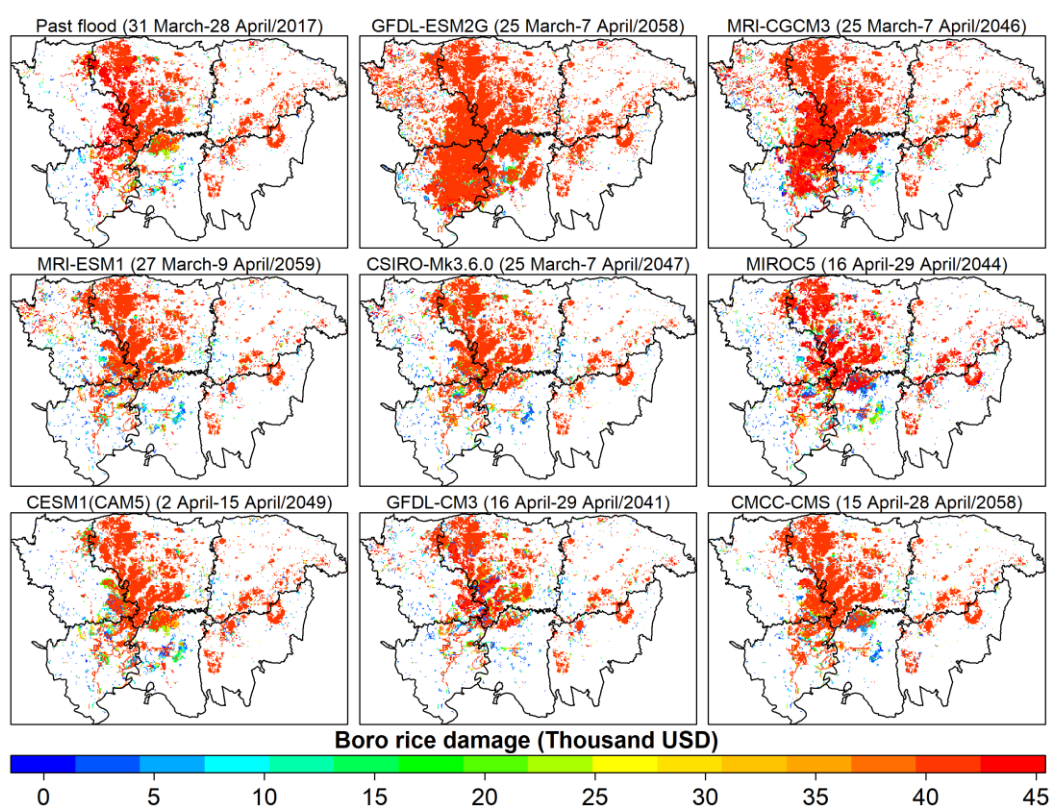


Figure 6.7: Flood damage maps estimated for Boro rice damage for different future flood events considering the changes in global climate and land use.

Similar to the calculated future hazard, two models showed an increase and the other six models showed a decrease in the extent of flood damage to Boro rice in future compared to that of the 2017 past flood. Although some models showed decreased extent of Boro rice damage in future, yet their total figure showed a huge amount of economic damage, as shown in Figure 6.8. The figure shows the total amount of flood damage to Boro rice in future calculated for the study area for each GCM. It was observed that the maximum total estimated damage to Boro rice by one GCM was amounted to 1049 million USD in future, a 124% increase compared to the damage estimated and validated for the 2017 flood. However, average estimated damage of all the models (GCMs) showed 543 million USD, a 16% increase in future compared to the past. The generated future damage maps will help detect the area vulnerable to agricultural flood risk and also investigate the benefits of implementing risk reduction measures (Olsen et al., 2015; Kefi et al., 2018).

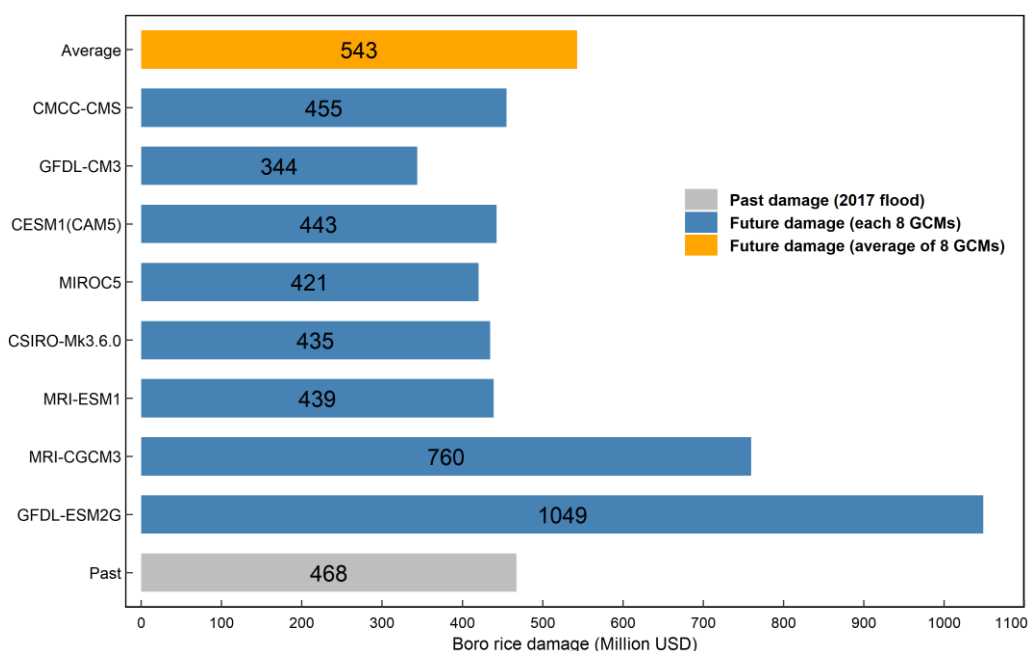


Figure 6.8: Total amount of flood damage to Boro rice in future calculated for the study area considering the flood events of each selected GCM.

6.5.5 Agricultural risk reduction

During abnormal flash floods in the study area, excess water need to be facilitated to reduce agricultural risk. For this purpose, this study recommends two possible alternatives together with the existing measures. One recommendation is based on structural measure and the other one is on non-structural measure. The structural measure includes river channel dredging and widening to mitigate agricultural damage as well as other damages (such as households, livestock, roads, etc.) during floods. The rivers in the study area get silted up for long, and they are never dredged to maintain the channel section of the rivers. To examine if the structural is measure is effective, the calibrated and validated RRI model was run for one GCM (MIROC5), as a sample case, with a changing river cross sections. The depths and widths of the river channels were increased by 2m and 5m respectively and accordingly the model was run for MIROC5 model to generate the hazard maps. Figure 6.9a–b, respectively, shows the hazard maps generated for the MIROC5 model without and with structural mitigation measure. Figure 6.10 compares the areas of inundation generated by the MIROC5 model for different sets of inundation depths without and with the mitigation measure. Together, the results showed a decrease in inundation areas and depths with the structural mitigation measure, indicating its effectiveness in reducing flood damage in the study area.

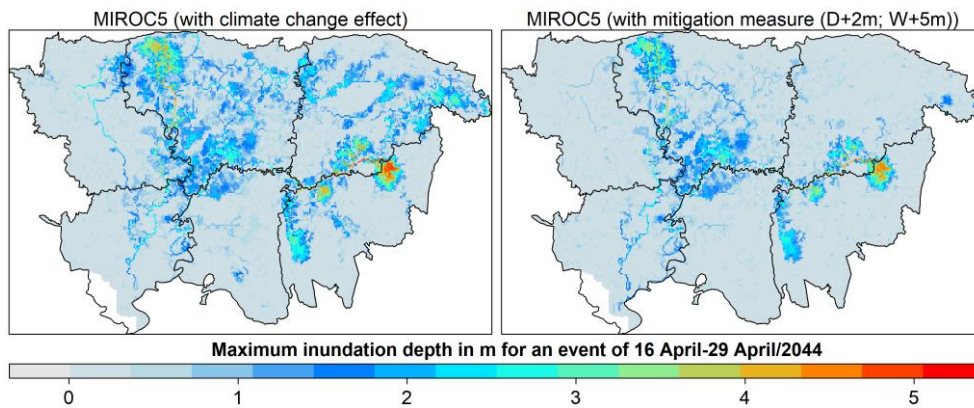


Figure 6.9: Hazard maps generated for the MIROC5 model (a) without and (b) with the structural measure (river channel dredging and widening).

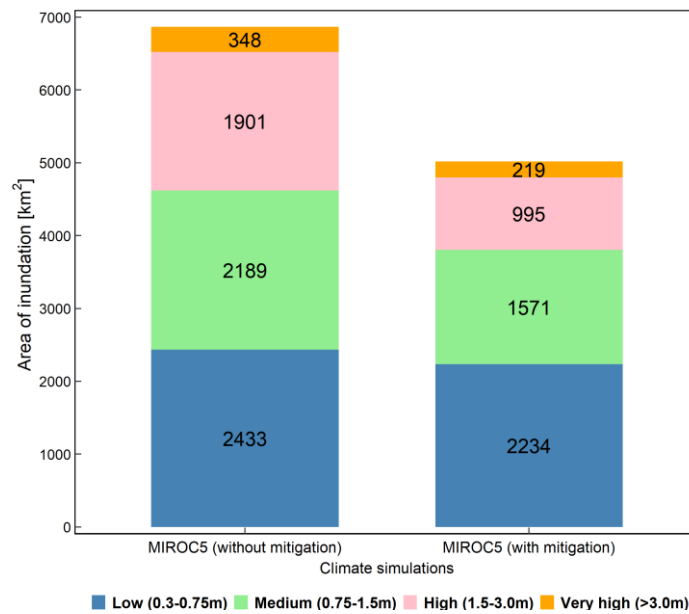


Figure 6.10: Comparison of flood inundation areas for different sets of flood inundation depths without and with the structural measure (river channel dredging and widening).

Agricultural flood damage (flood damage to Boro rice) without and with the mitigation measure for the aforesaid GCM was estimated and shown in Figure 6.11. The results showed a 41% decrease in agriculture damage with the structural mitigation measure (2m and 5m increase in river depths and widths, respectively).

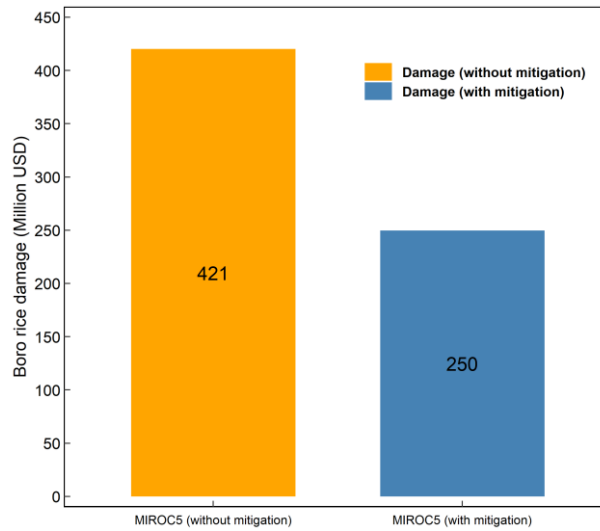


Figure 6.11: Flood damage to Boro rice without and with the structural measure (river channel dredging and widening).

Based on the results of this study, a non-structural measure is recommended to facilitate excess water during floods for reducing agricultural damage. This measure allows water to enter into the Haors of Boro fields in a regulated way up to an average of 25 cm water depth (the height at which rice tiller evolves). From the field survey results, it is revealed that flood water up to 25 cm of depth across the Boro field will cause no damage to rice, but duration of maturity may be longer by about 15 days. By applying this method, a huge volume of excess water can be stored temporarily in around 423 Haors in the area. To investigate the effectiveness of this non-structural measure, the calibrated and validated RRI model was run for the MIROC5 model (for one GCM as sample case) with pumping out water of $\sim 21 \times 10^8 \text{ m}^3$ from two rivers at border points, as shown in Figure 6.12a. The amount of water that pumped out was estimated considering an area downstream of the aforementioned two rivers, as shown in Figure 6.12a. The estimated area was about 8500 sq. km. Considering the 25 cm of water depth, the amount of water to be pumped out was calculated as $8500 \text{ sq. km} \times 25 \text{ cm} = 8500 \times 10^6 \times 0.25 \text{ m}^3 = 21 \times 10^8 \text{ m}^3$. Figure 6.12b shows the hazard map generated with the non-

structural measure marking the area with an oval shape considered for risk mitigation. Flood damage to Boro rice was estimated with this non-structural mitigation measure, and the results showed a 7% decrease in Boro rice damage, as shown in Figure 6.13. The RRI simulations will predict further decreases in flood damage to Boro rice by this non-structural mean if we consider pumping out water from all the rivers and the whole study area.

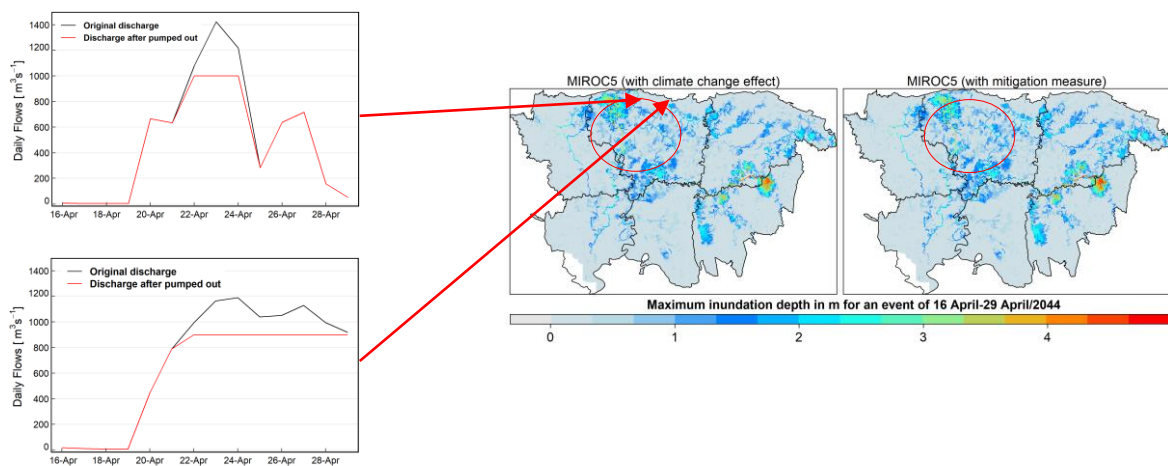


Figure 6.12: Hazard maps generated without and with the non-structural measure.

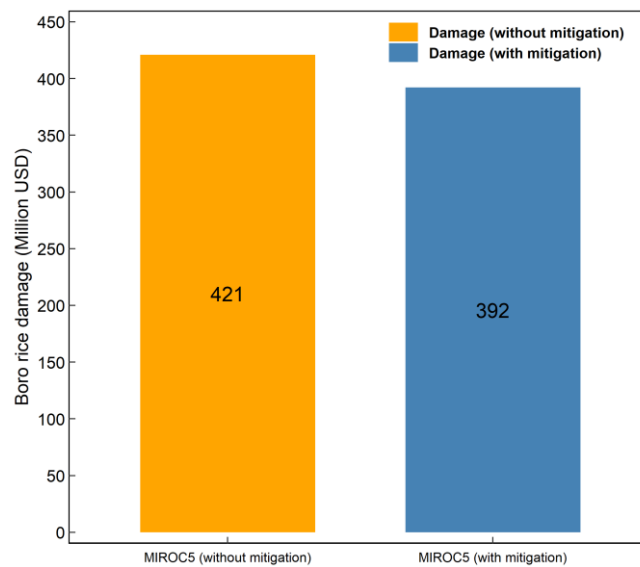


Figure 6.13: Flood damage to Boro rice without and with the non-structural measure.

6.6 Conclusion

Flood risk was assessed in the study area in terms of agricultural damage considering the effect of climate change and land use change. Flood hazard, exposure, and vulnerability were assessed first, and then combined them to estimate such flood damage. Eight selected Global Climate Models (GCMs) were used to map future hazard in terms of flood inundation depths, extent, and duration using the calibrated and validated RRI model. Flood hazard maps showed an increase in flood inundation depths as well as extent of flood inundation in future. Future exposure maps of Boro rice extent for the flood years of each GCM were predicted through a land change modeller that uses past land cover maps as input data. Present developed curves were used as vulnerability for this component of the study. By integrating hazard, exposure, and vulnerability components, future flood damage to Boro rice was estimated for each flood event of the selected GCMs. The maximum Boro rice damage estimated by a GCM amounted to 1049 million USD in future, a 124% increase compared to past damage. However, average estimated damage of all the models (GCMs) showed 543 million USD, a 16% increase in future. To facilitate excess water during floods for reducing agricultural flood damage, structural as well as non-structural measures were recommended. The results showed a significant decrease in flood damage to Boro rice through the recommended measures.

The hazard and risk maps generated for future climate in this study will help the decision makers formulate climate change adaptation plans in a short- and long-term basis. The findings can also be considered in policy making for preparedness and for reduction, management of current as well as future flood disaster risk.

Chapter 7: Summary and conclusions

7.1 Overall summary

In this study, a research framework is proposed to perform integrated flood risk assessment (IFRA) in an inaccessible and poorly gauged transboundary river basin, the Meghna, which is shared by India and Bangladesh. The Bangladesh part is mainly dominated by agriculture and greatly supports the country and its economy. Therefore IFRA is essential in this part of the country to strengthen preparedness for effective response to and recovery from flood events and to build back better based on the Sendai framework and globally supported sustainable development goals. However, because of various limitations, such as lack of local observed data and unavailability of hydro-meteorological and water use data from India, IFRA becomes difficult to perform for Bangladesh in the Meghna basin. Accordingly, the research framework for IFRA has been proposed by this study aiming to acquire evidence-based policy level information for sustainable development. An IFRA model consists of assessment of flood hazard, flood vulnerability, and flood exposure. Therefore, in support of the framework, this research focused on the hazard assessment for present and future climate using ground and satellite data, vulnerability assessment based on field survey results, and exposure assessment by using globally available observed and satellite information. By combining hazard, vulnerability, and exposure elements of IFRA model, flood damage and risk maps were produced for three different damage classes. Finally, policy implications through structural and non-structural means were proposed to reduce flood disaster risk for sustainable development of the study area. Summarized findings and conclusions are drawn in the following sub-sections.

7.1.1 Summary and findings on hazard assessment

Basin-wide rainfall data are required as driving force for any hydrological model to simulate the hazard parameters, such depth, duration, and extent of inundation. However, due to sparse local ground data and lack of upstream hydro-meteorological data in the Meghna basin, this study used globally available satellite rainfall estimates to simulate hazard parameters in the basin. To do so, four Gauge-adjusted Satellite Rainfall Products (GSRPs) were used to develop a reference rainfall data for the basin. Since satellite rainfall are affected by biases, the GSRPs were improved against locally available gauge rainfall by using several bias correction and merging techniques. Correction factors and merging weights were calculated at the local gauges and are spatially distributed by adopting an interpolation method to improve the GSRPs, both inside and outside Bangladesh. The combined use of merging and bias correction provided the best results, thus producing an improved reference dataset. The potential of this dataset was successfully investigated by calibrating and validating a 2D hydrological model called Rainfall-Runoff-Inundation (RRI) to the simulated streamflows. The calibrated and validated RRI model was then forced with the developed reliable rainfall data to generate hazard maps for a past climate in terms of inundation depths, duration, and extent across the basin. The major finding is that the globally available satellite rainfall products can overcome the data scarcity issues in transboundary river basins. Despite the limitation and uncertainty, reliable rainfall information can be created out of satellite products to simulate hydrological responses of a transboundary river basin for effective flood risk and water resources management for sustainable development.

7.1.2 Summary and findings on vulnerability assessment

Vulnerability is usually represented by depth-damage functions that can be of two types: empirical (developed from actual data) or synthetic (developed from questionnaire survey). However, due to the lack of integrated damage data, a structured questionnaire survey was conducted to collect damage data for the Boro rice (main crop of the study area) and different types of households. While analyzing the collected data, variability was observed within the dataset for each damage category, which might be due to the difference in experience and memories of each respondent. Other reason, in the case of household damage variability, could be the variety of building materials that the houses are constructed of. Despite the variability found in the collected dataset, their standard deviation was reasonably small in quantity for each damage category, which indicates that the actual damage might not differ from the damage collected during the questionnaire survey. However, to avoid least uncertainty, standard deviation (σ) obtained from the collected data for each damage class was integrated with the established damage curves as maxima ($+1\sigma$) and minima (-1σ). In such a way, this study established damage functions for Boro rice (considering its flowering through maturity stage as floods hit the study area at this stage of the rice), house building, and household property damage. The functions revealed that the flood damage is more serious with the increase of inundation depth. Rice damage becomes approximately 100% at 70–75 cm of water depth (the height at which grains start to flourish) and a flood duration of seven and/or more days. One important finding is that the Boro plants can tolerate the inundation depth up to an average of 25 cm (the height at which the tiller of the rice evolves). However, at this water depth, the maturity of the rice might be delayed by about 15–20 days. The functions also revealed that the household damage is mainly dependent on inundation height above floor

level, and the type of houses (e.g., Mud, Brick, and Concrete). Mud houses, compared to others, were found most vulnerable to flood due to their construction method and building materials.

7.1.3 Summary and findings on exposure assessment

In this study, exposure assessment was required for Boro rice extent and household distribution. Extent of Boro rice for the study area was extracted from a land cover map provided by IRRI. The Boro area by district calculated from the IRRI map was verified with the reported data collected from Department of Agricultural Extension, Bangladesh. The comparison found the calculated data satisfactorily agree with the reported data. For household exposure assessment, a household distribution map with the proportion of each type of house in the study area was required. However, neither such map nor such observed data for the study area was available. Therefore, this study prepared a grid based household distribution map using LandScan population distribution, average family size, and proportion of house types, by district. The calculated number of houses by district reasonably agree with the census data obtained from Bangladesh Bureau of Statistics. However, the distribution of houses in the prepared map might not agree with the actual house distribution of the area, which might produce uncertainties in household flood damage estimation.

7.1.4 Summary and findings on flood damage assessment

Potential damage to Boro rice and households (that includes house buildings and in-house properties) was estimated for the 2017 flood by combining the three components of IFRA model: flood hazard, vulnerability and exposures. The estimated area with Boro rice damage (~237 734 ha) was found to agree with the reported area (225 840 ha). The total damage to Boro rice was estimated to be 372, 589 and 468 million USD considering

minimum, maximum and average rice yield, respectively. Such reported damage obtained from three different sources, respectively, were 356, 612 and 450 million USD, which satisfactorily agree with the estimated Boro damage. The total household damage (house building plus in-house properties), on the other hand, amounted to 461 million USD, which couldn't be validated due to lack of reported data. However, the estimated number of affected households (~776 579) were compared with that of the reported figure (850 088), and was found to be underestimated, which might result from the household distribution map prepared considering population distribution and average household size by district. A precise household distribution map might overcome this issue. Altogether, the developed IFRA model was satisfactorily conducted and validated for a flood of past climate by this study.

7.1.5 Summary and findings on risk assessment due to global change

Flood risk due to the global changes in climate and land use was assessed by using the validated IFRA model to support the research framework of this study. Hazard parameters for future climate were simulated by using bias-corrected daily precipitation outputs of ten GCMs selected from 44 models considering the RCP scenario of 8.5. Rainfall analysis showed an increase in future rainfall for eight of the selected ten models. Daily rainfall outputs of these eight models were then used to produce hazard maps through the calibrated and validated RRI model for extreme flood events of each model. The flood events for each model were obtained based on a sequential 5-day maximum rainfall calculated from basin averaged rainfall of each model. The generated hazard maps revealed that the inundation depths and area are likely to be the main impacts of climate change. The results showed an increase in inundation areas with a depth over 75 cm at which approximately 100 percent of Boro rice damage occurs. The results also showed

that the Mud house type is likely to be more vulnerable in future as inundation areas with a depth over 1.5 m (at which the building and goods of Mud households are completely destroyed) will increase. Another finding is that the area of inundation with maximum inundation depths (over 2–3m) will decrease in future, which indicates that the agricultural damage is likely to be larger than the household damage.

In this study, only agricultural flood risk under global change (primarily for Boro rice) was assessed. This study has not considered to assess flood risk for household (that includes house building and in-house property damage) under global change for avoiding greater uncertainty that might be raised from household distribution map prepared by this study. To estimate agricultural flood risk, future vulnerability and exposure assessment are also required together with the future hazard assessment. For this purpose, the established Boro damage curves (at present value) were used to estimate flood vulnerability, and for exposure assessment, Boro land cover maps were predicted using a land change modeler that uses the changing trend of past Boro land cover maps provided by IRRI. Following the IFRA model, flood risk map for Boro rice in terms of potential flood damage was produced for each flood event of the selected GCMs by combining future hazard parameters with the predicted Boro land cover and present vulnerability. The maximum Boro rice damage estimated for a GCM amounted to 1049 million USD in future, a 124% increase, compared to the damage estimated for the 2017 flood. However, an average estimated damage of all the models (GCMs) showed 543 million USD, a 16% increase in future, compared to the past damage.

7.2 Contribution and applicability of the study

The contribution and applicability of this study's methodology are divided into several points and discussed as follows:

(1) This study developed a basin-wide reference rainfall data, as a first attempt, in a poorly gauged and inaccessible transboundary river basin by using locally available ground and globally available satellite rainfall data. The dataset was satisfactorily validated temporally and spatially on both point and basin scales and investigated for its potential to the simulated streamflows. Finally, this developed dataset was successfully used to map flood hazard in terms of inundation depth, duration, and extent for a past flood. The methodology of creating such reference rainfall data can also be applicable to other transboundary river basins to:

- Overcome transboundary data scarcity issues.
- Fill gaps to local ground measurements.
- Serve as reference data for various applications (e.g., flood modelling, hazard and risk assessment, construction of hydraulic structures, etc.)

The methodology can also be used to perform near-real-time (NRT) flood forecasting using freely available NRT satellite products.

(2) Due to the lack of integrated flood damage data in Bangladesh, this study, as a first attempt, established flood damage functions for agriculture and households through the data of a questionnaire survey conducted in the study area. The damage functions are useful for

- Post disaster flood damage assessment.
- Near-real-time flood damage assessment.
- Potential flood risk assessment

The methodology for establishing flood damage functions can also be used developing damage functions for other damage classes and for other areas of interest as well.

(3) This study, as a first attempt, developed an IFRA model in a transboundary river basin. The model was performed for estimating flood damage to agriculture and household for the study area considering a past flood event of 2017, and satisfactorily validated the estimated results with the reported statistics. Finally, the model was used to produce flood hazard, damage and risk maps under changing climate as well.

(4) Flood hazard maps (both past and future) showing flood depths and extent of inundation can help identify and map the flood prone areas at local scale. They can also be helpful to detect the areas at high risk to be prioritized and thus provide important information for flood risk management in the study area. In addition, the hazard maps can be used for land-use planning in flood prone areas. Moreover, flood hazard maps can increase awareness of flooding among the inhabitants of the study area. Such maps also encourage inhabitants to find out more about local flood risk and help them to take appropriate preparedness. Using the hazard maps, inhabitants can also identify the spots for safe evacuation during the time of flood.

(5) Flood damage and risk maps can be of great help for a number of stakeholders in policy making for flood risk reduction and management to achieve the goals of Sendai framework and sustainable development goals. Past maps can help introduce and strengthen flood forecasting and early warning system by constructing observation network in the study area, especially along the Bangladesh–India border. Future maps can help formulate climate adaptation plans, strengthen emergency preparedness by allocating resource and funds, and identify priority measures. They can also be useful for planning and designing structural as well as non-structural measures. Moreover, they can be used for cost-benefit analysis of various risk reduction measures.

(6) This study can be extended and applied to other floods and regions of Bangladesh, such as Ganges and Brahmaputra basins. However, created reference rainfall data need to be validated, and their potential also need to be investigated through a hydrological model to simulated streamflows. In addition, damage functions for various damage classes that might be different from the classes considered in this study are also required to be established.

(7) The methodology of this study can benefit the upstream nations of a transboundary river. If any upstream country faces data scarcity issues (ungauged, poorly gauged or transboundary issues), the methodology of this study can be used to create a reliable distributed rainfall data to simulate hydrological responses of the basins for effective flood risk management. India can use such methodology in the Ganges and Brahmaputra basins as hydro-meteorological data are not available from Nepal, Bhutan, and China, the upstream countries of these basins. The methodology can also be used as a tool for investigating, analyzing, and assessing the common issues present in the transboundary basins between the riparian countries, which can lead to create a data exchange framework and provide a win-win situation. Between Bangladesh and India, this study can be a pioneer to promote mutual collaboration, trust, and cooperation, which is importantly necessary for sustainable development of the two nations.

(8) Similar to the Meghna river basin, many other transboundary river basins throughout the world have been facing challenges in flood risk management for sustainable development. Despite the presence of Nile Basin Initiative (NBI), one of Africa's largest and important river basin spanning over ten countries, the Nile faces problems of basin-wide coordinated water policy and lack of hydro-meteorological and water use data and information to predict floods and droughts. For these reasons,

integrated flood management becomes crucial for the riparian countries, especially for the countries of the eastern Nile basin (Ethiopia, Sudan, and Egypt). Other transboundary river basins, such as Ganges, Brahmaputra, Niger, Mekong, La Plata, Volta, Euphrates, etc. face the same challenges as the Meghna and Nile do. Any country under these river basins can prepare long-term reliable rainfall information to overcome the data limitations and perform better flood risk management practices following the method used by this study. Therefore, the methodology developed in this study for a transboundary river basin, the Meghna, can also be applicable to other transboundary basins to improve the existing risk mitigation measures by providing evidence based information for practicing better flood risk management and for sustainable development of the basins. By understanding the benefits derived from the methodology of this study, a win-win situation can be created between the countries of a transboundary river basin, and accordingly policies can be formulated to share the benefits.

7.3 Limitations of the study

This study has the following limitations that are recommended to address in future studies.

(1) The questionnaire survey conducted for this study to collect flood damage data was limited to three main damage classes (Boro rice, house building and in-house properties). It is recommended to conduct such questionnaire survey in future study for other damage classes too, such as road damage, livestock damage, etc.

(2) The damage data for the said damage classes were collected considering two main driving factors: flood depths and duration for Boro rice damage, and only depths for household damage. It is recommended to collect such data for a future study by including

other factors, such as age, gender, and income of the respondents, distance of household from rivers, building materials of same household type, etc.

(3) The flood damage estimation in this study was limited to agriculture (Boro rice) and household damage (building and property) for past climate and that to agriculture damage for future climate. It is recommended to estimate flood damage in future study for other damage classes as well if damage data/functions are available.

(4) The house distribution map was prepared in this study using population distribution and average household size. It is recommended to prepare an actual household distribution map through field survey or by using finer resolution satellite map.

(5) Structural and non-structural measures are proposed by this study for reducing the agricultural flood risk in the study area. It is recommended to assess cost benefit analysis in future study for the proposed risk reduction measures.

(6) The IFRA methodology is developed for the rural northeastern Bangladesh located downstream of the Meghna river basin. To conduct such methodology in an urban area might require other parameters to be considered, such as drainage facilities to be incorporated in hydrological model, building materials for establishing damage functions, etc.

Chapter 8: Policy implications

8.1 Existing policy approaches

To reduce flood risk in the Meghna basin area, Bangladesh has been adopting both structural and non-structural measures together. Structural measures include submergible embankments (SEs) and river embankments (REs). SEs, up to a certain level of design height, are meant to be constructed to protect Boro rice that are cultivated inside Haors (draining depressions). REs, on the other hand, are discontinuously constructed along river banks to prevent river bank erosion and to reduce structure and property damage, such as households, livestock, private properties, mosques, historical places, etc. As a non-structural measure, an inundation map (hazard map showing only extent of inundation) with a 3-day probabilistic forecasting is produced by assuming fixed river discharge and water level at the country's border, and made available online only in order to warn the residents of the area to save their lives and assets. However, these existing measures didn't work out in reducing agriculture, structure, and property damage during the past floods of 2004, 2010, 2016, and 2017. Therefore, together with the existing approaches, this study recommends several additional measures for the policy makers based on the results and findings to reduce flood risk in the area.

8.2 Policy recommendations

Under the research framework of this study, first, local and transboundary data scarcity issues in the Meghna river basin was addressed, and accordingly a reliable distributed rainfall dataset was developed for the basin by using both ground observations and satellite estimates. Such developed rainfall were used as reference data for hydrological simulations in the basin. This study also addressed local flood damage data issues and accordingly established damage functions for Boro rice, different types of

house buildings, and in-house properties through the data of a questionnaire survey conducted in the study area. These functions were used as reference damage functions for the said damage classes in order to assess flood vulnerability in the study area. Finally, this study successfully conducted an Integrated Flood Risk Assessment (IFRA) model to generate flood hazard and risk maps for the past as well as future climates in order to achieve evidence-based policy level information for sustainable development of the study area and for building back better. The results revealed a number of findings, which have several policy level implications useful for different stakeholders. The decision makers under the Government of Bangladesh (GoB), non-government organizations (NGOs), and various development partners (DP) can utilize these findings in policy making for preparedness, recovery, reduction, prevention, and management of flood disaster risk. In the following paragraphs, several soft (non-structural) and hard (structural) policy measures are recommended based on the findings for reducing flood risk in the study area.

By following the methodology of this study, Bangladesh Water Development Board (BWDB) can create reliable rainfall data using near-real-time (NRT) satellite estimates for producing NRT flood forecasting along with the existing 3-day probabilistic forecasting. BWDB can install an automatic rainfall observation network near the borders between Bangladesh and India to further validate the created rainfall data and make it more reliable for effective NRT flood forecasting. BWDB can also set priorities of various development works and so make budget allocation in terms of location and timing using the results of this study for effective flood risk management. Benefit-cost analysis of such development works can also be performed by using the results of this study. Department of Agricultural Extension (DAE) and Department of Disaster Management

(DDM) of Bangladesh can utilize this study's methodology to collect flood damage data for a number of damage classes after a flood event to create a flood damage databank. The databank can be used to further validate the damage functions established by this study. It can also be used for establishing damage functions other than the damage classes considered in this study.

Detailed flood hazard maps of the study area can be prepared using this studies' results. Such prepared hazard maps will be able to show safe and danger water levels, spots of evacuation centers, and a lot of other important information such as personal information that can be used during flood time, etc. For their best utilization by the inhabitants, these hazard maps should be disseminated to the local government authority for providing information to the residents to increase their awareness during flood time. To fully implement the hazard maps in the local area and promote their maximum use, training programs are necessary to make the hazard maps understandable for the inhabitants. Implementation of such training program can help the inhabitants to enhance appropriate preparedness and identify the spots for safe evacuation during flood time, and thus local flood risk can greatly be reduced.

Apart from the above soft mitigation measures, another non-structural measure based on the new finding of this study is proposed to facilitate excess water for reducing agricultural risk during flood time. This non-structural measure allows water to enter into the Haors of Boro fields in a regulated way up to an average of 25 cm water depth (the height at which rice tiller evolves). From the field survey results, it is revealed that flood water up to that height across the Boro field will cause no damage to rice, although duration of maturity may be longer by about 15 days. By applying this method, a huge volume of excess water can be stored temporarily in around 423 Haors in the area.

Introduction of flood insurance program in the study area can be another soft solution to reduce flood disaster risk in case of big and abnormal floods. However, to establish a local flood insurance program, hazard, damage and risk maps are required, not for the current climate only, but for future climate as well, for which this study can be a pioneer to provide necessary maps for establishing local flood insurance program.

Introduction of flood insurance program can also effectively help reduce disaster risk if floods occur earlier than the expected time. Current pre-monsoon flash flooding usually occurs in the study area from late March to late April at the full height of Boro rice (from flowing through maturity stage). Hazard assessment due to climate change also showed the said range of duration for pre-monsoon flooding in the area. Flood risk reduction by allowing water into the Boro field up to an average of 25 cm depth is possible at the mentioned stage of the rice. However, if floods hit the area much earlier than the said duration at other earlier growth stages of the rice (such as seedling, vegetative stage), risk reduction by implementing this policy may not be effective. In such cases, flood insurance program can play an important role in reducing flood disaster risk in the area.

The results of household damage revealed that the Mud houses, which are dominant in the study area, are more vulnerable to flood due to their construction method and building materials. The construction cost of a Mud house is about USD 3500, whereas those of the Brick and Concrete houses respectively are USD 8500 and USD 16800. By reconstructing the Mud houses to Brick house under the aegis of GoB and NGOs, flood risk to households can significantly be reduced. Flood risk to households can also be reduced by elevating floor level from the ground (PL), as found from this study.

As a structural measure for reducing flood risk, dredging and widening of river channels are investigated by this study as the rivers of the area get silted up for long and never be dredged and widened to maintain their channel sections. As mentioned before, SEs and REs are the existing structural measures for reducing flood risk in the study area, but they were not effective during past floods. However, for reducing flood risk to more extent, high-cost permanent embankments with abnormal crest height or concrete embankments cannot be constructed as the environment and ecology of the area need to be preserved for aquaculture activities. Therefore, as an alternative structural measure, river dredging and widening is investigated and found effective during the pre-monsoon flood (March-April) in the Meghna basin. However, this measure might cause more inundation in the downstream area of the basin, which has not been investigated by this study. Therefore, the non-structural measures (soft measures) proposed by this study, such as near-real-time flood forecasting and warning, dissemination and implementation of hazard maps, allowing excess water into the Boro fields up to a 25 cm or more water height, and introduction of flood insurance program, were found more effective and environmentally friendly than the dredging and widening of river channels. These non-structural measures proposed by this study have to be promoted by the government as well as non-governments organizations for reducing increasing flood risk in the study area. The author who is an executive engineer of BWDB will make a presentation to the Director General, showing the results and findings of this study, and accordingly propose the recommended policies to be implemented as a pilot basis for reducing future flood disaster risk.

Appendix A.1

Sample questionnaire for Boro yield damage due to floods
[Please consider maturity stage (10-20 days before harvesting) of Boro paddy (BR-28/BR-29) during pre-monsoon flash flood (April flood)]

Name of interviewee:

District:

Occupation:

Sub-district:

Union:

a) Please provide general information of Boro paddy at maturity stage

1. Type of Farm holding: **Small** (5 – 249 decimal of operating land)
 Medium (250 – 749 decimal of operating land)
 Large (> 749 decimal of operating land)

2. Full Length/height of Boro paddy = _____ ft. _____ inch

3. Average expected yield = _____ Maund/Bigha

4. How many days your Boro paddy was inundated for?

Floods	2004	2010	2016	2017	Comments
Days					

5. What was the maximum inundation depth your Boro paddy experienced?

Floods	2004	2010	2016	2017	Comments
Depth (ft.)					

6. How much was the actual Boro rice production (**Maund/Bigha**)?

Floods	2004	2010	2016	2017	Comments
Production					

b) Please provide information of reduced Boro production due to inundation depth and duration

Inundation depth (ft.)	Reduced Production (Maund/Bigha)			Comments
	1-3 Days	4-6 Days	7 & above Days	
0.75	Average expected yield = _____ Maund/Bigha			
1				
1.5				
2				
2.5				
> 3				

Unit conversion: *1 Maund = 37.3242 kg.; 1 Bigha = 33 decimal*
 1 ft. = 12 inch; 1 inch = 2.54 cm

Appendix A.2

Sample questionnaire for house and household assets damage due to floods (Both Pre-monsoon and monsoon floods are considered)

Name of interviewee:

District:

Occupation:

Sub-district:

Union:

a) Please provide general information on house and household assets:

1. Type of house (with photograph):
 - Packa (Concrete)** (made of brick, cement, sand; concrete/CI sheet roof)
 - Semi-Packa (Brick)** (made of brick column and CI sheet; CI sheet roof)
 - Kaccha (Mud)** (made of mud and clay; Straw/CI sheet roof)
2. Floor level from ground = _____ ft. _____ inch
3. Approximate value of house = Thousand taka _____
4. Approximate value of household assets = Thousand taka _____
5. How many days your house was inundated for?

Floods	2004	2010	2016	2017	2018	Comments
Days						

6. How maximum the inundation depth above floor level your house was experienced?

Floods	2004	2010	2016	2017	2018	Comments
Depth (ft.)						

7. How much was the house recovery cost after flood (**Thousand taka**)?

Floods	2004	2010	2016	2017	2018	Comments
Cost						

8. How much was the loss of household assets in the flood (**Thousand taka**)?

Floods	2004	2010	2016	2017	2018	Comments
Loss						

b) Please provide information on recovery cost of house according to inundation depth

Inundation depth (ft.)	Recovery cost (Thousand taka) after floods	Comments
< *FL	No damage → Value of house = Thousand taka _____	
1		
2		
3		
4		
5		
6		
7		
8 and above		

* FL = Floor level from ground

c) Please provide information on loss of household assets according to inundation depth

Inundation depth (ft.)	Recovery cost (Thousand taka) after floods	Comments
< *FL	No damage → Value of assets = Thousand taka _____	
1		
2		
3		
4		
5		
6		
7 and above		

* FL = Floor level from ground

Unit conversion: *1 ft. = 12 inch; 1 inch = 2.54 cm*

Appendix B

Pictures taken from the questionnaire survey activities



References

- Ahmad QK, Ahmed A. (2003) Regional Cooperation in Flood Management in the Ganges-Brahmaputra-Meghna Region: Bangladesh Perspective. *Natural Hazards* 28:191–198. doi: 10.1023/A:1021186203100
- Aonashi K, Awaka J, Hirose M, et al (2009) GSMaP Passive Microwave Precipitation Retrieval Algorithm: Algorithm Description and Validation. *Journal of the Meteorological Society of Japan Ser II* 87A:119–136. doi: 10.2151/jmsj.87A.119
- Arias-Hidalgo M, Bhattacharya B, Mynett AE, van Griensven A (2013) Experiences in using the TMPA-3B42R satellite data to complement rain gauge measurements in the Ecuadorian coastal foothills. *Hydrol Earth Syst Sci* 17:2905–2915. doi: 10.5194/hess-17-2905-2013
- Bakker MHN (2009a) Transboundary river floods: examining countries, international river basins and continents. *Water Policy* 11:269–288
- Bakker MHN (2009b) Transboundary River Floods and Institutional Capacity. *JAWRA Journal of the American Water Resources Association* 45:553–566. doi: 10.1111/j.1752-1688.2009.00325.x
- Balthrop C, Hossain F (2010) Short note: A review of state of the art on treaties in relation to management of transboundary flooding in international river basins and the Global Precipitation Measurement mission. *Water Policy* 12:635–640. doi: 10.2166/wp.2009.117
- Beck HE, van Dijk AIJM, Levizzani V, et al (2017a) MSWEP: 3-hourly 0.25° global gridded precipitation (1979–2015) by merging gauge, satellite, and reanalysis data. *Hydrol Earth Syst Sci* 21:589–615. doi: 10.5194/hess-21-589-2017
- Beck HE, Vergopolan N, Pan M, et al (2017b) Global-scale evaluation of 22 precipitation datasets using gauge observations and hydrological modeling. *Hydrol Earth Syst Sci* 21:6201–6217. doi: 10.5194/hess-21-6201-2017
- Bhatti HA, Rientjes T, Haile AT, et al (2016) Evaluation of Bias Correction Method for Satellite-Based Rainfall Data. *Sensors (Basel)* 16:. doi: 10.3390/s16060884
- Biswas AK (2004) Integrated Water Resources Management: A Reassessment. *Water International* 29:248–256. doi: 10.1080/02508060408691775
- Blomquist W, Schlager E (2005) Political Pitfalls of Integrated Watershed Management. *Society & Natural Resources* 18:101–117. doi: 10.1080/08941920590894435
- Chen J, Brissette FP, Chaumont D, Braun M (2013) Finding appropriate bias correction methods in downscaling precipitation for hydrologic impact studies over North America. *Water Resour Res* 49:4187–4205. doi: 10.1002/wrcr.20331

- Chen J, St-Denis BG, Brissette FP, Lucas-Picher P (2016) Using Natural Variability as a Baseline to Evaluate the Performance of Bias Correction Methods in Hydrological Climate Change Impact Studies. *J Hydrometeor* 17:2155–2174. doi: 10.1175/JHM-D-15-0099.1
- Chowdhury MR (2000) An Assessment of Flood Forecasting in Bangladesh: The Experience of the 1998 Flood. *Natural Hazards* 22:139–163. doi: 10.1023/A:1008151023157
- Chowdhury MR, Ward N (2004) Hydro-meteorological variability in the greater Ganges–Brahmaputra–Meghna basins. *Int J Climatol* 24:1495–1508. doi: 10.1002/joc.1076
- Christensen JH, Boberg F, Christensen OB, Lucas-Picher P (2008) On the need for bias correction of regional climate change projections of temperature and precipitation. *Geophys Res Lett* 35:L20709. doi: 10.1029/2008GL035694
- Clark Labs (2019) Land Change Modeller for ArcGIS (Brochure). Available online: <https://clarklabs.org/landchange-modeler-for-arcgis/> (last accessed on 17 March, 2019).
- Dirks KN, Hay JE, Stow CD, Harris D (1998) High-resolution studies of rainfall on Norfolk Island: Part II: Interpolation of rainfall data. *Journal of Hydrology* 208:187–193. doi: 10.1016/S0022-1694(98)00155-3
- Dixit A (2003) Floods and Vulnerability: Need to Rethink Flood Management. *Natural Hazards* 28:155–179. doi: 10.1023/A:1021134218121
- Drieschova A, Giordano M, Fischhendler I (2008) Governance mechanisms to address flow variability in water treaties. *Global Environmental Change* 18:285–295. doi: 10.1016/j.gloenvcha.2008.01.005
- Dutta D, Herath S, Musiaka K (2003) A mathematical model for flood loss estimation. *Journal of Hydrology* 277:24–49. doi: 10.1016/S0022-1694(03)00084-2
- Ebert EE, Janowiak JE, Kidd C (2007) Comparison of Near-Real-Time Precipitation Estimates from Satellite Observations and Numerical Models. *Bull Amer Meteor Soc* 88:47–64. doi: 10.1175/BAMS-88-1-47
- Ehret U, Zehe E, Wulfmeyer V, et al (2012) HESS Opinions “Should we apply bias correction to global and regional climate model data?” *Hydrol Earth Syst Sci* 16:3391–3404. doi: 10.5194/hess-16-3391-2012
- Enserink, B., D. Kamps, E. Mostert (2003) Public Participation in River Basin Management in the Netherlands: (not) Everybody’s Concern. RBA-Centre, Delft University of Technology, Delft, the Netherlands.
- Fang GH, Yang J, Chen YN, Zammit C (2015) Comparing bias correction methods in downscaling meteorological variables for a hydrologic impact study in an arid

- area in China. *Hydrol Earth Syst Sci* 19:2547–2559. doi: 10.5194/hess-19-2547-2015
- FAO (2012) Food and Agriculture Organization of the United Nations: Irrigation in Southern and Eastern Asia in Figures, AQUASTAT Survey-2011, FAO Water Report #37, Rome.
- Farr TG, Rosen PA, Caro E, et al (2007) The Shuttle Radar Topography Mission. *Rev Geophys* 45:RG2004. doi: 10.1029/2005RG000183
- Felbermayr G, Gröschl J (2014) Naturally negative: The growth effects of natural disasters. *Journal of Development Economics* 111:92–106. doi: 10.1016/j.jdeveco.2014.07.004
- Funk C, Hoell A, Shukla S, et al (2014) Predicting East African spring droughts using Pacific and Indian Ocean sea surface temperature indices. *Hydrol Earth Syst Sci* 18:4965–4978. doi: 10.5194/hess-18-4965-2014
- Funk C, Peterson P, Landsfeld M, et al (2015) The climate hazards infrared precipitation with stations—a new environmental record for monitoring extremes. *Scientific Data* 2:sdata201566. doi: 10.1038/sdata.2015.66
- Gain AK, Hoque MM (2013) Flood risk assessment and its application in the eastern part of Dhaka City, Bangladesh. *Journal of Flood Risk Management* 6:219–228. doi: 10.1111/jfr3.12003
- Gain AK, Mojtahed V, Biscaro C, et al (2015) An integrated approach of flood risk assessment in the eastern part of Dhaka City. *Natural Hazards* 79:1499–1530. doi: 10.1007/s11069-015-1911-7
- Gopalakrishnan C, Tortajada C, Biswas AK (eds) (2005) *Water Institutions: Policies, Performance and Prospects*. Springer, the Netherlands
- Gopikrishnan S, Vinay T (2016) Validation of a Questionnaire for Objective Evaluation of Performance of Built Facilities. *Journal of Performance of Constructed Facilities* 30:04014191. doi: 10.1061/(ASCE)CF.1943-5509.0000705
- Grahn T, Nyberg L (2017) Assessment of pluvial flood exposure and vulnerability of residential areas. *International Journal of Disaster Risk Reduction* 21:367–375. doi: 10.1016/j.ijdr.2017.01.016
- Guo H, Chen S, Bao A, et al (2015) Inter-Comparison of High-Resolution Satellite Precipitation Products over Central Asia. *Remote Sensing* 7:7181–7211. doi: 10.3390/rs70607181
- Gusyev MA, Kwak Y, Khairul MI, et al (2015) Effectiveness of water infrastructure for river flood management – Part 1: Flood hazard assessment using hydrological models in Bangladesh. In: *Proceedings of the International Association of Hydrological Sciences*. Copernicus GmbH, pp 75–81

- Habib E, Haile AT, Sazib N, et al (2014) Effect of Bias Correction of Satellite-Rainfall Estimates on Runoff Simulations at the Source of the Upper Blue Nile. *Remote Sensing* 6:6688–6708. doi: 10.3390/rs6076688
- Haile AT, Habib E, Rientjes THM (2013) Evaluation of the climate prediction center CPC morphing technique CMORPH rainfall product on hourly time scales over the source of the Blue Nile river. *Hydrological processes* 27:1829–1938. doi: 10.1002/hyp.9330
- Hasan MM, Sharma A, Johnson F, et al (2016) Merging radar and in situ rainfall measurements: An assessment of different combination algorithms. *Water Resour Res* 52:8384–8398. doi: 10.1002/2015WR018441
- Hasanzadeh Nafari R, Amadio M, Ngo T, Mysiak J (2017) Flood loss modelling with FLF-IT: a new flood loss function for Italian residential structures. *Natural Hazards and Earth System Sciences* 17:1047–1059. doi: <https://doi.org/10.5194/nhess-17-1047-2017>
- Hay LE, Clark MP (2003) Use of statistically and dynamically downscaled atmospheric model output for hydrologic simulations in three mountainous basins in the western United States. *Journal of Hydrology* 282:56–75. doi: 10.1016/S0022-1694(03)00252-X
- Hay LE, Wilby RL, Leavesley GH (2000) A Comparison of Delta Change and Downscaled Gcm Scenarios for Three Mountainous Basins in the United States1. *JAWRA Journal of the American Water Resources Association* 36:387–397. doi: 10.1111/j.1752-1688.2000.tb04276.x
- Heistermann M, Kneis D (2011) Benchmarking quantitative precipitation estimation by conceptual rainfall-runoff modeling. *Water Resour Res* 47:W06514. doi: 10.1029/2010WR009153
- Hopson TM, Webster PJ (2010) A 1–10-Day Ensemble Forecasting Scheme for the Major River Basins of Bangladesh: Forecasting Severe Floods of 2003–07. *J Hydrometeor* 11:618–641. doi: 10.1175/2009JHM1006.1
- Huffman GJ, Bolvin DT, Nelkin EJ, et al (2007) The TRMM Multisatellite Precipitation Analysis (TMPA): Quasi-Global, Multiyear, Combined-Sensor Precipitation Estimates at Fine Scales. *J Hydrometeor* 8:38–55. doi: 10.1175/JHM560.1
- Ines AVM, Hansen JW (2006) Bias correction of daily GCM rainfall for crop simulation studies. *Agricultural and Forest Meteorology* 138:44–53. doi: 10.1016/j.agrformet.2006.03.009
- IPCC (2014) *Climate Change 2014: Impacts, Adaptation, and Vulnerability. Part B: Regional Aspects. Contribution of Working Group II to the Fifth Assessment Report of the Intergovernmental Panel on Climate Change* [Barros, V.R., C.B. Field, D.J. Dokken, M.D. Mastrandrea, K.J. Mach, T.E. Bilir, M. Chatterjee, K.L.

- Ebi, Y.O. Estrada, R.C. Genova, B. Girma, E.S. Kissel, A.N. Levy, S. MacCracken, P.R. Mastrandrea, L.L. White (eds.)]. Cambridge University Press, Cambridge, United Kingdom and New York, NY, USA, 688 pp.
- Islam AS, Haque A, Bala SK (2010) Hydrologic characteristics of floods in Ganges–Brahmaputra–Meghna (GBM) delta. *Nat Hazards* 54:797–811. doi: 10.1007/s11069-010-9504-y
- Islam MN, Uyeda H (2007) Use of TRMM in determining the climatic characteristics of rainfall over Bangladesh. *Remote Sensing of Environment* 108:264–276. doi: 10.1016/j.rse.2006.11.011
- Jiang S, Ren L, Hong Y, et al (2012) Comprehensive evaluation of multi-satellite precipitation products with a dense rain gauge network and optimally merging their simulated hydrological flows using the Bayesian model averaging method. *Journal of Hydrology* 452–453:213–225. doi: 10.1016/j.jhydrol.2012.05.055
- JICA (1991) Japan International Cooperation Agency. Master plan for greater Dhaka flood protection project, FAP 8A, main REPORT and supporting report-II. Dhaka: Japan International Cooperation Agency
- Jongman B, Hochrainer-Stigler S, Feyen L, et al (2014) Increasing stress on disaster-risk finance due to large floods. *Nature Climate Change* 4:264–268. doi: 10.1038/nclimate2124
- Joyce RJ, Janowiak JE, Arkin PA, Xie P (2004) CMORPH: A Method that Produces Global Precipitation Estimates from Passive Microwave and Infrared Data at High Spatial and Temporal Resolution. *J Hydrometeor* 5:487–503. doi: 10.1175/1525-7541(2004)005<0487:CAMTPG>2.0.CO;2
- Kefi M, Mishra BK, Kumar P, et al (2018) Assessment of Tangible Direct Flood Damage Using a Spatial Analysis Approach under the Effects of Climate Change: Case Study in an Urban Watershed in Hanoi, Vietnam. *ISPRS International Journal of Geo-Information* 7:29. doi: 10.3390/ijgi7010029
- Khan D, Rahman S, Haque AK, et al (2012) Flood damage assessment for Dhaka City, Bangladesh
- Kibler KM, Biswas RK, Juarez Lucas AM (2014) Hydrologic data as a human right? Equitable access to information as a resource for disaster risk reduction in transboundary river basins. *Water Policy* 16:36–58. doi: 10.2166/wp.2014.307
- Kreibich H, Seifert I, Merz B, Thielen AH (2010) Development of FLEMOcs – a new model for the estimation of flood losses in the commercial sector. *Hydrological Sciences Journal* 55:1302–1314. doi: 10.1080/02626667.2010.529815
- Kubota T, Shige S, Hashizume H, et al (2007) Global Precipitation Map Using Satellite-Borne Microwave Radiometers by the GSMaP Project: Production and Validation.

- IEEE Transactions on Geoscience and Remote Sensing 45:2259–2275. doi: 10.1109/TGRS.2007.895337
- Kummerow C, Simpson J, Thiele O, et al (2000) The Status of the Tropical Rainfall Measuring Mission (TRMM) after Two Years in Orbit. *J Appl Meteor* 39:1965–1982. doi: 10.1175/1520-0450(2001)040<1965:TSOTTR>2.0.CO;2
- Kwak Y, Gusyev M, Arifuzzaman B, et al (2015) Effectiveness of Water Infrastructure for River Flood Management: Part 2 – Flood Risk Assessment and Its Changes in Bangladesh. In: *Proceedings of the International Association of Hydrological Sciences*. Copernicus GmbH, pp 83–87
- Kwak Y, Takeuchi K, Fukami K, Magome J (2012) A new approach to flood risk assessment in Asia-Pacific region based on MRI-AGCM outputs. *Hydrological Research Letters* 6:70–75. doi: 10.3178/hrl.6.70
- Lafon T, Dadson S, Buys G, Prudhomme C (2013) Bias correction of daily precipitation simulated by a regional climate model: a comparison of methods. *Int J Climatol* 33:1367–1381. doi: 10.1002/joc.3518
- Lehner B, Verdin K, Jarvis A (2008) New global hydrography derived from spaceborne elevation data. *Eos, Transactions American Geophysical Union* 89:2. doi: 10.1029/2008EO100001
- Lenderink G, Buishand A, van Deursen W (2007) Estimates of future discharges of the river Rhine using two scenario methodologies: direct versus delta approach. *Hydrol Earth Syst Sci* 11:1145–1159. doi: 10.5194/hess-11-1145-2007
- Marsalek J, Stancalie G, Balint G (eds) (2006) *Transboundary Floods: Reducing Risks Through Flood Management*. In: *Proceedings of the NATO Advanced Research Workshop on Transboundary Floods: Reducing Risks and Enhancing Security Through Improved Flood Management Planning*, Baile Felix (Oradea), Romania, May 4-8, 2005. Springer, Berlin
- Masood M, Takeuchi K (2012) Assessment of flood hazard, vulnerability and risk of mid-eastern Dhaka using DEM and 1D hydrodynamic model. *Nat Hazards* 61:757–770. doi: 10.1007/s11069-011-0060-x
- Menne MJ, Durre I, Vose RS, et al (2012) An Overview of the Global Historical Climatology Network-Daily Database. *J Atmos Oceanic Technol* 29:897–910. doi: 10.1175/JTECH-D-11-00103.1
- Merz B, Kreibich H, Schwarze R, Thielen A (2010) Review article “Assessment of economic flood damage.” *Natural Hazards and Earth System Sciences* 10:1697–1724. doi: <https://doi.org/10.5194/nhess-10-1697-2010>
- Messner F, Meyer V (2005) Flood damage, vulnerability and risk perception - challenges for flood damage research. Helmholtz Centre for Environmental Research (UFZ), Division of Social Sciences (ÖKUS)

- Mirza MMQ (2003) Three Recent Extreme Floods in Bangladesh: A Hydro-Meteorological Analysis. *Natural Hazards* 28:35–64. doi: 10.1023/A:1021169731325
- Mirza MMQ, Warrick RA, Ericksen NJ (2003) The Implications of Climate Change on Floods of the Ganges, Brahmaputra and Meghna Rivers in Bangladesh. *Climatic Change* 57:287–318. doi: 10.1023/A:1022825915791
- MLIT (2005) Ministry of Land, Infrastructure, Transport and Tourism. Manual for economic analysis for flood control projects. Publication of MLIT, Japan
- MOC (1996) Outline of River Improvement Economic Research Investigation, Technical Report, River Engineering Bureau, Ministry of Construction (MOC), Japan
- Mudelsee M, Börngen M, Tetzlaff G, Grünewald U (2003) No upward trends in the occurrence of extreme floods in central Europe. *Nature* 425:166. doi: 10.1038/nature01928
- Nishat B, Rahman SMM (2009) Water Resources Modeling of the Ganges-Brahmaputra-Meghna River Basins Using Satellite Remote Sensing Data. *JAWRA Journal of the American Water Resources Association* 45:1313–1327. doi: 10.1111/j.1752-1688.2009.00374.x
- Nyunt CT, Koike T, Yamamoto A (2016) Statistical bias correction for climate change impact on the basin scale precipitation in Sri Lanka, Philippines, Japan and Tunisia. *Hydrology and Earth System Sciences Discussions* 1–32. doi: <https://doi.org/10.5194/hess-2016-14>
- Okamoto K, Takahashi N, Iwanami K, et al (2008) High precision and high resolution global precipitation map from satellite data. In: 2008 Microwave Radiometry and Remote Sensing of the Environment. pp 1–4
- Okazumi T, Miyamoto M, Shrestha BB, Gusyev M (2014a) Uncertainty Estimation During the Process of Flood Risk Assessment in Developing Countries – Case Study in the Pampanga River Basin –. *Journal of Disaster Research* 9:69–77. doi: 10.20965/jdr.2014.p0069
- Okazumi T, Tanaka S, Kwak Y, et al (2014b) Flood vulnerability assessment in the light of rice cultivation characteristics in Mekong River flood plain in Cambodia. *Paddy Water Environ* 12:275–286. doi: 10.1007/s10333-013-0403-1
- Olesen L, Löwe R, Arnbjerg-Nielsen K (2017) Flood damage assessment – Literature review and recommended procedure. Cooperative Research Centre for Water Sensitive Cities, Melbourne, Australia
- Olsen AS, Zhou Q, Linde JJ, Arnbjerg-Nielsen K (2015) Comparing Methods of Calculating Expected Annual Damage in Urban Pluvial Flood Risk Assessments. *Water* 7:255–270. doi: 10.3390/w7010255

- Parry BL (2013) Think the weather bad's here? Spare a thought for these Indian villagers who live in the wettest place in the world with 40 FEET of rain a year. In: Mail Online. <http://www.dailymail.co.uk/news/article-2471421/Indias-Mawsynram-villagers-live-wettest-place-world-40-FEET-rain-year.html>. Accessed 2 Aug 2017
- Paul SK, Routray JK (2010) Flood proneness and coping strategies: the experiences of two villages in Bangladesh. *Disasters* 34:489–508. doi: 10.1111/j.1467-7717.2009.01139.x
- Piani C, Weedon GP, Best M, et al (2010) Statistical bias correction of global simulated daily precipitation and temperature for the application of hydrological models. *Journal of Hydrology* 395:199–215. doi: 10.1016/j.jhydrol.2010.10.024
- Prasanna V, Subere J, Das DK, et al (2014) Development of daily gridded rainfall dataset over the Ganga, Brahmaputra and Meghna river basins. *Met Apps* 21:278–293. doi: 10.1002/met.1327
- Qi W, Zhang C, Fu G, et al (2016) Evaluation of global fine-resolution precipitation products and their uncertainty quantification in ensemble discharge simulations. *Hydrol Earth Syst Sci* 20:903–920. doi: 10.5194/hess-20-903-2016
- Romali NS, Sulaiman MSAK, Yusop Z, Ismail Z (2015) Flood Damage Assessment: A Review of Flood Stage–Damage Function Curve. In: Abu Bakar SH, Tahir W, Wahid MA, et al. (eds) ISFRAM 2014. Springer Singapore, pp 147–159
- Romilly TG, Gebremichael M (2011) Evaluation of satellite rainfall estimates over Ethiopian river basins. *Hydrol Earth Syst Sci* 15:1505–1514. doi: 10.5194/hess-15-1505-2011
- Rudolf B (1993) Management and analysis of precipitation data on a routine basis, in precipitation and evaporation. In: Proceedings of the 1968 23rd ACM National Conference. ACM, New York, NY, USA, pp 69–76
- Salio P, Hobouchian MP, García Skabar Y, Vila D (2015) Evaluation of high-resolution satellite precipitation estimates over southern South America using a dense rain gauge network. *Atmospheric Research* 163:146–161. doi: 10.1016/j.atmosres.2014.11.017
- Sayama T, Ozawa G, Kawakami T, et al (2012) Rainfall–runoff–inundation analysis of the 2010 Pakistan flood in the Kabul River basin. *Hydrological Sciences Journal* 57:298–312. doi: 10.1080/02626667.2011.644245
- Sayama T, Tatebe Y, Iwami Y, Tanaka S (2015a) Hydrologic sensitivity of flood runoff and inundation: 2011 Thailand floods in the Chao Phraya River basin. *Nat Hazards Earth Syst Sci* 15:1617–1630. doi: 10.5194/nhess-15-1617-2015

- Sayama T, Tatebe Y, Tanaka S (2015b) An emergency response-type rainfall-runoff-inundation simulation for 2011 Thailand floods. *J Flood Risk Management* 10:65–78. doi: 10.1111/jfr3.12147
- Seto S, Takahashi N, Iguchi T (2005) Rain/No-Rain Classification Methods for Microwave Radiometer Observations over Land Using Statistical Information for Brightness Temperatures under No-Rain Conditions. *J Appl Meteor* 44:1243–1259. doi: 10.1175/JAM2263.1
- Shah (2001) Sustainable Development of the Ganges-Brahmaputra-Meghna Basins - United Nations University. <https://unu.edu/publications/books/sustainable-development-of-the-ganges-brahmaputra-meghna-basins.html>. Accessed 12 Mar 2018
- Shen Y, Xiong A, Hong Y, et al (2014) Uncertainty analysis of five satellite-based precipitation products and evaluation of three optimally merged multi-algorithm products over the Tibetan Plateau. *International Journal of Remote Sensing* 35:6843–6858. doi: 10.1080/01431161.2014.960612
- Shepard D (1968) A Two-dimensional Interpolation Function for Irregularly-spaced Data. In: *Proceedings of the 1968 23rd ACM National Conference*. ACM, New York, NY, USA, pp 517–524
- Shrestha BB, Okazumi T, Miyamoto M, Sawano H (2016) Flood damage assessment in the Pampanga river basin of the Philippines. *Journal of Flood Risk Management* 9:355–369. doi: 10.1111/jfr3.12174
- Siddique-E-Akbor AHM, Hossain F, Sikder S, et al (2014) Satellite Precipitation Data–Driven Hydrological Modeling for Water Resources Management in the Ganges, Brahmaputra, and Meghna Basins. *Earth Interact* 18:1–25. doi: 10.1175/EI-D-14-0017.1
- Steen PJMV, Pellenbarg PH (2004) Water Management Challenges in the Netherlands. *Tijdschrift voor economische en sociale geografie* 95:590–599. doi: 10.1111/j.0040-747X.2004.00343.x
- Stock J, Watson M (1999) *Cointegration, Causality and Forecasting: A Festschrift for Clive W.J. Granger*. Oxford University Press, Oxford
- Stock JH, Watson MW (2003) How Did Leading Indicator Forecasts Perform during the 2001 Recession? Social Science Research Network, Rochester, NY
- Stock JH, Watson MW (2004) Combination forecasts of output growth in a seven-country data set. *J Forecast* 23:405–430. doi: 10.1002/for.928
- Su F, Hong Y, Lettenmaier DP (2008) Evaluation of TRMM Multisatellite Precipitation Analysis (TMPA) and Its Utility in Hydrologic Prediction in the La Plata Basin. *J Hydrometeor* 9:622–640. doi: 10.1175/2007JHM944.1

- Sun F, Roderick ML, Lim WH, Farquhar GD (2011) Hydroclimatic projections for the Murray-Darling Basin based on an ensemble derived from Intergovernmental Panel on Climate Change AR4 climate models. *Water Resour Res* 47:W00G02. doi: 10.1029/2010WR009829
- Takahashi N, Awaka J (2005) Introduction of a melting layer model to a rain retrieval algorithm for microwave radiometers. In: *Proceedings. 2005 IEEE International Geoscience and Remote Sensing Symposium, 2005. IGARSS '05.* pp 3404–3409
- Takeuchi K, Hapuarachchi P, Zhou M, et al (2008) A BTOP model to extend TOPMODEL for distributed hydrological simulation of large basins. *Hydrological Processes* 22:3236–3251. doi: 10.1002/hyp.6910
- Tateishi R, Hoan NT, Kobayashi T, et al (2014) Production of Global Land Cover Data – GLCNMO2008. *Journal of Geography and Geology* 6:99. doi: 10.5539/jgg.v6n3p99
- Taylor KE (2001) Summarizing multiple aspects of model performance in a single diagram. *J Geophys Res* 106:7183–7192. doi: 10.1029/2000JD900719
- Teutschbein C, Seibert J (2012) Bias correction of regional climate model simulations for hydrological climate-change impact studies: Review and evaluation of different methods. *Journal of Hydrology* 456:12–29. doi: 10.1016/j.jhydrol.2012.05.052
- Thiemeßl MJ, Gobiet A, Heinrich G (2012) Empirical-statistical downscaling and error correction of regional climate models and its impact on the climate change signal. *Climatic Change* 112:449–468. doi: 10.1007/s10584-011-0224-4
- Thiemeßl MJ, Gobiet A, Leuprecht A (2011) Empirical-statistical downscaling and error correction of daily precipitation from regional climate models. *Int J Climatol* 31:1530–1544. doi: 10.1002/joc.2168
- Tingsanchali T, Karim MF (2005) Flood hazard and risk analysis in the southwest region of Bangladesh. *Hydrological Processes* 19:2055–2069. doi: 10.1002/hyp.5666
- Tol RSJ, van der Grijp N, Olsthoorn AA, van der Werff PE (2003) Adapting to climate: a case study on riverine flood risks in the Netherlands. *Risk Anal* 23:575–583
- Ushio T, Sasashige K, Kubota T, et al (2009) A Kalman Filter Approach to the Global Satellite Mapping of Precipitation (GSMaP) from Combined Passive Microwave and Infrared Radiometric Data. *Journal of the Meteorological Society of Japan Ser II* 87A:137–151. doi: 10.2151/jmsj.87A.137
- Ushio T, Tashima T, Kubota T, Kachi M (2014) Gauge adjusted Global Satellite Mapping of Precipitation (GSMaP_Gauge). In *Proceedings of the 2014 XXXIth URSI on General Assembly and Scientific Symposium (URSI GASS), Beijing, China, 16–23 August 2014.* ISTS 87A:137–151. doi: 10.2151/jmsj.87A.137

- Valeriano OCS, Koikel T, Rahman M (2010) TOWARDS GLOBAL RIVER DISCHARGE ASSESSMENT USING A DISTRIBUTED HYDROLOGICAL MODEL AND GLOBAL DATA SETS. *Revista Investigación & Desarrollo* 1:
- Velasco M, Cabello À, Russo B (2016) Flood damage assessment in urban areas. Application to the Raval district of Barcelona using synthetic depth damage curves. *Urban Water Journal* 13:426–440. doi: 10.1080/1573062X.2014.994005
- Vila DA, de Goncalves LGG, Toll DL, Rozante JR (2009) Statistical Evaluation of Combined Daily Gauge Observations and Rainfall Satellite Estimates over Continental South America. *J Hydrometeor* 10:533–543. doi: 10.1175/2008JHM1048.1
- Viviroli D, Mittelbach H, Gurtz J, Weingartner R (2009) Continuous simulation for flood estimation in ungauged mesoscale catchments of Switzerland – Part II: Parameter regionalisation and flood estimation results. *Journal of Hydrology* 377:208–225. doi: 10.1016/j.jhydrol.2009.08.022
- Wang J, Hong Y, Li L, et al (2011) The coupled routing and excess storage (CREST) distributed hydrological model. *Hydrological Sciences Journal* 56:84–98. doi: 10.1080/02626667.2010.543087
- Wilcke RAI, Mendlik T, Gobiet A (2013) Multi-variable error correction of regional climate models. *Climatic Change* 120:871–887. doi: 10.1007/s10584-013-0845-x
- Win S, Zin WW, Kawasaki A, San ZMLT (2018) Establishment of flood damage function models: A case study in the Bago River Basin, Myanmar. *International Journal of Disaster Risk Reduction* 28:688–700. doi: 10.1016/j.ijdr.2018.01.030
- Winsemius HC, Beek LPHV, Jongman B, et al (2013) A framework for global river flood risk assessments. *Hydrology and Earth System Sciences* 17:1871–1892. doi: <https://doi.org/10.5194/hess-17-1871-2013>
- Woldemeskel FM, Sivakumar B, Sharma A (2013) Merging gauge and satellite rainfall with specification of associated uncertainty across Australia. *Journal of Hydrology* 499:167–176. doi: 10.1016/j.jhydrol.2013.06.039
- Wood AW, Leung LR, Sridhar V, Lettenmaier DP (2004) Hydrologic Implications of Dynamical and Statistical Approaches to Downscaling Climate Model Outputs. *Climatic Change* 62:189–216. doi: 10.1023/B:CLIM.0000013685.99609.9e
- Xie P, Arkin PA (1996) Analyses of Global Monthly Precipitation Using Gauge Observations, Satellite Estimates, and Numerical Model Predictions. *J Climate* 9:840–858. doi: 10.1175/1520-0442(1996)009<0840:AOGMPU>2.0.CO;2
- Yong B, Hong Y, Ren L-L, et al (2012) Assessment of evolving TRMM-based multisatellite real-time precipitation estimation methods and their impacts on hydrologic prediction in a high latitude basin. *J Geophys Res* 117:D09108. doi: 10.1029/2011JD017069

Zappa M, Rotach MW, Arpagaus M, et al (2008) MAP D-PHASE: real-time demonstration of hydrological ensemble prediction systems. *Atmosph Sci Lett* 9:80–87. doi: 10.1002/asl.183

Zhai G, Fukuzono T, Ikeda S (2005) MODELING FLOOD DAMAGE: CASE OF TOKAI FLOOD 2000. *Journal of the American Water Resources Association* 41:77–92. doi: 10.1111/j.1752-1688.2005.tb03719.x